Elsevier Editorial System(tm) for Regulatory Toxicology and Pharmacology

Manuscript Draft

Manuscript Number: RTP-16-274R1

Title: Evaluation of the Tobacco Heating System 2.2. Part 7: Systems toxicological assessment of a mentholated version revealed reduced cellular and molecular exposure effects compared with mentholated and non-mentholated cigarette smoke

Article Type: PMI Supplement

Keywords: modified risk tobacco product; systems toxicology; transcriptomics; proteomics; lipidomics; subchronic inhalation toxicity

Corresponding Author: Dr. Julia Hoeng,

Corresponding Author's Institution:

First Author: Ulrike Kogel

Order of Authors: Ulrike Kogel; Bjoern Titz, Ph.D.; Walter K Schlage; Catherine Nury; Florian Martin; Alberto Oviedo; Stefan Lebrun; Ashraf Elamin; Emmanuel Guedj; Keyur Trivedi; Nikolai V Ivanov; Patrick Vanscheeuwijck; Manuel C Peitsch; Julia Hoeng

Abstract: Modified risk tobacco products (MRTPs) are being developed with the aim of reducing smoking-related health risks. The Tobacco Heating System 2.2 (THS2.2) is a candidate MRTP that uses the heat-not-burn principle. Here, systems toxicology approaches were engaged to assess the respiratory effects of mentholated THS2.2 (THS2.2M) in a 90-day rat inhalation study (OECD test guideline 413). The standard endpoints were complemented by transcriptomics and quantitative proteomics analyses of respiratory nasal epithelium and lung tissue and by lipidomics analysis of lung tissue. The adaptive response of the respiratory nasal epithelium to conventional cigarette smoke (CS) included squamous cell metaplasia and an inflammatory response, with high correspondence between the molecular and histopathological results. In contrast to CS exposure, the adaptive tissue and molecular changes to THS2.2M aerosol exposure were much weaker and were limited mostly to the highest THS2.2M concentration in female rats. In the lung, CS exposure induced an inflammatory response, triggered cellular stress responses, and affected sphingolipid metabolism. These responses were not observed or were much lower after THS2.2M aerosol exposure. Overall, this system toxicology analysis complements and reconfirms the results from classical toxicological endpoints and further suggests potentially reduced health risks of THS2.2M.

Philip Morris International,
Philip Morris Products SA
Quai Jeanrenaud 5
2000 Neuchâtel
Switzerland

23 September, 2016

To the Editor of
Regulatory Toxicology and Pharmacology

Re: Ulrike Kogel, Bjoern Titz, Walter K. Schlage, Catherine Nury, Florian Martin, Alberto Oviedo, Stefan Lebrun, Ashraf Elamin, Emmanuel Guedj, Keyur Trivedi, Nikolai V. Ivanov, Patrick Vanscheeuwijck, Manuel C. Peitsch, Julia Hoeng

Evaluation of the Tobacco Heating System 2.2. Part 7: Systems toxicological assessment of a mentholated version revealed reduced cellular and molecular exposure effects compared with mentholated and non-mentholated cigarette smoke

Dear Dr. Gori,

We would like to thank the editors for the opportunity to submit a revised version of the manuscript.

We would be grateful if you would consider publishing the above manuscript, Part 7 of a series of nine manuscripts, in a special issue of Regulatory Toxicology and Pharmacology. The series of manuscripts describes the toxicological assessment and a clinical study on the Tobacco Heating System 2.2.

We also thank the reviewers for a careful and thoughtful review of our document, and we believe that the incorporation of each of the suggestions has resulted in an improved manuscript.

Taken together, we feel that the revised manuscript fulfills the Reviewer's requirements and that thanks to their input the quality of the paper has been improved.

We are looking forward to hearing from you soon.

Yours sincerely,

Dr. Julia Hoeng

Director System Toxicology

Philip Morris International,
Philip Morris Products SA
Quai Jeanrenaud 5
2000 Neuchâtel
Switzerland

20th September, 2016

To the Editor of
Regulatory Toxicology and Pharmacology

Ms. No.: RTP-16-274
Title: Evaluation of the Tobacco Heating System 2.2. Part 7: Systems toxicological assessment of a mentholated version revealed reduced cellular and molecular exposure effects compared with mentholated and non-mentholated cigarette smoke

Corresponding Author: Julia Hoeng

We thank the reviewers for the very helpful and constructive comments. We have addressed the comments as outlined in our point-by-point response below, in blue font.

Reviewer #1: REVIEW OF RTP-16-274

OVERALL

A key aspect of any toxicological investigation is a complete, unambiguous description of each test article. For example, there is sufficient information on the 3R4F reference cigarette to understand that chemical and physical properties of the cigarette to manufacture a duplicate product. Indeed, there is sufficient information on the product that it could be duplicated by a third-party manufacturer without extensive analytical work. However, there is insufficient information in this manuscript on the MRC(LM) and MRC(HM) to understand the chemical and physical properties of these cigarettes. Moreover, the figures associated with the manuscript appear to show that the mainstream smoke from MRC(LM) has different toxicological properties than the mainstream smoke from MRC(HM). This finding is unexpected given classical inhalation toxicology of mainstream smoke from mentholated cigarettes versus nonmentholated cigarettes (for example, the authors citation of the research by Gaworski and co-workers). It appears that the authors have been remiss in the not understanding the toxicological properties of their reference cigarettes before using them as comparison with the THS cigarettes.
Until this is done, the scientific validity of this manuscript is in question.

We thank the reviewer for this suggestion and have included more details on the mentholated reference cigarettes (MRC) in part 6 of this series, which is focused on the overall design and classical endpoints of this inhalation study:

“MRC have been manufactured by Philip Morris International, Neuchatel, Switzerland for the purpose of the present study. Tar levels were 9.9 and 10.5 mg/cig, nicotine 0.64 and 0.64 mg/cig and CO 11.4 and 11.3 mg/cig for MRC(LM) and MRC(HM) respectively. In 3R4F tar is 9.4 mg/cig, nicotine 0.7 mg/cig and CO 12.0 mg/cig. For MRC(LM), L-menthol (CAS 2216-51-5) was added to 11.1 mg/cig (9.0 mg/cig in the filter, 2.1 mg/cig pack inner liner), for MRC(HM) 18.4 mg/cig (9.0 mg/cig in the filter, 3.9 mg/cig pack inner liner, 5.5 mg/cig cut filler or tobacco rod). The L-menthol used had a purity >99%”.” In this manuscript, part 7 of the series, we have now added: “For more details see (part 6, (Oviedo et al., submitted (this issue))).” in the “Reference cigarettes and THS2.2M” section.

In addition, we would like to clarify that our study was designed for the comparison between THS2.2M aerosol and CS from reference cigarettes – rather than for the comparison between the different reference cigarettes. To this end, we included mentholated reference cigarettes, in addition to the common 3R4F reference, to further support the comparative assessment of THS2.2M aerosol. For this, we manufactured the reference cigarettes, based on the specifications of 3R4F, but with menthol added in quantities that deliver similar menthol levels as those found in aerosol from THS2.2M.

While some differences between the reference cigarettes are found in our data, the few potential differences in the biological responses do not show an overall consistent pattern. Clear differences are only observed between the (group of) references on THS2.2M, whereas –over the whole data set—the three references rather seem to show an overall consistent (and often strong) biological response.

Moreover, the clarity of the figures in both the main manuscript and the supplementary material is unsatisfactory. Perhaps the artwork needs to be prepared at 2400 bpi so that it does not lose clarity when put into a PDF.

We apologize for this inconvenience, which was likely due to a conversion issue: all figures were available as vector graphics in the PDF format, but were converted to a bitmap format for review purposes. We have submitted the higher quality original PDF figure files for the revised manuscript.

Also, to describe machine smoking of cigarettes using the ISO standards, both 3308 and 4387 need to be cited. Moreover, smoke menthol measurements should have been done according to ISO 13110:2012: Cigarettes -- Determination of menthol in smoke condensates -- Gas-chromatographic method.

We used only ISO 3308 in the text, and added this now also to the reference list.

The method for measuring menthol is described in part 2 of the series, in detail; see 2.7.15 “analysis of menthol”). ISO 4387 and others were used to determine the smoke constituents by International Organization for Standardization as described in part 2 of this series. For all those chemical analysis we now refer to part 2 of the series.

Thus, it will take a major revision to bring this manuscript up to the standards of THIS JOURNAL.

We thank the reviewer for the suggestions how to improve the presentation of the methods and results. We have now revised the different, interconnected parts of this series of manuscripts to ensure that this important information is available to the reader.

Reviewer #2: General comments

This is a well-written manuscript that provides useful information to add to the general series.

Much more information (in lines 120 onwards) is needed on the way menthol is added to the cigarettes, including (if possible), the amounts. What was the source of the "mentholated reference cigarettes"?

The current manuscript is focused on the systems toxicology assessment component of the OECD inhalation study that is described in more detail by Oviedo et al. (part 6 of this series). In the current manuscript, we refer the reader to part 6 for more details on the exposure system and the mentholated reference cigarettes. To more clearly guide the reader to this information, we have now added the sentence "For more details see (part 6, (Oviedo et al., submitted (this issue)))." in the "Reference cigarettes and THS2.2M" section.

As the referenced manuscript by Oviedo et al. (part 6) manuscript was also lacking some details, we have added this information in part 6:

A) Details on the MRCs have been added to the manuscript (see our response to reviewer 1, above).
B) Concentrations of nicotine, Tar, CO, menthol were included

Throughout the text, the inference is made that the authors consider that nicotine could be a causative agent for some of the responses. I am unaware of the rationale for this inference, since nicotine inhalation studies have not shown such activity.

We thank the reviewer for pointing this out. With the exception of Cyp1a1 expression in the lung, we did not intend to identify nicotine as a likely agent for the responses. In our study, nicotine is used as a dosing reference to support the comparison between reference cigarette smoke (CS) and THS2.2M aerosol – with matching nicotine concentrations between the medium THS2.2M concentration and reference CS. This is why we state on effects of the aerosol/CS concentrations with matching or higher nicotine concentrations – but we did not intent to articulate that the observed responses are to be attributed to nicotine rather than, for example, the complex mixture of other CS components for the reference cigarettes. We have now slightly restated how we refer to the applied aerosol concentration, e.g. "…these remained well below the changes induced by the reference cigarettes (at twice the concentration with respect to the applied nicotine concentration)." [page 14], "…supported the overall conclusion that the effects of THS2.2M exposure were strongly reduced (even for the highest concentration of 50 µg/L nicotine) compared with CS exposure."[page 33], and "this systems toxicology analysis supported an integrated product risk assessment of THS2.2M. Consistently, the THS2.2M aerosols (even at the highest nicotine concentration)…" [page 36].

For Cyp1a1 we have some evidence for a nicotine-related effect in lung. In a previous rat inhalation study, we had found that Cyp1a1 shows a clear up-regulation upon nicotine-only exposure in the lung (Phillips et al., 2015). We discuss the observed up-regulation of Cyp1a1 in the current study in this context: "Cyp1a1 was the only xenobiotic enzyme that was significantly up-regulated upon THS2.2M exposure, which could likely be explained — in the absence of CS-typical inducers such as polycyclic aromatic hydrocarbons by the up-regulation effect that nicotine-only exposure had on the expression of this gene (Phillips et al., 2015)."

How is this manuscript different from another one (similar title) in the series?

The manuscript by Oviedo et al. "Evaluation of the Tobacco Heating System 2.2. Part 6: 90-day OECD 413 rat inhalation study with systems toxicology endpoints demonstrates reduced exposure effects of a mentholated version compared with mentholated and non-mentholated cigarette smoke." is presenting the overall design of this inhalation study and is focusing on the "standard" endpoints. Omics results are included at the highest level (e.g. numbers of differentially expressed genes/proteins) to summarize the overall response trends. In contrast, the current manuscript is specifically focused on the systems toxicology data analyses (transcriptomics, proteomics, lipidomics) and on "mechanistic" insights. "Standard" endpoints are discussed in regard how they complement each other. With this, both manuscripts provide complementary views on the overall toxicological and biological responses observed in this 90-day rat inhalation study.

Specific comments

Data on the possible pyrolysis of menthol at 350 °C would be helpful.

We are not aware of any publication mentioning menthol pyrolysis at 350°C. However, given the menthol physicochemical properties, the pyrolysis of menthol at 350°C should produce even less decomposition products than at 900°C.

The pyrolysis of menthol was studied in the frame of the potential influence of ingredients on the cigarette smoke composition. Therefore, this work was performed at ~900°C and not at 350°C. However, menthol is a molecule which easily sublimes. Therefore, it escapes before decomposition. In a book by Moldoveanu (Moldoveanu, S., Pyrolysis of Organic Molecules with Applications to Health and Environmental Issues, Elsevier, 2010, Elsevier), it was reported: "Menthol, being volatile, is transferred from the tobacco to smoke by a distillation process before reaching the temperatures necessary for decomposition. Experimental pyrolysis of menthol using [..] pyrolysis conditions [..] to mimic a burning cigarette, showed that over 99% of initial menthol is transferred during pyrolysis in intact form, with only 0.4% decomposed to menthene and 0.1% into menthone". Moldoveanu refers to (Baker, R. R., Bishop, J., 2004. The pyrolysis of tobacco ingredients. Journal of Applied Pyrolysis. 71, 223) which describes the pyrolysis of several ingredients. In addition, in an old publication, Jenkins explored the transfer of labeled menthol when spiked into Conventional Cigarettes. Similar transfer yields and decomposition products were observed when smoking the spiked cigarettes (Jenkins, R. W., Jr., Newman, R. H., Chavis, M. K., 1970. Cigarette Smoke Formation Studies: II. Smoke Distribution and Mainstream Pyrolytic Composition of Added 14C-Menthol (U). Beiträge zur Tabakforschung / Contributions

to Tobacco Research. 5, 299. www.degruyter.com/view/j/cttr.1970.5.issue-6/cttr-2013-0254/cttr-2013-0254.xml).

Lines 271-276 appear to contain non-scientific information.

The login information for the public data repository was intended for review purposes only and was removed for this revision.

Details on the smoke exposure apparatus are missing.

We now refer to part 6 of this series, which is focused on the overall design and classical endpoints of this inhalation study: "For more details including on the smoke and aerosol generation, monitoring of the aerosol composition, exposure conditions, and markers of exposure see the part 6 of this series (Oviedo et al., submitted (this issue))." Detailed descriptions can be found in "Test atmosphere generation and exposure", section 2.4.

This reviewer would like to see comparative statements on the strengths and weaknesses of the study.

We had included strengths of this study in the "discussion and conclusion" sections, e.g. complementation and added benefits of the systems toxicology approaches and the use of three complementary omics technologies. Some of the weaknesses/limitations were already mentioned in the discussion section, e.g. the inability of the used methods to spatially resolve the observed changes. However, especially, in the conclusion section the limitations were not well reflected. For this, we have now changed the 2nd half of the conclusions as follows:
"… Limitations of the employed omics technologies included the lack of spatial and cellular resolution of the detected changes, the lack of global activity measurements for the detected proteins, and the lack of information how the observed molecular changes are specifically linked to disease outcomes. In the future, complementary technologies could be adapted to fill these gaps and, importantly, the dense matrix of the systems biology-derived molecular data could be used to more directly link the outcomes from the general purpose 90-day OECD TG413 subchronic inhalation studies to the more disease-specific results from animal models of, for example, COPD, cardiovascular disease, and lung cancer."

The list of references seems slightly excessive and I suggest some reduction.

We agree, but would also remark that this is partly due to the diversity of topics (e.g., biological and technical aspects) covered. We have now (slightly) reduced the number of references, whenever possible.

Reviewer #3: RTP-16-274

This is a well written manuscript which is a part of the series of manuscripts that addressed the effects of exposure to cigarette smoke and aerosol from THS2.2. Multiple lines of evidence, including transcriptomic, proteomic and lipidomic data reveal that

cigarette smoke exposure elicits marked perturbations in several key biological pathways in respiratory nasal epithelium and lung. The bioinformatic analyses were performed using the previously described systems approach by the same group and compared the network perturbations from two different treatments. Overall the study is well conducted and results are generally well described.

The authors have not made an attempt to compare/relate the transcriptomic or proteomic results to exposure-nicotine or menthol levels in different treatment groups. In the absence of actual exposure information, it is difficult to assess the true significance of the findings. The authors may wish to address this point.

We thank the reviewer for this comment and would first like to emphasize that our study was designed and analyzed to compare the biological impact of THS2.2M aerosol with (a group of) relevant CS references. Please, also see our response to the related comments of reviewer 1 (1st comment on menthol) and reviewer 2 (2nd comment on nicotine). To ensure relevant comparability between THS2.2M aerosol and the references, we use the nicotine concentration in the aerosol/smoke for a relevant normalization and designed the study with identical nicotine concentrations for the three references and the medium concentration of THS2.2M. In addition to 3R4F, two versions with different menthol concentrations were included as references to better support the comparison for the mentholated version of THS2.2. Three concentrations of THS2.2M were included (also according to OECD TG) to evaluate potential dose responses and designed to also include a twice as high concentration as the references (by nicotine normalization) to reveal potential effects, when the aerosol concentration is further increased compared to the references. As pointed out in our response to reviewer 2, we understand that the observed responses are not necessarily linked to nicotine and would agree that our study was not designed to reveal nicotine-specific effects. Of note, we have a recent publication, in which we investigate potential nicotine effects in more detail (Phillips et al, 2015; Inhalation toxicology 27.9 (2015): 405-431) and, for example, based on this study we suggest that the observed effect on Cyp1a1 expression is due to nicotine. Similarity, as pointed out in our response to reviewer 1, the study was not designed to compare the effects of menthol in the set of the three reference cigarettes, but these additional references were rather included to further support the main comparison between THS2.2M and the (group of) these three references. While, as pointed out, there might be a low level variation in the response to these three references, we could not identify any clear consistent pattern and it is clear that the main difference is always between THS2.2M aerosol and reference CS exposure.

With respect to the (lacking) exposure information, we have now included more details on the mentholated reference cigarettes in part 6 of this series. In addition, we would like to emphasize that the exposure was characterized by measuring the uptake of nicotine and menthol in blood of the rats and these data are reported in part 6 of the series, which also has several more details on the exposure.

Other comments include:

* The font sizes of labels of some figures (example, fig Supp 2) are not legible
* All acronyms need to be defined (example, Supp fig 2)

We increased the font size of the heatmaps. Supp Figures will be only available online and we will make sure that we provide a high resolution pdf which allows to zoom-in.
We have included in the sup fig legend the acronyms which were used in the supp fig as CST for cell stress.

Reviewer #4:

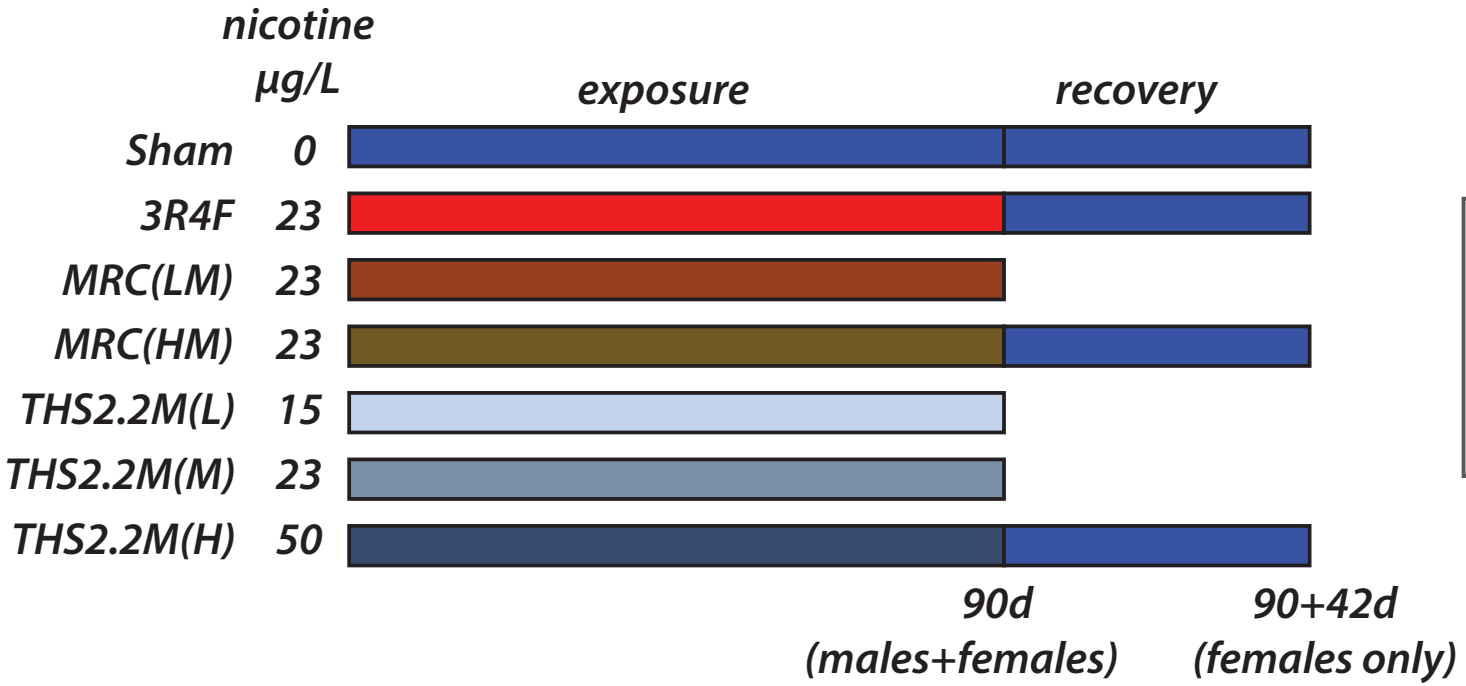
Very involved but well written. Heat maps are somewhat hard to read because of the amount of information.

We thank the reviewer for the positive feedback. We agree that heatmaps can be challenging to read, but would hope that the readers still appreciate these rather compact representations of the extensive molecular responses.

Highlights

- Systems toxicology assessment of candidate modified risk tobacco product (THS2.2M)
- Systems toxicology analyses were used to compare THS2.2M with a reference cigarette
- Assessment of exposure effects using proteomics, transcriptomics, and lipidomics
- Exposure showed lower effects of THS2.2M aerosol on rat nose and lung tissue
- Molecular insights on inflammation or cell stress complemented apical endpoints

Figure 1

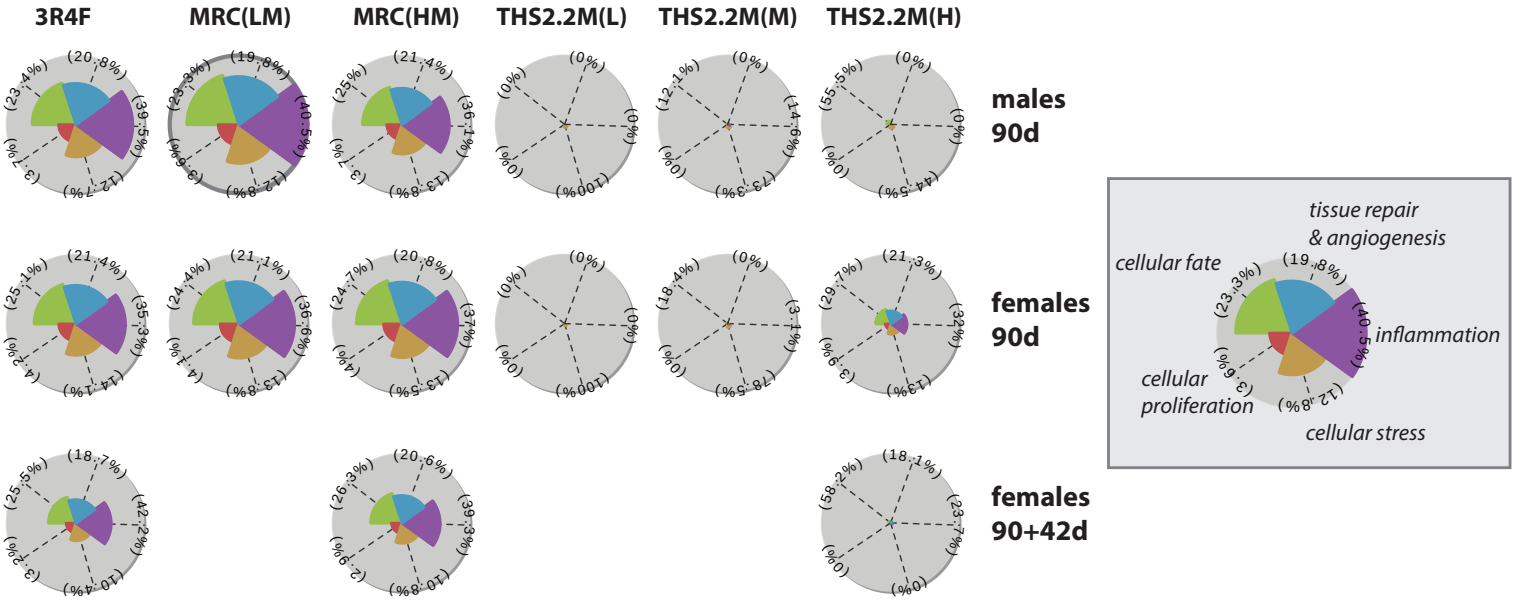


(molecular) endpoints

	nose	lung
Histopathology	*X*	*X*
Transcriptomics	*X*	*X*
Proteomics	*X*	*X*
Lipidomics		*X*

Figure 2

A


3R4F
MRC(LM)
MRC(HM)
THS2.2M(L)
THS2.2M(M)
THS2.2M(H)
males 90d
females 90d
females 90+42d
tissue repair & angiogenesis
cellular fate
inflammation
cellular proliferation
cellular stress

B

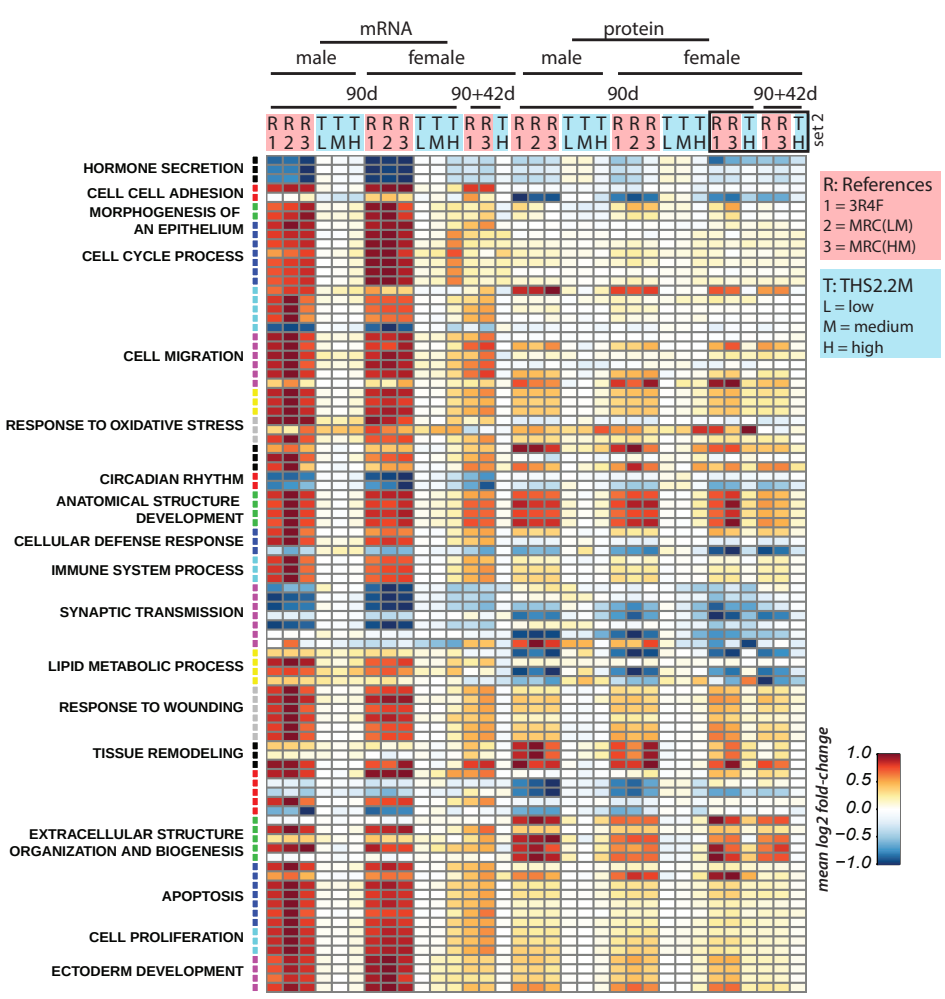

mRNA
protein
male
female
90d
90+42d
set 2
HORMONE SECRETION
CELL CELL ADHESION
MORPHOGENESIS OF AN EPITHELIUM
CELL CYCLE PROCESS
CELL MIGRATION
RESPONSE TO OXIDATIVE STRESS
CIRCADIAN RHYTHM
ANATOMICAL STRUCTURE DEVELOPMENT
CELLULAR DEFENSE RESPONSE
IMMUNE SYSTEM PROCESS
SYNAPTIC TRANSMISSION
LIPID METABOLIC PROCESS
RESPONSE TO WOUNDING
TISSUE REMODELING
EXTRACELLULAR STRUCTURE ORGANIZATION AND BIOGENESIS
APOPTOSIS
CELL PROLIFERATION
ECTODERM DEVELOPMENT
R: References
1 = 3R4F
2 = MRC(LM)
3 = MRC(HM)
T: THS2.2M
L = low
M = medium
H = high
mean log2 fold-change
1.0
0.5
0.0
−0.5
−1.0

Figure 3

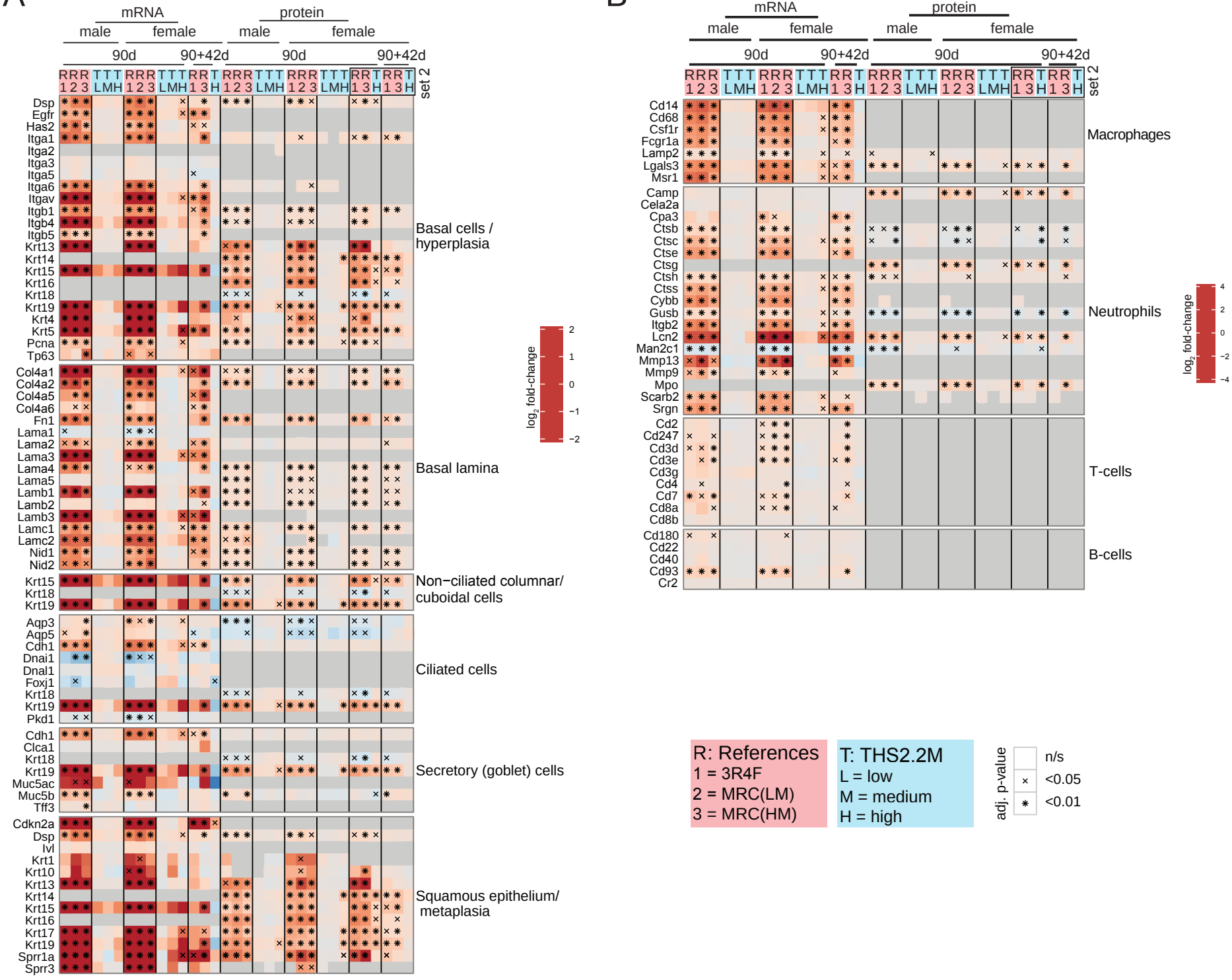

A
B
mRNA
protein
male
female
90d
90+42d
set 2
Basal cells / hyperplasia
Basal lamina
Non−ciliated columnar/ cuboidal cells
Ciliated cells
Secretory (goblet) cells
Squamous epithelium/ metaplasia
Macrophages
Neutrophils
T-cells
B-cells
log2 fold-change
R: References
1 = 3R4F
2 = MRC(LM)
3 = MRC(HM)
T: THS2.2M
L = low
M = medium
H = high
adj. p-value
n/s
<0.05
<0.01

Figure 4

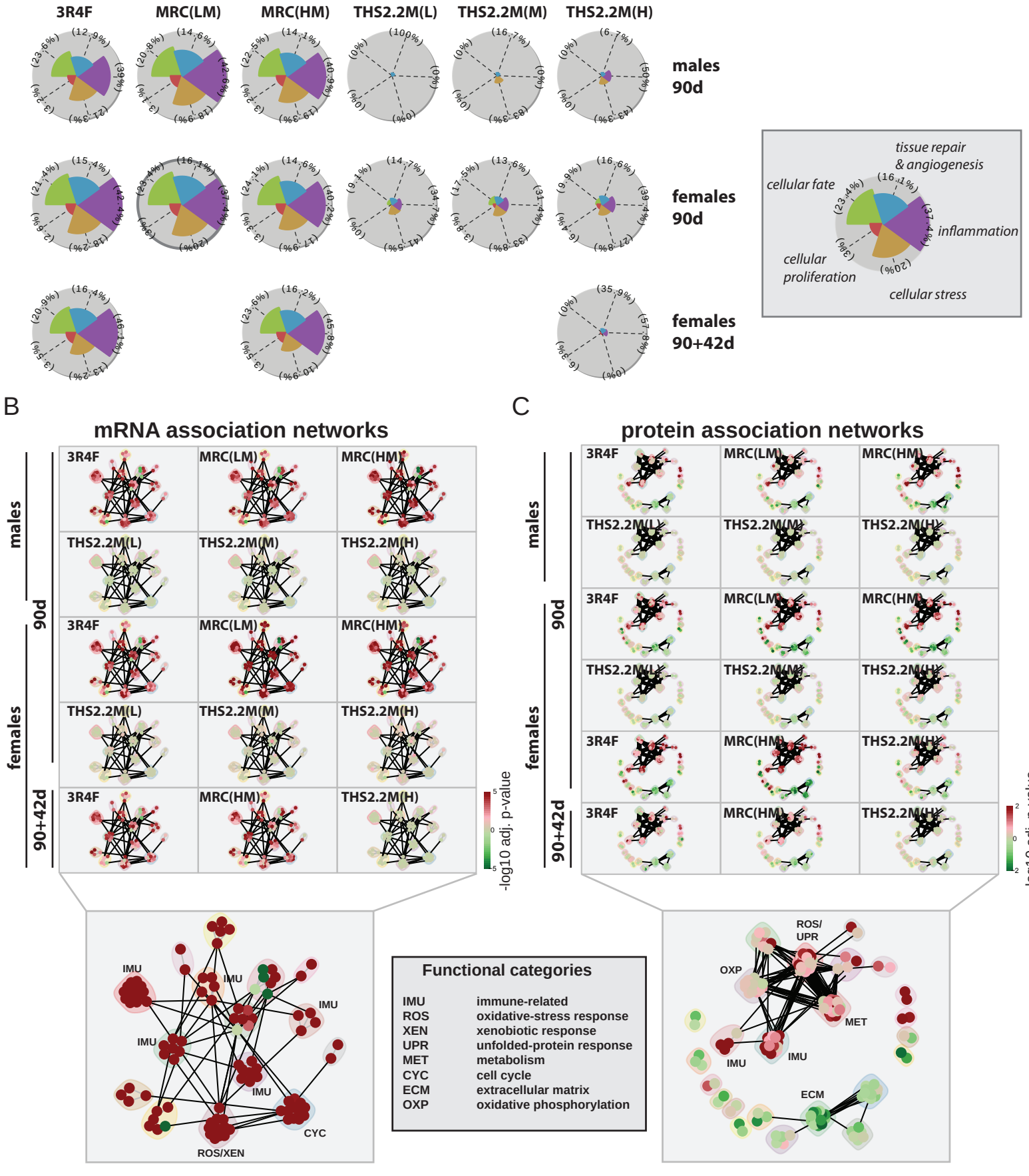
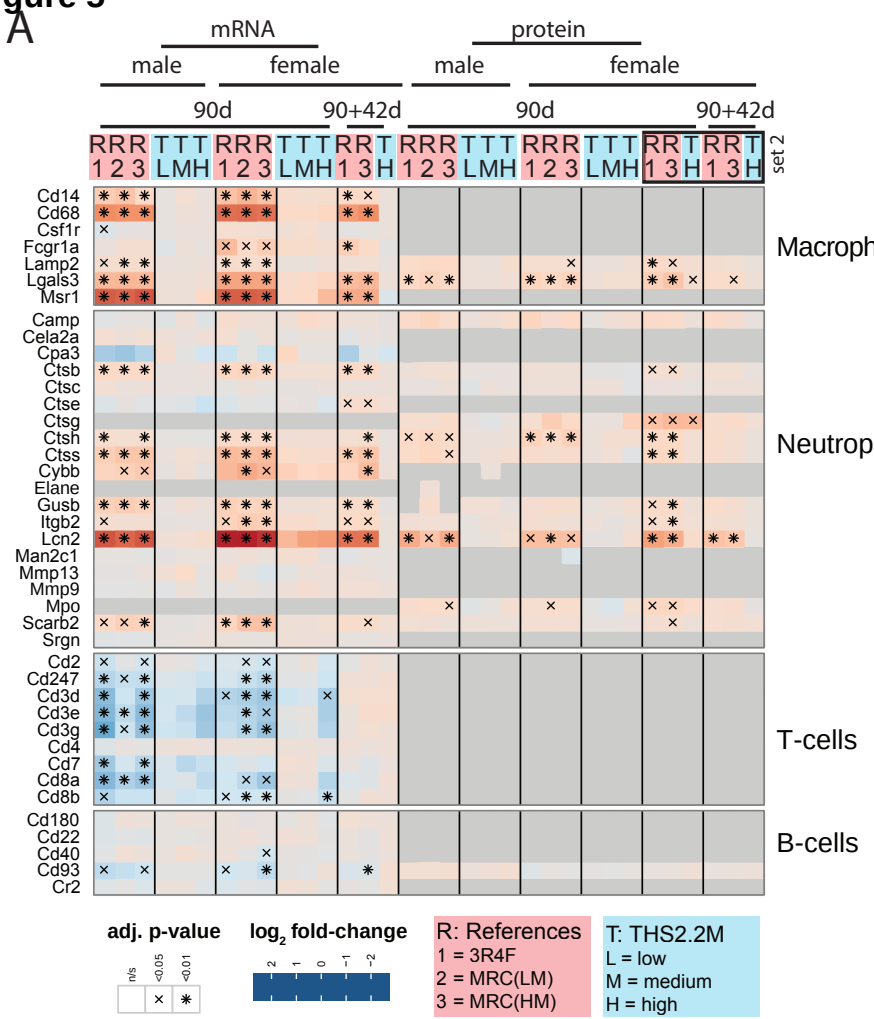
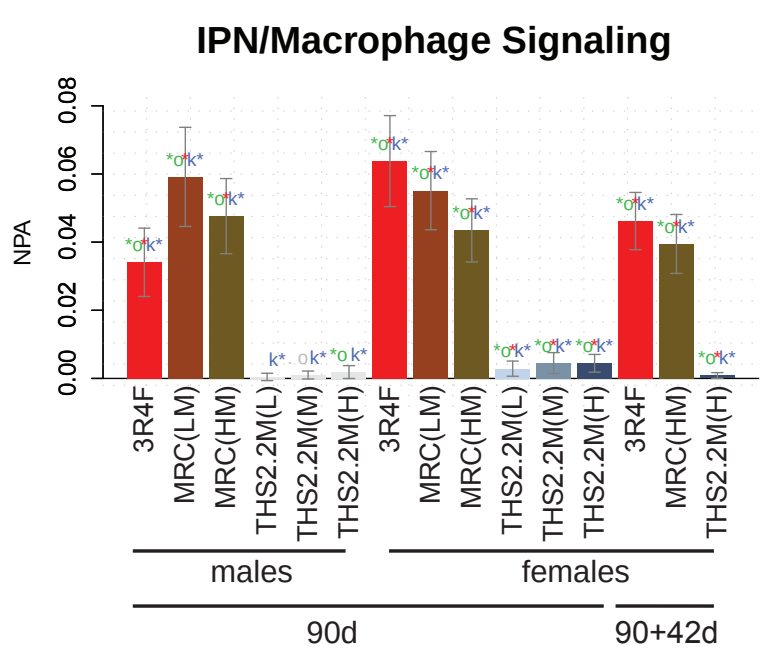
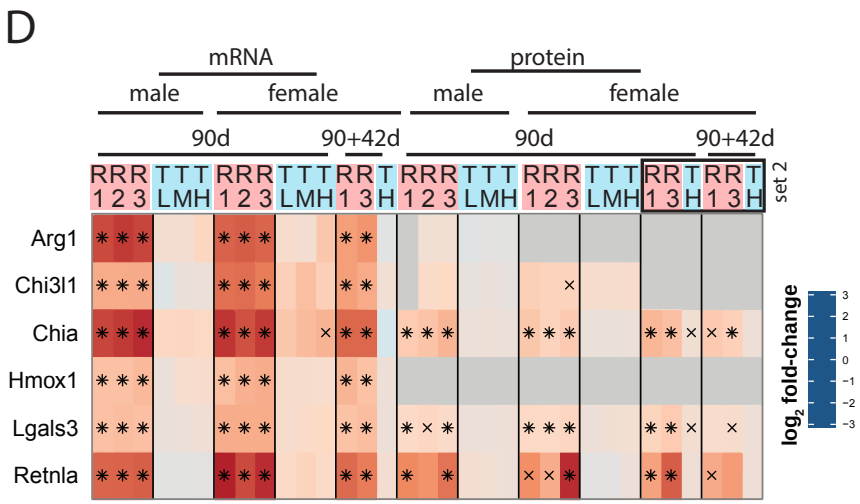

A
3R4F
MRC(LM)
MRC(HM)
THS2.2M(L)
THS2.2M(M)
THS2.2M(H)
males 90d
females 90d
females 90+42d
tissue repair & angiogenesis
cellular fate
inflammation
cellular proliferation
cellular stress
B
mRNA association networks
C
protein association networks
males
females
90d
90+42d
-log10 adj. p-value
IMU
ROS/XEN
CYC
ROS/ UPR
OXP
MET
ECM
Functional categories
IMU immune-related
ROS oxidative-stress response
XEN xenobiotic response
UPR unfolded-protein response
MET metabolism
CYC cell cycle
ECM extracellular matrix
OXP oxidative phosphorylation

Figure 5


A
mRNA
protein
male
female
90d
90+42d
set 2
Macrophages
Neutrophils
T-cells
B-cells
Cd14
Cd68
Csf1r
Fcgr1a
Lamp2
Lgals3
Msr1
Camp
Cela2a
Cpa3
Ctsb
Ctsc
Ctse
Ctsg
Ctsh
Ctss
Cybb
Elane
Gusb
Itgb2
Lcn2
Man2c1
Mmp13
Mmp9
Mpo
Scarb2
Srgn
Cd2
Cd247
Cd3d
Cd3e
Cd3g
Cd4
Cd7
Cd8a
Cd8b
Cd180
Cd22
Cd40
Cd93
Cr2
adj. p-value
log2 fold-change
R: References
1 = 3R4F
2 = MRC(LM)
3 = MRC(HM)
T: THS2.2M
L = low
M = medium
H = high


B
IPN/Macrophage Signaling
NPA
3R4F
MRC(LM)
MRC(HM)
THS2.2M(L)
THS2.2M(M)
THS2.2M(H)
males
females
90d
90+42d


D
mRNA
protein
male
female
90d
90+42d
set 2
Arg1
Chi3l1
Chia
Hmox1
Lgals3
Retnla
log2 fold-change

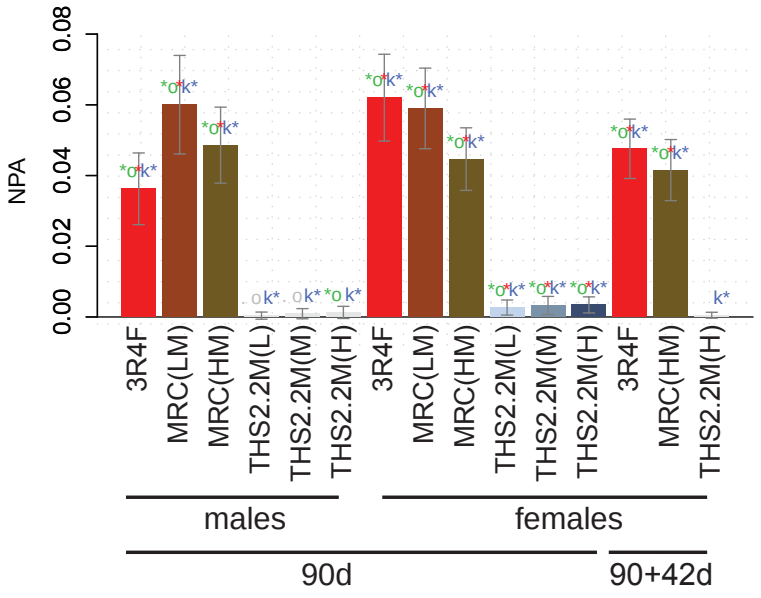

C
IPN/Neutrophil Signaling
NPA
3R4F
MRC(LM)
MRC(HM)
THS2.2M(L)
THS2.2M(M)
THS2.2M(H)
males
females
90d
90+42d

Figure 6

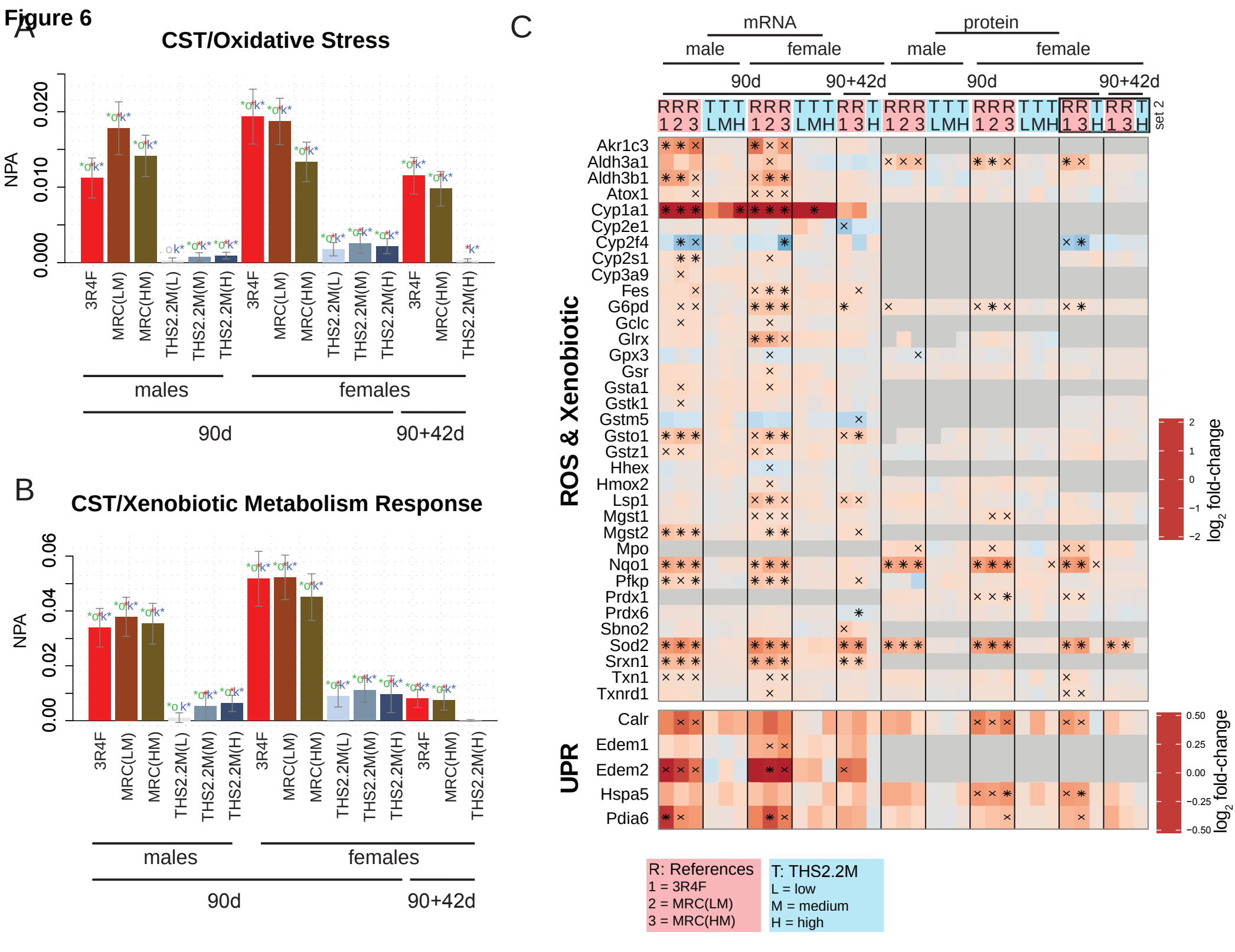
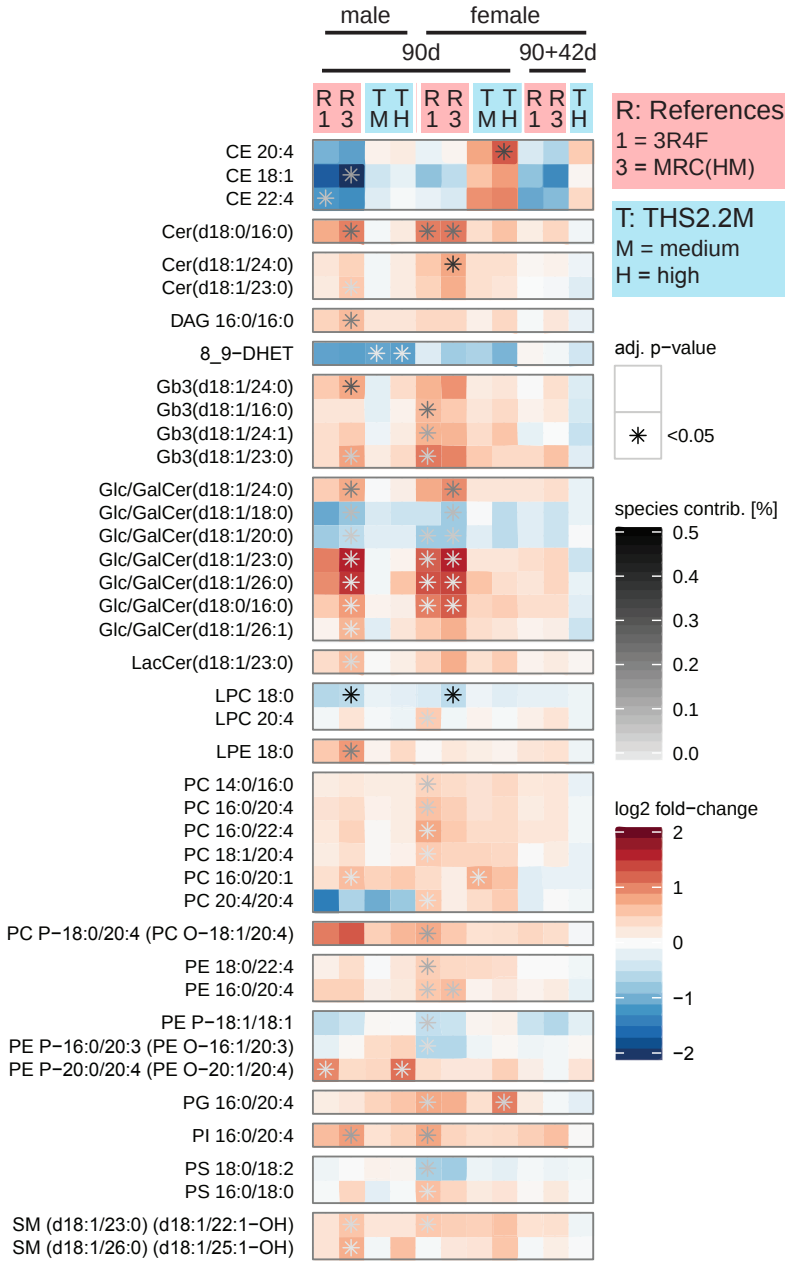
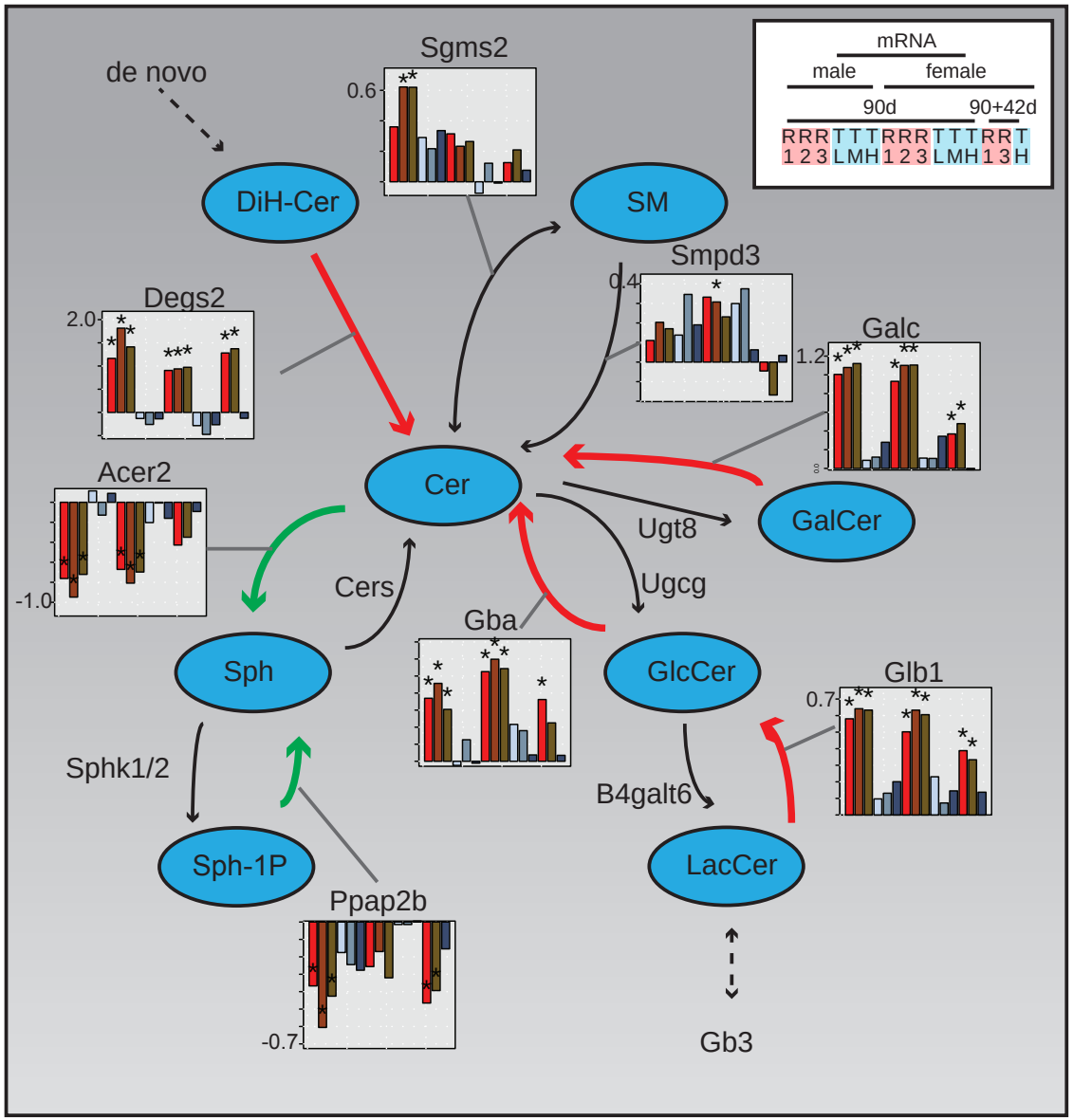

A
CST/Oxidative Stress
NPA
0.000
0.010
0.020
3R4F
MRC(LM)
MRC(HM)
THS2.2M(L)
THS2.2M(M)
THS2.2M(H)
males
females
90d
90+42d
B
CST/Xenobiotic Metabolism Response
NPA
0.00
0.02
0.04
0.06
C
mRNA
protein
male
female
90d
90+42d
set 2
ROS & Xenobiotic
UPR
Akr1c3
Aldh3a1
Aldh3b1
Atox1
Cyp1a1
Cyp2e1
Cyp2f4
Cyp2s1
Cyp3a9
Fes
G6pd
Gclc
Glrx
Gpx3
Gsr
Gsta1
Gstk1
Gstm5
Gsto1
Gstz1
Hhex
Hmox2
Lsp1
Mgst1
Mgst2
Mpo
Nqo1
Pfkp
Prdx1
Prdx6
Sbno2
Sod2
Srxn1
Txn1
Txnrd1
Calr
Edem1
Edem2
Hspa5
Pdia6
log2 fold-change
R: References
1 = 3R4F
2 = MRC(LM)
3 = MRC(HM)
T: THS2.2M
L = low
M = medium
H = high

Figure 7

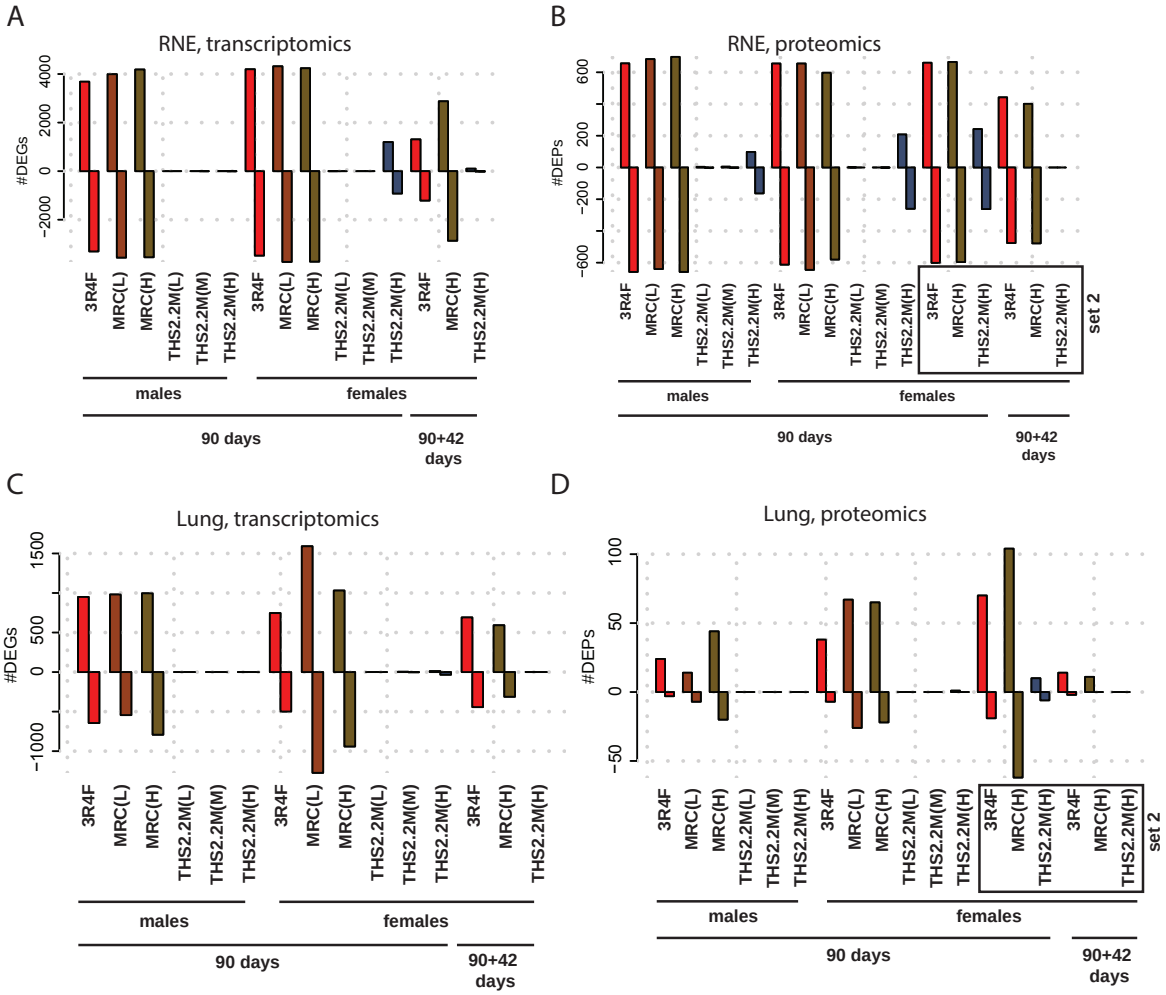
A


male
female
90d
90+42d
R R T T R R T T R R T
1 3 M H 1 3 M H 1 3 H
CE 20:4
CE 18:1
CE 22:4
Cer(d18:0/16:0)
Cer(d18:1/24:0)
Cer(d18:1/23:0)
DAG 16:0/16:0
8_9−DHET
Gb3(d18:1/24:0)
Gb3(d18:1/16:0)
Gb3(d18:1/24:1)
Gb3(d18:1/23:0)
Glc/GalCer(d18:1/24:0)
Glc/GalCer(d18:1/18:0)
Glc/GalCer(d18:1/20:0)
Glc/GalCer(d18:1/23:0)
Glc/GalCer(d18:1/26:0)
Glc/GalCer(d18:0/16:0)
Glc/GalCer(d18:1/26:1)
LacCer(d18:1/23:0)
LPC 18:0
LPC 20:4
LPE 18:0
PC 14:0/16:0
PC 16:0/20:4
PC 16:0/22:4
PC 18:1/20:4
PC 16:0/20:1
PC 20:4/20:4
PC P−18:0/20:4 (PC O−18:1/20:4)
PE 18:0/22:4
PE 16:0/20:4
PE P−18:1/18:1
PE P−16:0/20:3 (PE O−16:1/20:3)
PE P−20:0/20:4 (PE O−20:1/20:4)
PG 16:0/20:4
PI 16:0/20:4
PS 18:0/18:2
PS 16:0/18:0
SM (d18:1/23:0) (d18:1/22:1−OH)
SM (d18:1/26:0) (d18:1/25:1−OH)
R: References
1 = 3R4F
3 = MRC(HM)
T: THS2.2M
M = medium
H = high
adj. p−value
<0.05
species contrib. [%]
0.5
0.4
0.3
0.2
0.1
0.0
log2 fold−change
2
1
0
−1
−2

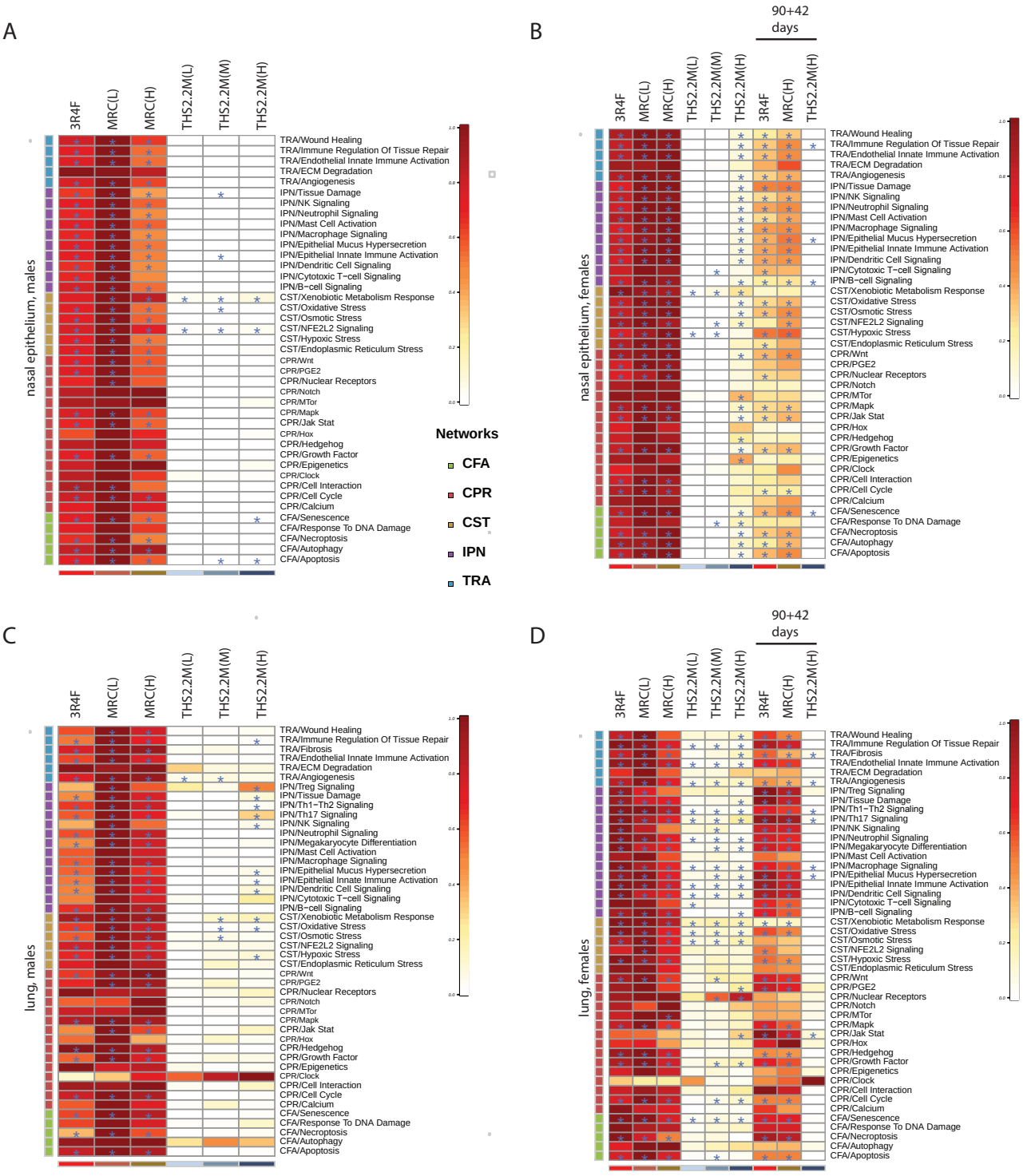
B


mRNA
male
female
90d
90+42d
R R R T T T R R R T T T R R T
1 2 3 L M H 1 2 3 L M H 1 3 H
de novo
DiH-Cer
Sgms2
0.6
SM
Smpd3
0.4
Degs2
2.0
Galc
1.2
Acer2
-1.0
Cer
GalCer
Ugt8
Ugcg
Cers
Gba
Sph
GlcCer
Glb1
0.7
Sphk1/2
B4galt6
Sph-1P
LacCer
Ppap2b
-0.7
Gb3

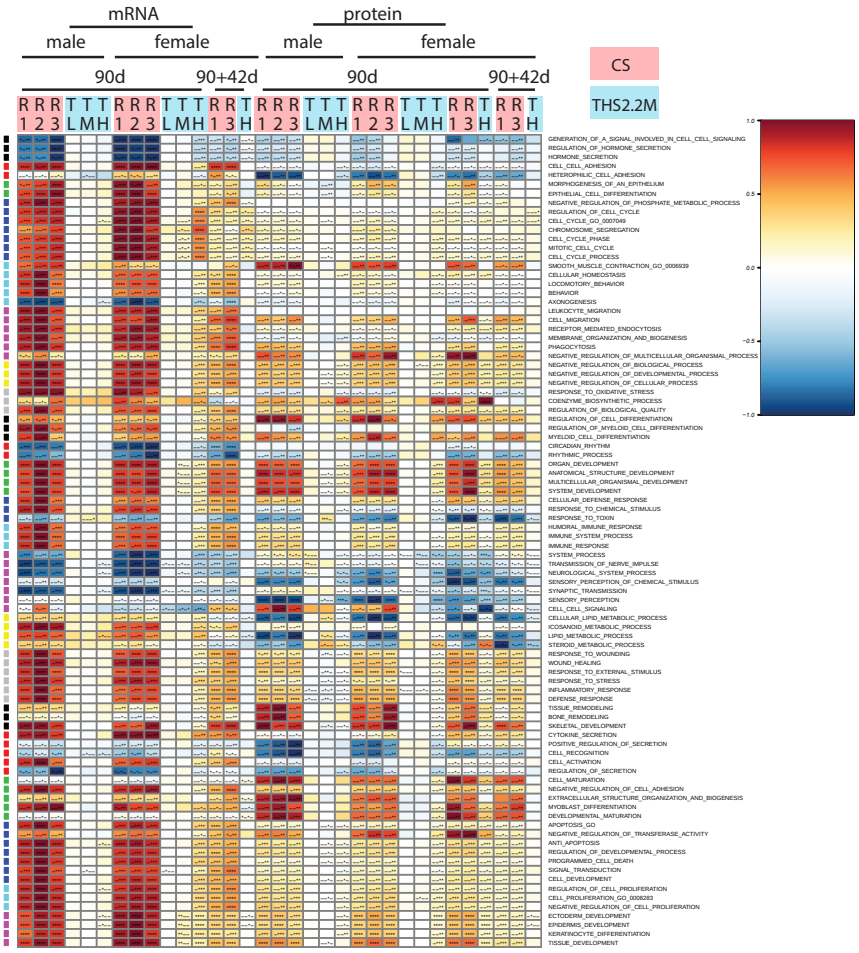
Supplementary Figure 1



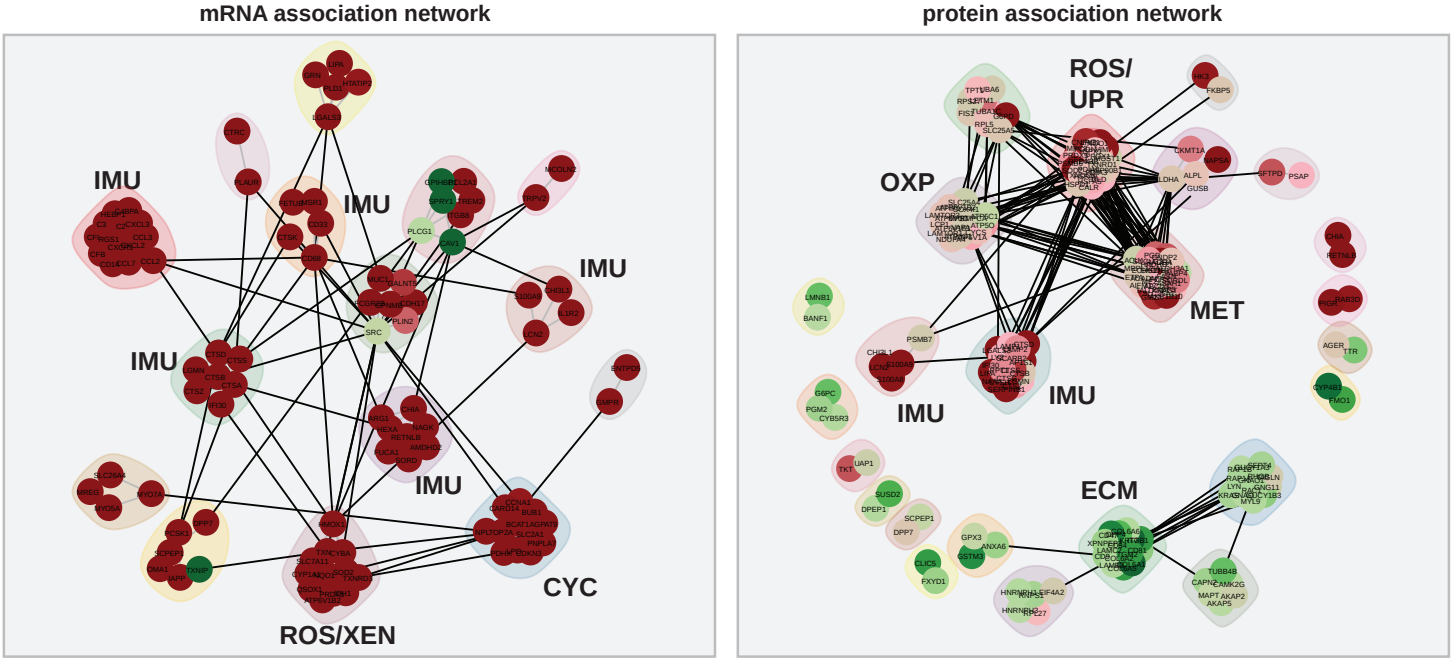
Supplementary Figure 2



Supplementary Figure 3

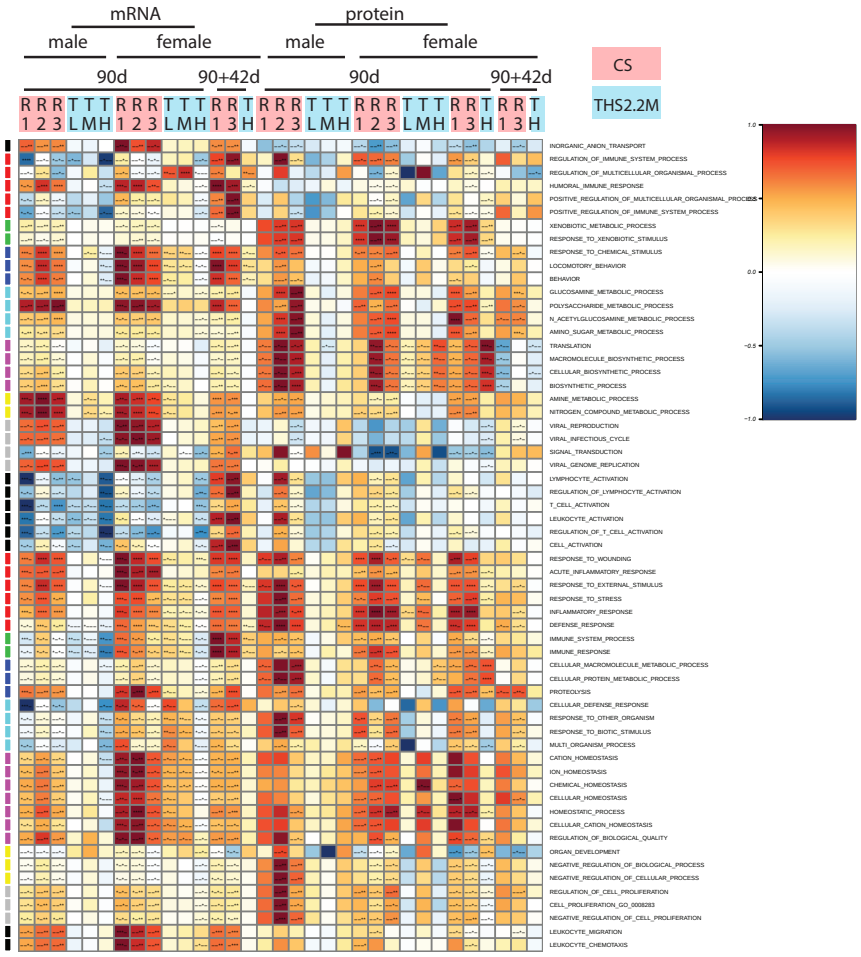


Supplementary Figure 4

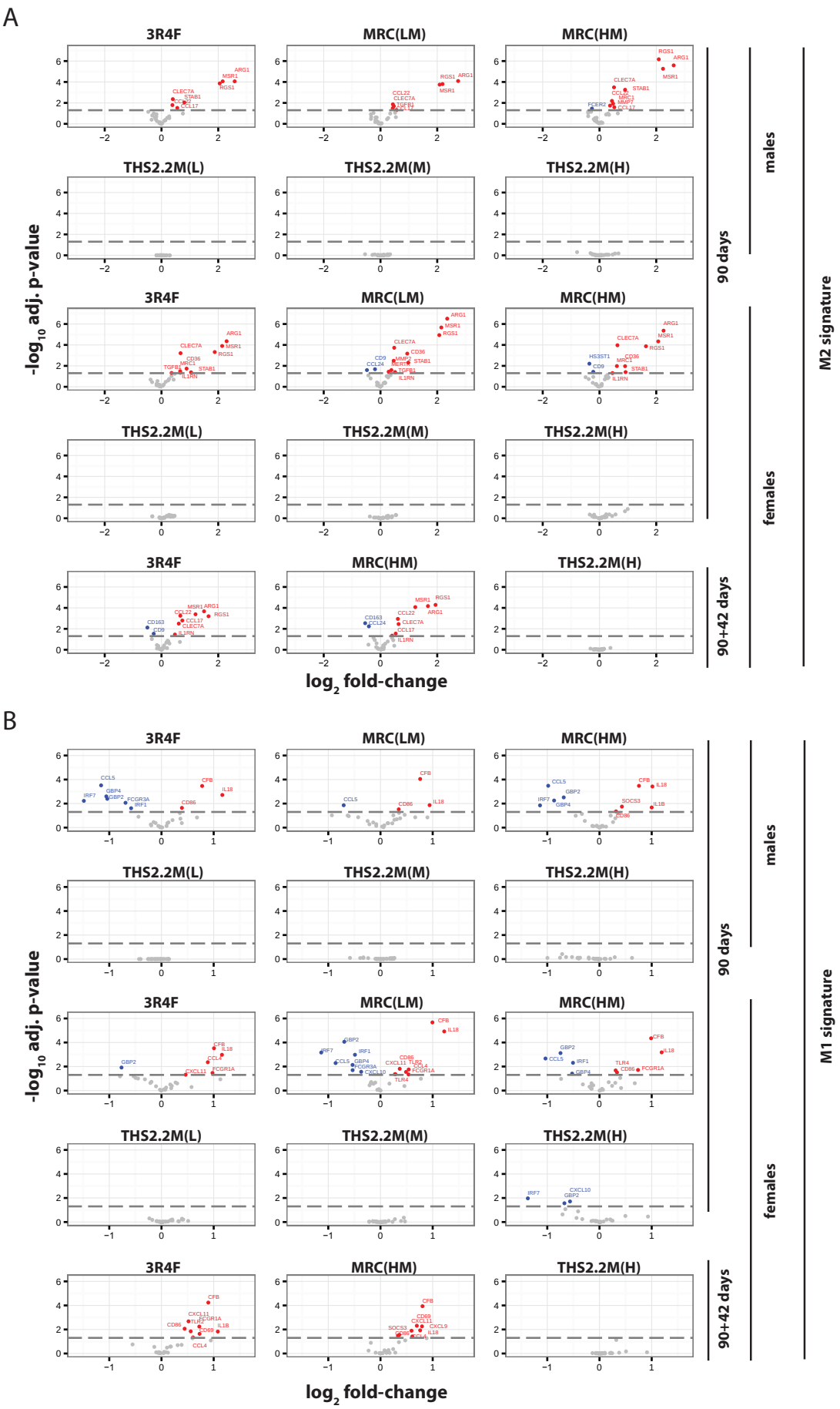


Functional categories	
IMU	immune-related
ROS	oxidative-stress response
XEN	xenobiotic response
UPR	unfolded-protein response
MET	metabolism
CYC	cell cycle
ECM	extracellular matrix
OXP	oxidative phosphorylation

Supplementary Figure 5

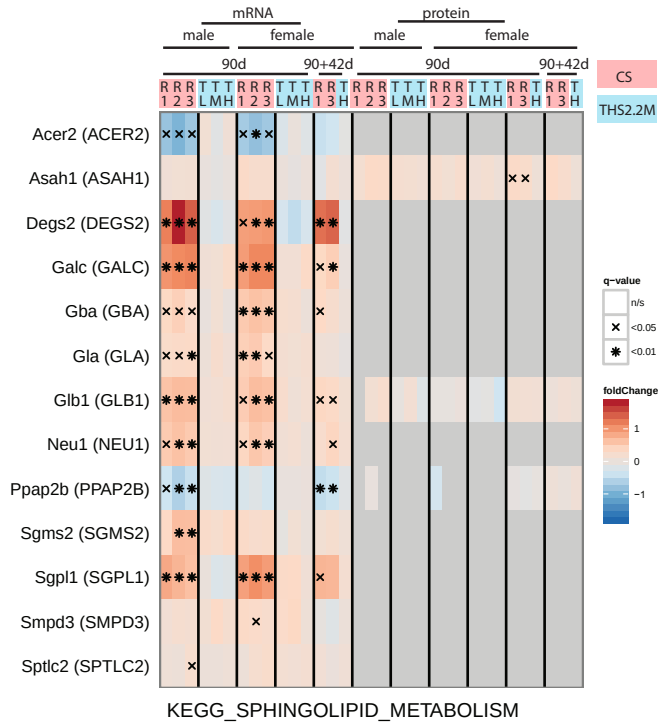


Supplementary Figure 6

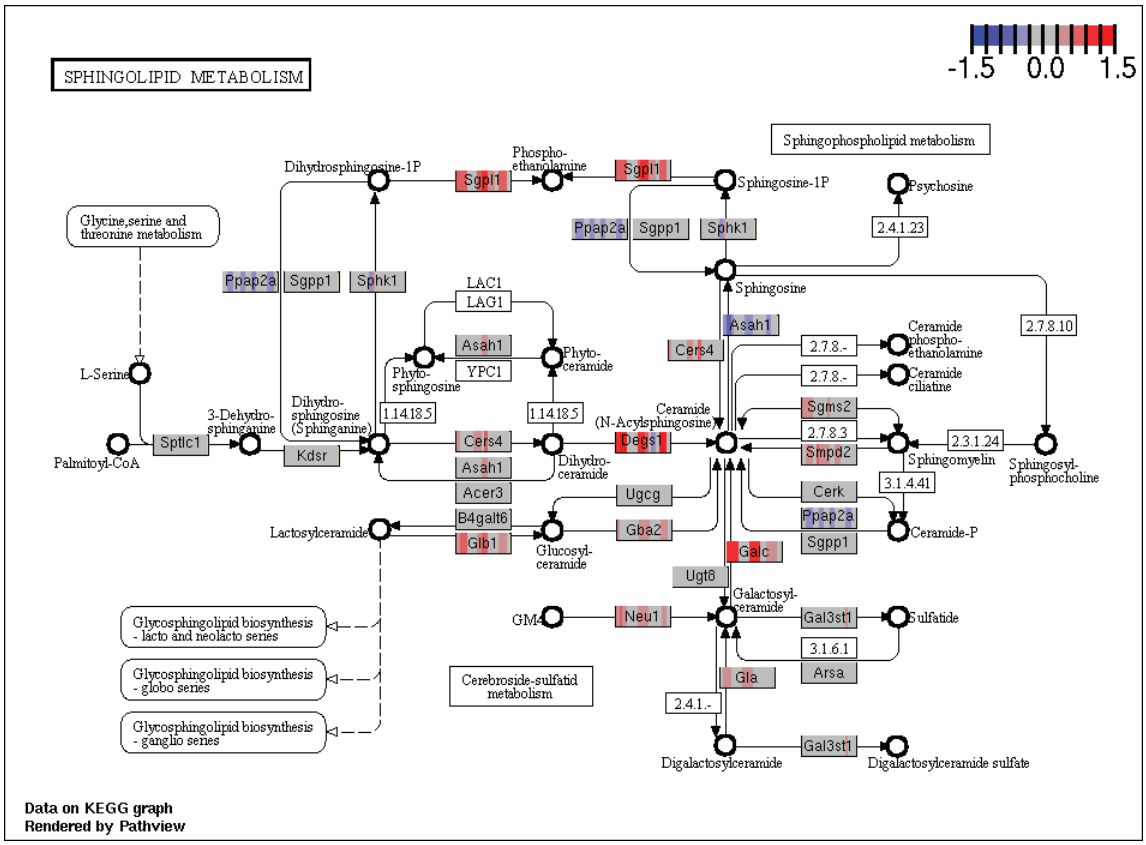


Supplementary Figure 7

A



B



Supplementary Table 1

Click here to download Supplemental Materials: UKogel_BTitz_part 7_SysTox_THS2.2M_SI_Table_1.xlsx

Supplementary Table 2

Click here to download Supplemental Materials: UKogel_BTitz_part 7_SysTox_THS2.2M_SI_Table_2.xlsx

*Clean version of Revised Manuscript
Click here to view linked References

Evaluation of the Tobacco Heating System 2.2. Part 7: Systems toxicological assessment of a mentholated version revealed reduced cellular and molecular exposure effects compared with mentholated and non-mentholated cigarette smoke

Ulrike Kogel[a,*], Bjoern Titz[a,*], Walter K. Schlage[b], Catherine Nury[a], Florian Martin[a], Alberto Oviedo[c], Stefan Lebrun[a], Ashraf Elamin[a], Emmanuel Guedj[a], Keyur Trivedi[a], Nikolai V. Ivanov[a], Patrick Vanscheeuwijck[a], Manuel C. Peitsch[a], Julia Hoeng[a]

[a] Philip Morris International Research and Development, Philip Morris Products S.A., Quai Jeanrenaud 5, 2000 Neuchatel, Switzerland (part of Philip Morris International group of companies)

[b] Biology consultant, Max-Baermann-Str. 21, 51429 Bergisch Gladbach, Germany

[c] Philip Morris International Research Laboratories, 50 Science Park Road, Singapore, Singapore (part of Philip Morris International group of companies)

[*] UK and BT contributed equally to this manuscript.

Corresponding author:

Julia Hoeng, PhD

E-mail: julia.hoeng@pmi.com

Tel: +41 (58) 242 2214

Fax: +41 (58) 242 2811

Abstract[1]

Modified risk tobacco products (MRTPs) are being developed with the aim of reducing smoking-related health risks. The Tobacco Heating System 2.2 (THS2.2) is a candidate MRTP that uses the *heat-not-burn* principle. Here, systems toxicology approaches were engaged to assess the respiratory effects of mentholated THS2.2 (THS2.2M) in a 90-day rat inhalation study (OECD test guideline 413). The standard endpoints were complemented by transcriptomics and quantitative proteomics analyses of respiratory nasal epithelium and lung tissue and by lipidomics analysis of lung tissue. The adaptive response of the respiratory nasal epithelium to conventional cigarette smoke (CS) included squamous cell metaplasia and an inflammatory response, with high correspondence between the molecular and histopathological results. In contrast to CS exposure, the adaptive tissue and molecular changes to THS2.2M aerosol exposure were much weaker and were limited mostly to the highest THS2.2M concentration in female rats. In the lung, CS exposure induced an inflammatory response, triggered cellular stress responses, and affected sphingolipid metabolism. These responses were not observed or were much lower after THS2.2M aerosol exposure. Overall, this system toxicology analysis complements and reconfirms the results from classical toxicological endpoints and further suggests potentially reduced health risks of THS2.2M.

Keywords: modified risk tobacco product; systems toxicology; transcriptomics; proteomics; lipidomics; subchronic inhalation toxicity

[1] *Abbreviations:* THS2.2, Tobacco Heating System 2.2; THS2.2M, mentholated THS2.2; HPHC, harmful and potentially harmful constituent; CS, cigarette smoke; MRTP, modified risk tobacco product; FDR, false-discovery rate; iTRAQ, isobaric tag for relative and absolute quantitation; MRC, mentholated reference cigarette; LM, low menthol; HM, high menthol.

Introduction

The U.S. Family Smoking Prevention and Tobacco Control Act (FSPTCA) defines a Modified Risk Tobacco Product (MRTP) as "any tobacco product that is sold or distributed for use to reduce harm or the risk of tobacco related disease associated with commercially marketed tobacco products" (Family Smoking Prevention and Tobacco Control Act). This publication is part of a series of nine publications describing the nonclinical and part of the clinical assessment of a candidate MRTP, THS2.2 regular and a mentholated version (THS2.2M). THS2.2 and THS2.2M are based on the concept that heating tobacco, rather than burning it, reduces or eliminates the formation of harmful and potentially harmful constituents in the inhaled aerosol. The series of publications provides part of the overall scientific program to assess the potential for THS2.2 to be a reduced risk product. The first publication in this series describes THS2.2 and the assessment program for MRTPs ((Smith et al., submitted (this issue))). This is followed by six publications, including this one, that describe the nonclinical assessment of THS2.2 regular and THS2.2M (Kogel et al., submitted (this issue));(Oviedo et al., submitted (this issue));(Schaller et al., submitted (this issue)-a; Schaller et al., submitted (this issue)-b);(Sewer et al., submitted (this issue); Wong et al., submitted (this issue)). The eighth publication in the series describes a clinical study to assess whether the reduced formation of Harmful and Potentially Harmful Constituents (HPHC) for THS2.2 regular also leads to reduced exposure to HPHCs when the product is used in a clinical setting (Haziza et al., submitted (this issue)). A final publication utilizes data gathered from the reduced exposure clinical study on THS2.2 regular to determine if a systems pharmacology approach can identify exposure response markers in peripheral blood of smokers switching to THS2.2 (Martin et al., submitted (this issue)).

In this part, the systems toxicology arm of a 90-day rat inhalation study for the assessment of THS2.2M compared with cigarette smoke (CS) from reference cigarettes is presented. The overall study was conducted according to OECD test guideline 413: the exposure characteristics, classical endpoints, and

global molecular response profiles are summarized in our accompanying manuscript (part 6 (Oviedo et al., submitted (this issue)).

A challenge with standard toxicological endpoints is that they are often detectable only after substantial damage has already occurred and therefore can lack sensitivity (Ellinger-Ziegelbauer et al., 2011). In addition, the limited mechanistic insights gained can hamper the refinement and eventual replacement of these traditional animal tests (OECD, 2013). Thus, (i) to increase sensitivity, (ii) to obtain additional insights into the molecular mechanisms of toxicity, and (iii) to gain knowledge that could eventually be applied to reduce the number of animal studies, we complement the standard endpoints in these studies with systems toxicology approaches – using transcriptomics, proteomics, and lipidomics measurements (Sauer et al., 2015; Sturla et al., 2014).

Briefly, in this study, groups of male and female rats were exposed for 90 days to three different concentrations of THS2.2M aerosol: 15 µg nicotine/L (low, THS2.2M(L)), 23 µg nicotine/L (medium, THS2.2M(M)), and 50 µg nicotine/L (high, THS2.2M(H)) (Figure 1). THS2.2M aerosol exposure was compared with CS from three different reference cigarettes: the 3R4F standard reference cigarette, and corresponding low (LM) and high (HM) mentholated reference cigarettes (MRCs). Importantly, the nicotine concentration in the CS of these reference cigarettes (23 µg/L) was matched to the nicotine concentration in the aerosol of the medium THS2.2M (THS2.2M(M)). In addition, for female subsets from the exposure groups Sham, 3R4F, MRC(HM), and THS2.2M(H), the recovery of the exposure-related effects after a subsequent fresh-air exposure for 42 days was assessed (Figure 1). For the systems toxicology analyses, respiratory nasal epithelium and lung tissue were collected and the molecular exposure responses of the transcriptome and proteome were measured. In addition, exposure effects on lung lipids were measured using lipidomics. These data were analyzed bioinformatically (Martin et al., 2014; Titz et al., 2014; Titz et al., 2015a) and evaluated in the context of the overall study, for example, in relationship to the histopathology results.

Altogether, our systems toxicology approach demonstrates the added benefit of these mechanistic details (e.g., on the decreased involvement of specific cell types and molecular response programs) and further supports the reduction in biological effects caused by THS2.2M aerosol exposure compared with CS from the reference cigarettes.

Materials and Methods

Experimental design

The study was conducted to characterize potential adverse effects caused by subchronic exposure to an aerosol from the mentholated tobacco heating system THS2.2M, a *heat-not-burn* tobacco product, and to compare them with the effects induced by CS generated from three reference cigarettes (Figure 1) (part 6, (Oviedo et al., submitted (this issue))). In addition to the recommendations in OECD TG413 for study designs, additional rats were included for the purpose of obtaining 'omics' endpoints. These rats were subjected to the same exposure conditions and handling times as the rats in the OECD study. As required, three dose levels of the THS2.2M aerosols were tested. Respiratory nasal epithelium and lung tissue were collected from the exposed rats and after a recovery period of 42 days, and used for the generation of transcriptomic, proteomics, and lipidomics data.

Reference cigarettes and THS2.2M

Standard reference 3R4F cigarettes were purchased from the University of Kentucky (Lexington, KY, USA, http://www.ca.uky.edu/refcig). In addition, two MRCs were produced by Philip Morris International, Neuchatel. The MRCs were designed so that the nicotine, total particulate matter, and CO levels in the smoke matched the levels of the 3R4F reference cigarette. The menthol yield in the smoke from the MRCs was 2.04 mg/cig (MRC(LM)) and 2.58 mg/cig (MRC(HM)) when smoked according to the ISO 3308 standard (International Organization for Standardization: 3308, 1991). For more details see (part 6, (Oviedo et al., submitted (this issue))). The reference cigarette 3R4F was used as the internal reference in this study.

THS2.2 has three distinct components: (i) a *tobacco stick* with unique processed tobacco made from tobacco powder, (ii) a holder into which the *tobacco stick* is inserted and which heats the tobacco material by means of an electronically controlled heating blade, and (iii) a charger that is used to

recharge the holder after each use. The holder heats the *tobacco stick* at a temperature not exceeding 350°C (for more details please refer to (Smith et al., submitted (this issue)). The mentholated version of THS2.2 (THS2.2M), assessed here (blend type *FR1/Menthol*), produces a menthol yield in the aerosol condensate of 2.09 mg/cig when smoked according to ISO 3308 standard (International Organization for Standardization: 3308, 1991). The THS2.2M were provided by Philip Morris Products S.A., Neuchâtel, Switzerland. For more details see (part 6, (Oviedo et al., submitted (this issue)); and for more information on the chemical analysis of smoke constituents see (Schaller et al., submitted (this issue)-a).

Animals

All procedures involving animals were performed in an AAALAC (Association for Assessment and Accreditation of Laboratory Animal Care International) accredited, AVA-licensed (Agri-Food & Veterinary Authority of Singapore) facility with approval from an Institutional Animal Care and Use Committee, in compliance with the National Advisory Committee for Laboratory Animal Research Guidelines on the Care and Use of Animals for Scientific Purposes.

Outbred male and female Sprague-Dawley rats [Crl:CD(SD)], bred under specific pathogen-free conditions, were obtained from Charles River, USA. The rats were approximately 6–7 weeks old on arrival and their health status was attested by the health check certificate provided by the breeder. The rats were kept and exposed in an animal laboratory with restricted access under controlled conditions of good hygiene. The laboratory air was filtered and positive pressure was maintained inside the laboratory. The room temperature was maintained at 22 ± 3°C and the relative humidity at 54 ± 4 %. The light/dark cycle was 12 h/12 h. All rats were individually identified by subcutaneously implanted transponders. The rats were acclimatized for a minimum of 16 days prior to exposure. For more details see (part 6, (Oviedo et al., submitted (this issue)).

Smoke and aerosol generation and animal exposure

The rats were nose-only exposed for a period of 13 weeks (6 h/d, 5 d/week) to filtered air (Sham), reference CS (23 µg/L nicotine) generated from the three reference cigarettes, or to three concentrations of THS2.2M aerosol (15, 23, 50 µg/L nicotine). For more details including on the smoke and aerosol generation, monitoring of the aerosol composition, exposure conditions, and markers of exposure see the part 6 of this series (Oviedo et al., submitted (this issue)).

For the molecular end points analyzed here, six male and six female rats were allocated to each of the following groups: the filtered, conditioned air group (Sham), and six smoke exposure groups, RC (3R4F) 23 µg nicotine/L; MRC(LM) 23 µg nicotine/L; MRC(HM) 23 µg nicotine/L; THS2.2M(L) 15 µg nicotine/L; THS2.2M(M) 23 µg nicotine/L; and THS2.2M(H) 50 µg nicotine/L. In addition, six female rats for each of the Sham, 3R4F, MRC(HM), and THS2.2M(H) groups were kept for a 42 days recovery period. For more details see (part 6, (Oviedo et al., submitted (this issue))).

Tissue preparation for 'omics' endpoints

Dissection was performed 16–20 hours after the last exposure. Prior to organ removal, a whole body perfusion with cold saline was performed. For the transcriptomics analysis, respiratory nasal epithelium (RNE) was isolated from the left side of the nose. For the proteomics analysis, RNE was isolated from the right side of the nose. The left lung lobe was cryosectioned into 40 µm slices, and the slices were collected alternating for transcriptomics and proteomics analysis.

Transcriptomics analysis

RNA from the RNE and lung samples was isolated using a miRNeasy extraction kit (Qiagen, Hilden, Germany) with the modification that RLT buffer (Qiagen) with beta-mercaptoethanol was used to lyse the lung slices. RNA was processed for hybridization on GeneChip® Rat Genome 230 2.0 Arrays (Affymetrix, Santa Clara, USA) using a High-Throughput 3' In Vitro Transcription PLUS kit (Affymetrix). Four RNE samples were eliminated because of low RNA concentration or poor RNA quality. Five lungs

samples were not processed in the Affymetrix pipeline because the RNA concentration or quality was insufficient.

Raw data files were processed in the custom Chip Description File environment Rat2302_Rn_ENTREZG v19.0.0 (rat2302rnentrezgcdf) (Dai et al., 2005) and normalized using frozen robust microarray analysis (fRMA) (McCall et al., 2010). The normalization vector needed for fRMA was created using a set of 1023 microarray rat samples from 11 tissues and the R package frmaTools version 1.18.0. Quality controls, including log-intensities, normalized-unscaled standard error (NUSE), relative log expression (RLE), median absolute value RLE (MARLE), and pseudo-images as well as raw image plots, were performed with the affyPLM package (Bioconductor, USA) (Bolstad et al., 2003). Following the quality control procedures, raw p-values were generated for contrasts between Sham and exposed groups with the limma package (Smyth, 2004), and adjusted using the Benjamini–Hochberg false discovery rate (FDR) multiple test correction (Gentleman et al., 2004).

Proteomics analysis

Proteome alterations were assessed by isobaric-tag based quantification using the iTRAQ® approach (Titz et al., 2015a). For this, rat right RNE samples were homogenized and sonicated in tissue lysis buffer (BioRad, Hercules, CA, USA) in random order and the proteins were precipitated with acetone. Frozen rat lung tissue slices were homogenized using a bead-assisted procedure in Tissue Lyser II (Qiagen, Valencia, CA, USA) in tissue lysis buffer before acetone precipitation. Protein precipitates were resuspended in 0.5 M triethylammonium bicarbonate (TEAB, Sigma-Aldrich, St. Louis, MO, USA), 1 M urea (Sigma-Aldrich) and 0.1% SDS (Sigma-Aldrich). Then, 50 µg of the suspension was processed using the iTRAQ 8-plex labeling procedure according to the manufacturer's instructions (AB Sciex, Framingham, MA, USA). Trypsin (Promega, Madison, WI, USA) was added to the samples in a 1:10 trypsin to protein ratio (w/w) followed by overnight digestion at 37°C. The tryptic digested samples were

185 labeled with the reporter-ion tags for the different exposure groups for two separate iTRAQ analysis
186 sets.

187 Two multiplexed iTRAQ analysis sets were prepared to allow for all relevant comparisons. iTRAQ set 1
188 contained all the 90-day time point samples. Each 8-plex labeling replicate set included one sample of
189 each 90-day exposed sample (Sham, RC(3R4F), MRC(LM), MRC(HM), THS2.2M(L), THS2.2M(M), and
190 THS2.2M(H)) and one pooled reference mix containing all replicates from the 90-day time point. For
191 each of the 12 replicates in iTRAQ set 1, either a male or female sample was picked randomly. Within
192 each replicate labeling set, the sample to channel mapping was randomized. iTRAQ set 2 was used to
193 focus on the exposure and 90+42d recovery effect for female rats only. Each 8-plex labeling set included
194 one of each 90+42-day sample (Sham, RC(3R4F), MRC(HM), and THS2.2M(H)) and a female sample of
195 each corresponding 90-day time point. Again, the biological replicates were randomly assigned to the
196 (six) replicate labeling sets and for each set the sample to channel mapping was randomized. Missing
197 samples were replaced randomly by another replicate from the same group. These duplicate,
198 placeholder samples were removed after data analysis and processing.

199 All the labeled samples that belonged to one iTRAQ replicate set were pooled and dried in a SpeedVac
200 (RVC 2-25 CD Plus, Martin Christ, Osterode am Harz, Germany). Samples were desalted by passing them
201 first through 0.5 mL bed volume detergent removal columns (Pierce, Rockford, IL, USA) and then
202 through 1 cc C18 reversed phase SepPak columns (Waters, Milford, MA, USA) according to the
203 manufacturers' manuals. Samples were dried in a SpeedVac and resuspended in nanoLC buffer A (5%
204 acetonitrile (Sigma-Aldrich), 0.2% formic acid (Sigma-Aldrich)).

205 Samples were analyzed in random order using an Easy nanoLC 1000 instrument (Thermo Scientific,
206 Waltham, MA, USA) connected online to a Q-Exactive (Thermo Scientific) mass-analyzer. Peptides were
207 separated on a 50 cm long C18 RP RSLC Easyspray column (2 µm particle size; Thermo Scientific) at a

flow rate of 200 nL/min with a 200 min gradient from nanoLC buffer A to 40% acetonitrile with 0.2% formic acid. Each sample was injected twice with two different analysis methods: a fast and a sensitive method, as described by Kelstrup et al. (Kelstrup et al., 2012), on the same column. The outputs of both mass-spectrometry runs were combined as merged mass-lists and searched against the rat reference proteome set (UniProt, version October 2013, canonical isoforms only) using Proteome Discoverer version 1.4.0.288 software (Thermo Scientific). SequestHT (implemented in Proteome Discoverer) was used as the search tool and iTRAQ-reporter ion intensities were determined from Proteome Discoverer. The Percolator node of Proteome Discoverer was used to estimate peptide-level adjusted p-values (q-values). iTRAQ peptide-level quantification data were exported and further processed in the R statistical environment (R Development Core Team, 2007). The quantification data were filtered for a q-value < 0.01 and for "unique" quantification results as defined in Proteome Discoverer. A global variance stabilizing normalization (VSN) was performed with the corresponding Bioconductor package in R (Huber et al., 2002; Hultin-Rosenberg et al., 2013). Each iTRAQ reporter ion set was normalized to its median and protein expression values were calculated as the median of these normalized peptide-level quantification values (Herbrich et al., 2013). To detect differentially abundant proteins, a linear model was fitted for each exposure condition and the corresponding Sham group, and p-values were calculated from moderated t-statistics with the empirical Bayes approach (Gentleman et al., 2004). The Benjamini-Hochberg False Discovery Rate (FDR) method was then used to correct for multiple testing effects. Proteins with an adjusted p-value < 0.05 were considered as differentially abundant.

Lipidomics analysis

Lipid molecules were extracted from lung tissue and quantified by Zora Biosciences (Espoo, Finland) according to internal Standard Operating Procedures, Lab Method Sheets, and data Processing Method Sheets (Ansari et al., 2016). Lipid levels were normalized to their respective internal standards and tissue weight. Concentrations of molecular lipids are presented as pmol/µg wet tissue.

232 Statistical analysis of the lipidomics data was similar to the analyses of the transcriptomics and
233 proteomics data. Samples with a total summed lipid concentration below the first quartile (1.5 x the
234 interquartile range) were excluded. For the detection of differentially abundant lipids, only lipid species
235 that were present/quantified in at least 50% of the samples of each compared group were included. A
236 linear model was fitted for each exposure condition and the corresponding Sham group, and p-values
237 from a moderated t-statistic were calculated with the empirical Bayes approach (Gentleman et al.,
238 2004). The Benjamini–Hochberg FDR method was used to correct for multiple testing effects. Lipids with
239 an adjusted p-value < 0.05 were considered differentially abundant.

240 ***Systems biology network analysis***

241 To quantitatively assess the perturbation of relevant biological response systems, we employed
242 previously defined cellular network models (Boué et al., 2015; Schlage et al., 2011) in conjunction with a
243 network scoring algorithm that predicts the activation of these cellular networks based on
244 transcriptomics data (Martin et al., 2014; Martin et al., 2012). Briefly, this approach relies on two-layer
245 causal network models, in which the lower layer represents the transcriptional changes and the upper
246 layer represents the actual causal network model. Both layers are linked and transcriptional changes in
247 the lower layer are used to deduce the activity of the components in the upper layer, which are then
248 aggregated into the final network score. The method uses gene expression data without a fold change or
249 p-value cut off. The biological mechanisms covered by the networks reflect relevant processes of the
250 respiratory system including inflammation, cellular fate, tissue repair and angiogenesis, cellular stress,
251 and cellular proliferation. Each network was built in a modular way, where each module (sub-network)
252 describes a specific biological aspect of the entire network. The modules can be decomposed to provide
253 another level of detail (Kogel et al., 2014).

254 ***Additional data analysis methods***

Gene sets were obtained from the Molecular Signatures Database (mSigDB) (Liberzon et al., 2011). Set analysis was supported by the Piano package in the R statistical environment (Väremo et al., 2013). Set enrichment was assessed by gene-set analysis with the (absolute) log2 fold-change as the gene/protein statistic and the mean as the set statistic. Gene/protein permutation and sample permutation were used to assess statistical significance. P-value adjustment was done with the Benjamini-Hochberg procedure. Sparse partial least squares approach was conducted in the canonical mode with the mixOmics package in R (Lê Cao et al., 2009). Functional associations among proteins were obtained from the STRING database (Szklarczyk et al., 2015). Functional clusters were annotated manually guided by ToppGene (Chen et al., 2009). Immune-cell markers were taken from the literature (Supplementary Table 1).

Data availability

The mass spectrometry proteomics data are available from the ProteomeXchange Consortium via the PRIDE partner repository (http://www.ebi.ac.uk/pride/archive/)(Vizcaíno et al., 2014). The database identifiers for the lung and respiratory nasal epithelium datasets are PXD003580 and PXD003591. The lipidomics data are available in Supplementary Table 2. The transcriptomics data have been submitted to ArrayExpress with the identifier E-MTAB-4493.

Results

Histological and molecular exposure response of the respiratory nasal epithelium

Consistent with the common exposure response to CS exposure (Gaworski et al., 1997; Kogel et al., 2014; Vanscheeuwijck et al., 2002), the reference cigarette exposures in this study resulted in several typical histopathological changes in the rat respiratory nasal epithelium (RNE) (see part 6, (Oviedo et al., submitted (this issue))). These changes included squamous cell metaplasia, basal cell hyperplasia, and mixed cell infiltrates in the submucosa. The latter indicated an inflammatory response in the tissue exposed to CS. In contrast, the RNE of rats exposed to THS2.2M aerosol showed fewer and less severe histopathological changes; only the highest THS2.2M aerosol concentration was associated with squamous cell metaplasia and a mixed cell infiltrate in the submucosa. Of note, after the 42-day recovery period several changes induced by CS-exposure including squamous cell metaplasia and the mixed cell infiltrate reverted only partially, whereas in the THS2.2M exposed groups the histopathological changes in the RNE reverted nearly completely.

To analyze the molecular changes that occurred in the RNE, we identified the significantly (FDR-adjusted p-value < 0.05) differentially expressed/abundant genes and proteins after exposure to CS from the reference cigarettes and THS2.2M aerosol compared with Sham exposure (Supplementary Figure 1A and B). Reference smoke exposure after 90 days induced extensive changes in both the transcriptome and the proteome. For example, more than 8000 genes and 1300 proteins were statistically significantly affected by the 90-day exposure to MRC(LM) in female rats. In contrast, the THS2.2M(L) and THS2.2M(M) aerosols induced a very low to absent differential response in the RNE. While THS2.2M(H) induced molecular changes, these remained well below the changes induced by the reference cigarettes (at twice the concentration with respect to the applied nicotine).

To reveal which biological processes were most prominently perturbed by the exposure conditions, a threshold-free, network-based systems biology approach was applied. This approach relies on our published collections of hierarchically structured biological network models (Boué et al., 2015; Gebel et al., 2013; Schlage et al., 2011; Westra et al., 2011; Westra et al., 2013). These manually curated models reflect relevant respiratory system processes that contribute to inflammation, cellular fate, tissue repair and angiogenesis, cellular stress, and cellular proliferation. For each of these network models, the degree of network perturbation caused by exposures to different aerosols is computed based on the measured changes in the transcriptome of the target tissue, and the overall biological impact for all networks is summarized based on the contributions of the different biological process categories (Martin et al., 2014). After 90 days of exposure to smoke from the three reference cigarettes, the transcriptomes of both male and female rats displayed network perturbations with similar levels of contributions from all five biological networks (Figure 2B). RNE exposed to aerosol from THS2.2M showed a much lower overall network perturbation; and a clear response was detected only for female rats exposed to THS2.2M(H). Exposure effects for 3R4F and MRC(HM) reverted partially after the 42-day recovery period. The perturbations detected for the subnetworks of these five biological processes are represented in Supplementary Figure 2 A and B.

To complement this analysis, we also identified significantly affected gene and protein sets (FDR-adjusted p-value < 0.05, Figure 2B, Supplementary Figure 3). Overall, the effects observed for gene sets were much less pronounced in RNE exposed to THS2.2M aerosol compared with CS exposure. Clustering of the enrichment results revealed several biological processes affected by CS exposure that could be linked to the observed adaptive changes of the RNE, such as epithelial cell differentiation, extracellular structure organization and tissue remodeling, and cell proliferation and migration processes (Figure 2B). Moreover, immune-response processes were found to be enriched.

Effects of exposure on molecular marker panels for respiratory nasal epithelium

To more specifically evaluate how the changes in tissue architecture are reflected at the molecular level, known markers for different epithelial cell types (e.g., basal cells, goblet cells, and squamous cells) and basal lamina components were assessed (Figure 3A, Supplementary Table 1A). This panel included several keratins, which have been identified as differentiation markers for rat nasal epithelium (Schlage et al., 1998a; Schlage et al., 1998b). For example, Krt14 and Krt15, which have been associated with a hyper- and metaplastic respiratory epithelium (Schlage et al., 1998b), were clearly up-regulated and increased in protein level abundance in the CS exposed groups. The small proline-rich proteins (Sprr1a and Sprr3) also were up-regulated on the gene expression level and increased partly in protein abundance. Sprr1a and Sprr3 are components of the cross-linked envelope of epithelial cells and a human ortholog has been identified as a biomarker for squamous metaplasia (Tesfaigzi and Carlson, 1999). Furthermore, basal lamina components were clearly up-regulated and increased in abundance, which likely reflects the active tissue remodeling processes in the CS-exposed RNE. The up-regulation and increased abundance of proliferating cell nuclear antigen (Pcna) supported an overall more proliferative state of the CS- exposed RNE. Overall, rats exposed to CS from the reference cigarettes showed a clear increase in these and other basal cell and squamous cell markers, which is in line with the histopathological observation of basal cell hyperplasia and squamous metaplasia without and with cornification. Further, the molecular analysis indicated an increase in goblet cell numbers and a goblet cell response (e.g., increase in the mucins Muc5ac and Muc5b). THS2.2M aerosols induced these markers of an adaptive tissue response to a much lower degree, and significant effects were observed only for the highest THS2.2M (THS2.2M(H)) concentration, in female rats.

In addition, a marker panel for immune cell types (Figure 3B, Supplementary Table 1B) was evaluated to investigate if the mixed cell infiltrate that was found in the histological evaluation could also be detected at the molecular level. Markers for both macrophages (e.g., Cd14, Cd68, and Lgals3) and neutrophils (e.g., Mpo, Lcn2, and Camp) were clearly up-regulated and increased in abundance upon CS exposure.

Markers for T-cells (e.g., the Cd3 T-cell receptor components) and B-cells also were up-regulated, but this was less pronounced and was detected only at the RNA level. In contrast, THS2.2M exposure only marginally affected these immune-cell markers; indeed, macrophage and neutrophil markers were up-regulated and increased in abundance only for THS2.2M(H) in female rats. While this response to THS2.2M(H) exposure was not detectable after the 42 day recovery period, a macrophage and neutrophil response was still detectable for 3R4F and MRC(HM) after the recovery period.

In summary, the systems toxicology analysis reconfirmed and complemented the histopathology results by providing insights into the effects on specific cell types and the cellular adaptation programs that were impacted by CS and to a lesser degree by THS2.2M aerosol exposure in the RNE.

Histological and molecular exposure response of the lung tissue

As described in the accompanying manuscript in this series (Oviedo et al., submitted (this issue)), histopathological evaluation of the lung revealed an increase of pigmented and unpigmented macrophages in the alveolar lumen, and goblet cell hyperplasia in the bronchi. Those are typical smoke-related as well as dose-dependent adaptive and inflammatory responses of the lung after exposure to CS in inhalation studies (Coggins et al., 1989; Piade et al., 2014; Vanscheeuwijck et al., 2002). In contrast, the histopathology evaluation of the lungs exposed to THS2.2M aerosol showed a lower response compared with the lungs from rats exposed to CS (part 6,(Oviedo et al., submitted (this issue))). Furthermore, whereas CS exposure resulted in an increase in the free cell counts in bronchoalveolar lavage fluid (BALF) including neutrophils and macrophages, and several inflammatory mediators such as Mcp1/3 and Csf1, THS2.2M aerosol exposure resulted in very limited changes in these immune-related endpoints (part 6, (Oviedo et al., submitted (this issue)).

To complement these comparisons and to gain further insights into the differential molecular responses, microarray-based mRNA expression profiling and quantitative proteomics was conducted for the lung

364 tissue. CS resulted in a maximum of 2865 differentially expressed genes for female rats exposed to
365 MRC(LM) (adjusted p-value < 0.05, Supplementary Figure 1C), while very few genes were differentially
366 expressed after THS2.2M exposure compared with the Sham group (a maximum of 45 genes were
367 differentially expressed in lung tissue from female rats exposed to THS2.2M(H)). After the 42-day
368 recovery phase, differentially expressed genes in response to CS were still detectable but their numbers
369 were reduced (Supplementary Figure 1C). On the whole, the differential protein abundance in response
370 to the exposures confirmed the trends observed for the transcriptomics data (Supplementary Figure
371 1D), but at the same significance threshold (adjusted p-value < 0.05) the number of differentially
372 abundant proteins was lower (a maximum of 166 proteins for females exposed to MRC(HM)) than the
373 number of differentially expressed genes.

374 Again, the threshold-free, network-based systems biology approach was applied for quantification of the
375 response of the network models based on the lung transcriptomics data (Figure 4A) (Martin et al., 2014).
376 After 90 days of exposure to CS from the three reference cigarettes, similar levels of network
377 perturbations were detected in the lung tissue of male and female rats with contributions from all five
378 networks: inflammation, cellular fate, tissue repair and angiogenesis, cellular stress, and cellular
379 proliferation. The responses of the individual scored subnetwork models are shown in Supplementary
380 Figure 2C and D. The THS2.2M aerosol produced a much lower overall network perturbation compared
381 with reference CS exposures. Overall, in male rats, the response to THS2.2M exposure was low and
382 increased slightly with concentration, whereas, in female rats, the response to THS2.2M exposure was
383 higher than in male rats, but well below the response to CS exposure. The effects induced by 3R4F and
384 MRC(HM) in females recovered only partially after the 42-days recovery period.

385 To further complement this analysis, a functional association clustering approach was applied to both
386 the transcriptomic and the proteomic data (Figure 4B and C, Supplementary Figure 4) (Fang and Gough,
387 2014; Titz et al., 2015a). Functionally associated genes/proteins were linked and differentially

expressed/abundant functional clusters were identified. The identified gene and protein clusters included immune-related, oxidative-stress and xenobiotic response, unfolded-protein response, oxidative phosphorylation, and metabolism clusters. In general, the components of these clusters were up-regulated upon exposure to CS from the reference cigarettes and to aerosols from THS2.2M; however, the exposure response to THS2.2M aerosol was lower. Thus, the data-driven functional interpretation approach confirmed the lower effects observed for THS2.2M aerosol exposure compared with CS exposure. Gene and protein set enrichment analyses further confirmed the overall trends and especially highlighted processes linked to the inflammatory response (Supplementary Figure 5).

Effects of exposure on molecular markers for the immune response in the lung

To follow-up on the effects of CS on the lung immune system, the expression/abundance of immune-cell markers was evaluated (Figure 5A). CS exposure resulted in a clear increase in macrophage markers such as Cd14 and Cd68 and of neutrophil-associated proteins/genes such as Lcn2 and Mpo. In contrast, lymphoid cell markers, especially T-cell markers such as Cd2 and Cd3, were significantly decreased in response to CS exposure. THS2.2M exposure did not significantly affect the abundance of macrophage or neutrophil markers; however, a dose-dependent reduction in T-cell markers was observed, with Cd3d and Cd8b being significantly reduced in female rats in response to THS2.2M(H) exposure.

To further support and quantify these differences, it was measured how the exposure conditions affected both the macrophage and the neutrophil signaling network models (Figure 5B and C). In both models, the response to THS2.2M exposure was very limited. Interestingly, both processes were found to be still activated in the CS exposed groups after the 42-day recovery period, which is in overall agreement with the marker profiles (Figure 5A), histopathological evaluation, and BALF profiling results (part 6, (Oviedo et al., submitted (this issue))).

It has been reported that CS induces an immune state, which involves polarization of macrophages toward the M2 phenotype (Shaykhiev et al., 2009; Stämpfli and Anderson, 2009; Titz et al., 2015b). Whereas M1 macrophages are associated with classical immune-responses, M2 macrophages have been, for example, implicated in tissue repair processes (Mantovani et al., 2013). Here, the prominent up-regulation of Retnla (resistin-like protein a) was noted (Figure 5D). Retnla (also called FIZZ1) is one of the key markers for M2 macrophages (Martinez et al., 2006). Other key M2 markers such as Arg1 and chitinases (Chi3l1/Ym-1, Chia), and important contributors to M2 polarization such as Hmox1 (Heme oxygenase-1) (Naito et al., 2014) and Lgals3 (galectin-3) (Novak et al., 2012; White and Gomer, 2015) were also increased upon CS exposure. Furthermore, CS exposure resulted in a general induction of markers that were defined previously for human M2 macrophages (Supplementary Figure 6A) (Shaykhiev et al., 2009). In contrast, however, the marker genes defined for human M1 macrophages did not show a clear trend; for example the M1 macrophage marker Cd86 was up-regulated and the M1-associated components of the interferon signaling axis (Irf1/7) was down-regulated (Supplementary Figure 6B). In addition, several cytokines that indicate a pro-inflammatory response were increased in BALF (e.g., Mcp1/3) (part 6, (Oviedo et al., submitted (this issue))). Of note, Csf1 (M-CSF), which is associated with M2 polarization, was also significantly increased upon CS exposure (Hamilton et al., 2014).

Overall, this analysis demonstrated a strong and specific effect of the CS from all three reference cigarettes on the lung immune system. In contrast, THS2.2M aerosol exposure resulted in a much more limited effect on the lung immune system.

Analysis of the cellular stress response in the lung tissue

Xenobiotic metabolism and oxidative stress responses are commonly induced by CS (Wooten et al., 2006). The response of the oxidative stress and the xenobiotic metabolism response subnetworks that

433 are part of the cellular stress (CST) network compendium were compared (Supplementary Figure 2C and
434 D). An oxidative stress response was observed in rats exposed to CS for all three reference cigarettes
435 (Figure 6A). Interestingly, this response was only partially reduced after the 42-day recovery period. In
436 contrast, the three tested THS2.2M aerosol concentrations induced only a limited (although, still
437 significant) effect on the oxidative stress network in both sexes. The xenobiotic metabolism response
438 network demonstrated a similar response difference between rats exposed to CS and THS2.2M aerosol,
439 but this response appeared to recover more completely after the 42-day exposure to filtered air (Figure
440 6B).

441 To reconfirm these observations and to obtain additional molecular detail, the differential expression
442 response of gene sets related to these cellular stress responses was evaluated; namely, the reactive-
443 oxygen species (ROS) and xenobiotic response, and the functionally related unfolded-protein response
444 (UPR) (Figure 6C). CS activated an extensive oxidative stress response program, which involved the
445 glutathione system (e.g., glutamate-cysteine ligase (Gclc), glutaredoxin (Glrx), glutathione-S-transferases
446 (GSTs)), the thioredoxin system (thioredoxin (Txn2) and thioredoxin reductase 1 (Txnrd1)), superoxide
447 dismutase 2 (Sod2) and quinone NAD(P)H dehydrogenase 1 (Nqo1), and metabolic adaptations toward
448 NAPDH generation (glucose-6-phosphate dehydrogenase (G6pd)). Other genes/proteins that were up-
449 regulated/increased by CS and involved in the xenobiotic response included aldehyde dehydrogenase 3
450 (Aldh3a1/Aldh3b1) and the aldo-keto reductase 1c3 (Akr1c3). Oxidative damage to proteins has been
451 reported to also induce endoplasmic reticulum stress and the unfolded-protein response (UPR)
452 (Hengstermann and Müller, 2008; Jorgensen et al., 2008; Kelsen et al., 2008). Here, CS induced the
453 expression of several UPR marker genes and, in female rats, significantly increased the abundance of the
454 UPR proteins calreticulin (Calr), Grp-78 (Hspa5), and Pdia6 (Mei et al., 2013). This suggests an adverse,
455 possibly ROS-mediated, effect of CS on lung protein metabolism, which was much reduced in the
456 THS2.2M aerosol exposure groups.

Taken together, these results suggest that CS exposure triggered a clear stress response in the lung tissue of the rats, which included broad oxidative stress, xenobiotic, and unfolded-protein responses and was confirmed at the transcriptome and the proteome levels. In contrast, THS2.2M aerosols, even at the highest concentration, triggered a much lower response in these cellular stress pathways.

Analysis of the lung lipidome

CS exposure has been associated with extensive alterations in the lung lipid metabolism (Bodas et al., 2015; Morissette et al., 2015; Telenga et al., 2014; Titz et al., 2016). Here, a lipidomics analysis revealed changes in lung lipids for the tested exposure conditions (Figure 7A). The most consistent effects on the lipidome observed in this study were on several sphingolipid classes: sphingomyelins (SM), ceramides (Cer), glucosyl-/galactosyl-ceramides (Glc/GalCer), lactosyl-ceramide (LacCer), and globotriaosyl-ceramides (Gb3), which was in line with previous studies (Bodas et al., 2015; Telenga et al., 2014; Titz et al., 2016; Yang and Uhlig, 2011). Of note, d18:1/18:0 and d18:1/20:0 Glc/GalCers decreased in response to CS exposure in this and a previous ApoE$^{-/-}$ mouse study (Titz et al., 2016), which likely indicates chain-length specific properties of these sphingolipids (Grösch et al., 2012).

Whether these changes in sphingolipid levels were reflected in the enzymes involved in sphingolipid metabolism was examined. While only a few of these enzymes were quantified at the protein level, several genes encoding sphingolipid metabolism enzymes showed significant differential mRNA expression (Supplementary Figure 7A). To determine whether the differential expression followed any particular pattern, the changes were mapped onto the sphingolipid metabolism map (Supplementary Figure 7B) and the main effects related to the measured sphingolipid classes are summarized in Figure 7B. The mRNA transcript of the *de novo* ceramide synthesis enzyme Degs2 and the transcripts of the degradation enzymes for the glycosylated-ceramide lipids (e.g., Gba, Galc, and Glb1) were significantly up-regulated by reference CS exposure. In contrast, the transcript of Acer2, an enzyme that converts

ceramide to sphingosine, was significantly down-regulated. These expression changes generally pointed to ceramide as the central component of the sphingolipid pathway — with the increase in the sphingolipid degradation enzymes supporting the role of dynamic sphingolipid equilibrium in the response to CS exposure.

In summary, reference CS significantly affected the sphingo-lipidome and transcriptome, whereas the effects of THS2.2M aerosol were much less and not statistically significant. While the expression changes of the genes encoding sphingolipid metabolic enzymes showed a distinct pattern, the relationship with the observed changes in lipid levels is complex. Nevertheless, these changes likely contribute to the dynamic sphingolipid equilibrium as part of the overall regulation of tissue responses.

Discussion

In this paper the results from the systems toxicology arm ("OECD PLUS") of a standard 90-day rat inhalation study are reported that was conducted according to the OECD TG413 (part 6, (Oviedo et al., submitted (this issue))). Molecular profiling results complemented the classical endpoints and showed a consistent reduction in the biological effects in the rat RNE and lung tissue for THS2.2M aerosol exposed compared with CS exposed rats.

Overall, this study exemplified how classical toxicology endpoints (e.g., histopathology) can be complemented effectively by extensive molecular measurements and computational analyses within a systems toxicology framework (Sturla et al., 2014). The systems toxicology approach facilitates a deeper (mechanistic) understanding of the complex biological responses to toxicant exposure, and supports a more comprehensive and possibly more sensitive assessment. Toxicants can affect all levels of the biological organization, including the transcriptome, proteome, and lipidome. Because of the maturity of the technology, transcriptomics analyses were engaged first to globally capture molecular responses to toxicants (Lovett, 2000; Nuwaysir et al., 1999). Although the potential benefits of including proteomics measurement for toxicity assessment were proposed much earlier (Burchiel et al., 2001), technical limitations made the effective use of proteomics for systems toxicology investigations challenging. However, with the development of new instrumentation, proteomics technology is now evolving rapidly and more and more studies are using proteomic data to support deeper insights into the mechanisms of toxicity (Titz et al., 2016; Titz et al., 2014). Similarly, lipidomics — also supported by the rapid progress in mass-spectrometry based assays — can be expected to contribute more and more to the elucidation of toxicological responses (Fernando et al., 2011). In this study, we applied all three technologies to compare the biological response of male and female rats to THS2.2M aerosol and CS. With this, we were able to identify the biological effects of CS exposure across these three levels of molecular organization. As expected, the detected responses were highly interconnected — including to the classical

histopathological endpoints. All in all, we found that the measurements on these three biological levels complemented each other (see below) and mutually increased the confidence in our conclusions, especially on the reduced biological effects of THS2.2M aerosol compared with CS exposure, which was found consistently on all three biological levels.

For RNE, we showed that in agreement with the observed massive adaptive changes in the architecture of this tissue, a large number of genes and proteins were significantly differentially regulated after CS exposure. By analyzing the enrichment of biological processes and signaling pathways, we found that there was high consistency between the molecular and histopathological findings. For example, we identified several processes affected by CS exposure that could be linked to the observed adaptive changes of the RNE, such as hyperplasia, stratification, and squamous differentiation of the RNE, extracellular matrix alteration and tissue remodeling, as well as cell proliferation and migration processes in general (Figure 2). Assuming that the up-regulation of specific cell markers largely reflects an increase of the respective cell types, we found an increase in basal cells and squamous-differentiated epithelial cells of squamous epithelium, specifically in the rats exposed to CS. In contrast, most of the tested markers that were differentially expressed in the RNE of rats exposed to CS, were not significantly affected in the RNE of rats exposed to THS2.2M aerosol. Some exceptions were found in female rats exposed to the high concentration of THS2.2M. For example markers such Sprr1 were significantly affected, which is also in concordance with the histological results (part 6, (Oviedo et al., submitted (this issue)).

Markers for ciliated cells such as Foxj1 and dynein subunits tended to be down-regulated, which correlates with the observed disappearance of ciliated cells in the areas of goblet cell hyperplasia and squamous metaplasia (see Figure 2). Ciliated cells are the hallmarks of respiratory epithelium and are found not only in the nasal cavity but throughout the respiratory tract; therefore, this finding is in line with previous literature, which showed that exposure to CS is associated with a decrease in cilia and

ciliated cells (Simet et al., 2010). The airway epithelium of smokers has shorter cilia than that of non-smokers (Leopold et al., 2009). Air-liquid interface *in vitro* cultures were shown to recapitulate the effect of CS on shortening cilia length and, in this system, CS extract was reported to have a broad inhibiting effect on the expression of a variety of genes related to ciliogenesis (Brekman et al., 2014). Further, the overexpression of the cilia-related transcription factor FOXJ1 was found to prevent the CS extract-mediated inhibition of cilia growth (Brekman et al., 2014).

Among the markers specific for secretory cells, Muc5b and, to a lesser degree, Muc5ac were found to be up-regulated in the RNE samples following CS exposure, although goblet cell hyperplasia (a higher number of mucus-producing cells) was observed in the histological sections of the region where the samples were taken from. This effect might be explained by the fact that a local loss of goblet cells was also found in other regions along the nasal septum and dorsal meatus (part 6, (Oviedo et al., submitted (this issue))). This observation represents a clear limit of molecular-level analyses. The spatial heterogeneity in tissues cannot be resolved, but separating different areas by laser capture microdissection may help overcome this shortcoming.

On the other hand, molecular methods were successful in characterizing the observed mixed cell infiltrates in more detail. Marker analysis indicated that these cells were likely macrophages and neutrophils, and less pronounced T- or B-cells. Young healthy smokers were reported to have increased numbers of macrophages, and exfoliated ciliated and goblet cells, as well as higher myeloperoxidase concentrations in their nasal lavage fluid compared with nonsmokers, and their nasal mucociliary clearance was higher (Nicola et al., 2014). However, other studies either found no differences in the nasal mucosa of smokers compared with non-smokers (Vachier et al., 2004), or reported reduced mucociliary clearance and ciliary motility, as well as a decreased ratio of ciliated to goblet cells in nasal mucosa biopsies from smokers compared with nonsmokers and former smokers (no difference was detected between nonsmokers and former smokers) (Pagliuca et al., 2015).

As obligate nose-breathers, rodents inhale CS exclusively through their nasal airways. In contrast, humans usually inhale CS through the mouth. Nasal tissue exposure in humans occurs mostly during exhalation of inhaled mainstream CS and additionally by some sidestream smoke in the surrounding atmosphere. Hence, the less pronounced and less consistent CS effects on human nasal epithelium must be seen against a background of individual variability in smoke uptake and smoking habit.

The airways of rats and mice generally undergo adaptive responses to CS exposure, and long-term exposure of lung tissue to CS can result in more permanent tissue changes in the deeper lung that are associated with chronic obstructive pulmonary disease (COPD) development (Chung and Adcock, 2008; Fischer et al., 2015; Titz et al., 2015b). In general, 90-day rat CS inhalation studies do not result in clear signs of a COPD-like disease such as emphysema; nevertheless, rats develop distinct pulmonary inflammation. It is generally recognized that rat models address asthma and chronic bronchitis, while emphysema development can be observed more easily in susceptible mouse strains (Wright and Churg, 2010; Yu et al., 2008). Accordingly, in this rat study, reference CS exposure resulted in an extensive inflammatory response, oxidative stress response, and perturbation of tissue repair networks, all of which are known to be associated with and contribute to the development of lung disease, including chronic bronchitis and small airway remodeling (Figure 4) (Chung and Adcock, 2008; Fischer et al., 2015; Zuo et al., 2014).

The inflammatory response of the lung was detected by transcriptome and the proteome analyses using three approaches: biological network-based analysis, gene-set analysis, and functional association clustering. Consistently, all three approaches showed the up-regulation of inflammatory processes upon exposure to CS but not to THS2.2M aerosol, and supported the overall conclusion that the effects of THS2.2M exposure were strongly reduced (even for the highest concentration) compared with CS exposure. Specifically, we found evidence of the involvement of macrophages and neutrophils in this CS response (Figure 5). These molecular profiling results were well aligned with the other endpoints of this

study (part 6, (Oviedo et al., submitted (this issue))). Free immune cells and inflammatory mediators also were specifically increased in the BALF of CS-exposed rats, and the histopathology showed an increase in macrophages scattered within alveoli and aggregated in alveolar spaces upon CS exposure.

An interesting observation was that markers for M2 macrophages (e.g., Retnla, Arg1, and Chi3l1) were increased in lung tissue upon CS exposure (Figure 5D, Supplementary Figure 6A). The M1/M2 polarization concept of macrophages was initially defined as analogous to the Th1/Th2 T-cell concept, and the two states have been associated with different modes of activation (e.g., IFNγ vs. IL-4/IL-13) and different immune responses (e.g., viral vs. parasite clearance) (Mantovani et al., 2013). Consistent with our finding for CS exposure, several studies have reported the polarization of macrophages toward the M2 phenotype (Shaykhiev et al., 2009; Stämpfli and Anderson, 2009; Titz et al., 2015b). All in all, the engagement of the M2 macrophage population, which is known to be involved in lung repair processes (Johnston et al., 2012), suggests they may help the lung tissue to cope with the effects of CS exposure. However, it is important to note that macrophage differentiation and response is clearly more complex and does not fully fit into binary schemes (Martinez and Gordon, 2014) — as exemplified here by the less consistent response of the M1 polarization markers (Supplementary Figure 6A). Our observations can further motivate more systematic investigations into how the full spectrum of macrophage activation states contributes to the response of the lung to toxicological challenges (e.g., (Morissette et al., 2015; Xue et al., 2014)).

T-cell markers were lower in the lung tissues of CS-exposed rats than in the lung tissues of sham-exposed animals. Furthermore, gene/protein enrichment analysis indicated down-regulation of T cell activation (Supplementary Figure 5). For example, *in vitro* activated T cells cultured in the presence of CS extract were found to display a dose-dependent decrease in cell proliferation, which was associated with the induction of cellular apoptosis (Hernandez et al., 2013). The T cell receptor (TCR) is a multimeric protein complex composed of a clonotypic αβ heterodimer, a CD3 γδε chains, and a ζ homodimer

609 (Valitutti et al., 1997). Here, we found that the CD3 γδε and ζ chains in the lung tissue decreased upon
610 CS exposure. Interestingly, the process of TCR-antigen (peptide-MHC) interaction is self-limited. The
611 triggered TCRs are rapidly removed from the cell surface and are degraded in the lysosomes (Valitutti et
612 al., 1997). Therefore, lower T-cell numbers or TCR down-regulation are possible alternative explanations
613 that can best be resolved with additional experiments in future studies.

614 The constituents in CS pose an extensive xenobiotic and oxidative challenge for the lung tissue (Talhout
615 et al., 2011). To counteract this challenge, lung tissue activates several oxidative and xenobiotic stress
616 response systems (Cantin, 2010). Inflammatory and oxidative stress are tightly interconnected and likely
617 facilitate each other (Morissette et al., 2015; Zuo et al., 2014). Here, we observed a clear xenobiotic and
618 oxidative stress response in the lung upon CS exposure, and this response was much more limited upon
619 exposure to THS2.2M aerosol (Figure 6). Cyp1a1 was the only xenobiotic enzyme that was significantly
620 up-regulated upon THS2.2M exposure, which could likely be explained — in the absence of CS-typical
621 inducers such as polycyclic aromatic hydrocarbons — by the up-regulation effect that nicotine-only
622 exposure had on the expression of this gene (Phillips et al., 2015). Further supporting the strong
623 xenobiotic and oxidative stress burden upon CS exposure, the lung tissue also showed a clear unfolded-
624 protein response (UPR). The UPR reflects stress on the endoplasmic reticulum caused by proteins that
625 have unfold as a result of, for example, oxidative damage (Hengstermann and Müller, 2008; Jorgensen
626 et al., 2008; Kelsen et al., 2008). Taken together, the molecular analyses clearly revealed a strong stress
627 burden on the lung tissue by CS exposure, and this burden was much reduced for all concentrations of
628 THS2.2M aerosol exposure.

629 CS exposure also has been associated with extensive alterations in lung lipid metabolism (Lee et al.,
630 2015; Lundstrom et al., 2011; Morissette et al., 2015; Telenga et al., 2014; Titz et al., 2016). The most
631 consistent effect of CS exposure observed in this study was a significant increase in several sphingolipids
632 (SM, Cer, Glc/GalCer, LacCer, and Gb3) (Figure 7A). Previously, we observed similar increases in

633 sphingolipids in the lung of mice upon CS exposure (Titz et al., 2016). Of note, this finding might also be
634 related to accumulating literature evidence that indicates the involvement of sphingolipid alterations in
635 several lung diseases including COPD (Lee et al., 2015; Yang and Uhlig, 2011). In a recent example,
636 Telenga et al. profiled the sputum lipidome of COPD subjects and found increased levels of several
637 sphingolipids, including ceramide and glycosphingolipids, compared with sputum lipidome of smokers
638 without COPD (Telenga et al., 2014). Of these glycosphingolipids, CS-induced accumulation of LacCer in
639 the lung of COPD subjects has been specifically implicated in processes that lead to emphysema (Bodas
640 et al., 2015). While the observed changes in the abundances of sphingolipid metabolic enzymes are
641 more difficult to interpret, overall they support changes in the dynamic equilibrium of sphingolipids —
642 centered on ceramide — that are induced by CS exposure (Figure 7B). As such, these effects likely reflect
643 the complex sphingosine network response, including feedback mechanisms, that as a whole
644 determines their phenotypic effects (Köberlin et al., 2015). We can conclude that CS had a clear effect
645 on the sphingolipid metabolism and induced a state that is similar to previously reported disease-related
646 changes. In contrast, THS2.2M aerosol exposure had much lower effects on sphingolipid metabolism.

647 **Conclusion**

648 In summary, this systems toxicology analysis supported an integrated product risk assessment of
649 THS2.2M. Consistently, the THS2.2M aerosols (even at the highest concentration) showed much lower
650 effects compared with smoke from reference cigarettes on the molecular profiles and molecular
651 response networks of respiratory nasal epithelium and lung tissue. They included biological processes
652 crucially linked to the development of lung disease, such as inflammation- and oxidative stress-related
653 processes. Thus, our systems toxicology endpoints complemented and augmented the more classical
654 endpoints of this OECD TG413 90-day rat inhalation study. Furthermore, this study revealed activated
655 toxicity pathways and associated candidate biomarkers that could further facilitate the development of
656 21st century toxicology assessment approaches (Krewski et al., 2010; Langley et al., 2015; Stephens et

al., 2012). Limitations of the employed omics technologies included the lack of spatial and cellular resolution of the detected changes, the lack of global activity measurements for the detected proteins, and the lack of information how the observed molecular changes are specifically linked to disease outcomes. In the future, complementary technologies could be adapted to fill these gaps and, importantly, the dense matrix of the systems biology-derived molecular data could be used to more directly link the outcomes from the general purpose 90-day OECD TG413 subchronic inhalation studies to the more disease-specific results from animal models of, for example, COPD, cardiovascular disease, and lung cancer.

Acknowledgements

The authors would like to thank the study team, especially acknowledging the technical assistance and support of Camille Schilt, Lola Hamied, Karine Baumer, Polina Mironova, Remi Dulize, Sophie Scheuner, Sophie Dijon, Sam Ansari as well as Jenny Ho, Wei Teck Tan, Subash Krishnan and the bioresearch and aerosol team at PMIRL Singapore. The authors thank Maurice Smith and Emilija Veljkovic for their critical review.

Conflict of interest statement

The work reported in this publication involved a candidate Modified Risk Tobacco Product developed by Philip Morris International (PMI) and was solely funded by PMI. All authors are (or were) employees of PMI R&D or worked for PMI R&D under contractual agreements.

References

Ansari, S., et al., 2016. Comprehensive systems biology analysis of a 7-month cigarette smoke inhalation study in C57BL/6 mice. Sci Data. 3**,** 150077.

Bodas, M., et al., 2015. Lactosylceramide-accumulation in lipid-rafts mediate aberrant-autophagy, inflammation and apoptosis in cigarette smoke induced emphysema. Apoptosis. 20**,** 725-739.

Boué, S., et al., 2015. Causal biological network database: a comprehensive platform of causal biological network models focused on the pulmonary and vascular systems. Database. 2015**,** bav030.

Brekman, A., et al., 2014. FOXJ1 prevents cilia growth inhibition by cigarette smoke in human airway epithelium in vitro. Am J Respir Cell Mol Biol. 51**,** 688-700.

Burchiel, S. W., et al., 2001. Analysis of genetic and epigenetic mechanisms of toxicity: potential roles of toxicogenomics and proteomics in toxicology. Toxicological Sciences. 59**,** 193-195.

Cantin, A. M., 2010. Cellular response to cigarette smoke and oxidants: adapting to survive. Proc Am Thorac Soc. 7**,** 368-75.

Chen, J., et al., 2009. ToppGene Suite for gene list enrichment analysis and candidate gene prioritization. Nucleic Acids Res. 37**,** W305-11.

Chung, K., Adcock, I., 2008. Multifaceted mechanisms in COPD: inflammation, immunity, and tissue repair and destruction. The European respiratory journal. 31**,** 1334.

Coggins, C. R., et al., 1989. Ninety-day inhalation study in rats, comparing smoke from cigarettes that heat tobacco with those that burn tobacco. Fundam Appl Toxicol. 13**,** 460-83.

Ellinger-Ziegelbauer, H., et al., 2011. The enhanced value of combining conventional and "omics" analyses in early assessment of drug-induced hepatobiliary injury. Toxicol Appl Pharmacol. 252**,** 97-111.

Family Smoking Prevention and Tobacco Control Act. Public Law No. 111-131 (June 22, 2009).

Fang, H., Gough, J., 2014. The 'dnet' approach promotes emerging research on cancer patient survival. Genome Med. 6**,** 64.

Fernando, H., et al., 2011. Lipidomic changes in rat liver after long-term exposure to ethanol. Toxicol Appl Pharmacol. 255**,** 127-37.

Fischer, B. M., et al., 2015. COPD: balancing oxidants and antioxidants. Int J Chron Obstruct Pulmon Dis. 10**,** 261-276.

Gaworski, C. L., et al., 1997. 13-week inhalation toxicity study of menthol cigarette smoke. Food Chem Toxicol. 35**,** 683-92.

Gebel, S., et al., 2013. Construction of a computable network model for DNA damage, autophagy, cell death, and senescence. Bioinformatics and biology insights. 7**,** 97.

Gentleman, R. C., et al., 2004. Bioconductor: open software development for computational biology and bioinformatics. Genome biology. 5**,** R80.

Grösch, S., et al., 2012. Chain length-specific properties of ceramides. Progress in lipid research. 51**,** 50-62.

Hamilton, T. A., et al., 2014. Myeloid colony-stimulating factors as regulators of macrophage polarization. Front Immunol. 5**,** 554.

Haziza, C., et al., submitted (this issue). Evaluation of the Tobacco Heating System 2.2. Part 8: 5-Day randomized reduced exposure clinical trial in Poland.

Hengstermann, A., Müller, T., 2008. Endoplasmic reticulum stress induced by aqueous extracts of cigarette smoke in 3T3 cells activates the unfolded-protein-response-dependent PERK pathway of cell survival. Free Radical Biology and Medicine. 44**,** 1097-1107.

Herbrich, S. M., et al., 2013. Statistical Inference from Multiple iTRAQ Experiments without Using Common Reference Standards. Journal of proteome research. 12, 594-604.
Hernandez, C. P., et al., 2013. Effects of cigarette smoke extract on primary activated T cells. Cell Immunol. 282, 38-43.
Huber, W., et al., 2002. Variance stabilization applied to microarray data calibration and to the quantification of differential expression. Bioinformatics. 18, S96-S104.
Hultin-Rosenberg, L., et al., 2013. Defining, comparing, and improving iTRAQ quantification in mass spectrometry proteomics data. Mol Cell Proteomics. 12, 2021-31.
International Organization for Standardization: 3308, ISO 3308. Routine analytical cigarette-smoking machine. Definitions and standard conditions. Amended 2000. International Organization for Standardization Geneva, Switzerland, 1991.
Johnston, L. K., et al., 2012. Pulmonary macrophage subpopulations in the induction and resolution of acute lung injury. American journal of respiratory cell and molecular biology. 47, 417-426.
Jorgensen, E., et al., 2008. Cigarette smoke induces endoplasmic reticulum stress and the unfolded protein response in normal and malignant human lung cells. BMC cancer. 8, 229.
Kelsen, S. G., et al., 2008. Cigarette smoke induces an unfolded protein response in the human lung: a proteomic approach. American journal of respiratory cell and molecular biology. 38, 541-550.
Kelstrup, C. D., et al., 2012. Optimized fast and sensitive acquisition methods for shotgun proteomics on a quadrupole orbitrap mass spectrometer. Journal of proteome research. 11, 3487-3497.
Köberlin, M. S., et al., 2015. A conserved circular network of coregulated lipids modulates innate immune responses. Cell. 162, 170-183.
Kogel, U., et al., 2014. A 28-day rat inhalation study with an integrated molecular toxicology endpoint demonstrates reduced exposure effects for a prototypic modified risk tobacco product compared with conventional cigarettes. Food and Chemical Toxicology. 68, 204-217.
Kogel, U., et al., submitted (this issue). Evaluation of the Tobacco Heating System 2.2. Part 7: Systems toxicological assessment of a mentholated version revealed reduced cellular and molecular exposure effects compared with mentholated and non-mentholated cigarette smoke.
Krewski, D., et al., 2010. Toxicity testing in the 21st century: a vision and a strategy. Journal of Toxicology and Environmental Health, Part B. 13, 51-138.
Langley, G., et al., 2015. Lessons from Toxicology: Developing a 21st-Century Paradigm for Medical Research. Environ Health Perspect. 123, A268-72.
Lê Cao, K.-A., et al., 2009. integrOmics: an R package to unravel relationships between two omics datasets. Bioinformatics. 25, 2855-2856.
Lee, J., et al., 2015. Sphingolipids as cell fate regulators in lung development and disease. Apoptosis. 20, 740-57.
Leopold, P. L., et al., 2009. Smoking is associated with shortened airway cilia. PLoS One. 4, e8157.
Liberzon, A., et al., 2011. Molecular signatures database (MSigDB) 3.0. Bioinformatics. 27, 1739-1740.
Lovett, R. A., 2000. Toxicogenomics. Toxicologists brace for genomics revolution. Science. 289, 536-7.
Lundstrom, S. L., et al., 2011. Lipid mediator profiling in pulmonary disease. Curr Pharm Biotechnol. 12, 1026-52.
Mantovani, A., et al., 2013. Macrophage plasticity and polarization in tissue repair and remodelling. The Journal of pathology. 229, 176-185.
Martin, F., et al., 2014. Quantification of biological network perturbations for mechanistic insight and diagnostics using two-layer causal models. BMC Bioinformatics. 15, 238.
Martin, F., et al., submitted (this issue). Evaluation of the Tobacco Heating System 2.2. Part 9: Application of systems pharmacology to identify exposure response markers in peripheral blood of smokers switching to THS2.2.

Martin, F., et al., 2012. Assessment of network perturbation amplitudes by applying high-throughput data to causal biological networks. BMC systems biology. 6**,** 54.

Martinez, F. O., Gordon, S., 2014. The M1 and M2 paradigm of macrophage activation: time for reassessment. F1000prime reports. 6.

Martinez, F. O., et al., 2006. Transcriptional profiling of the human monocyte-to-macrophage differentiation and polarization: new molecules and patterns of gene expression. The Journal of Immunology. 177**,** 7303-7311.

Mei, Y., et al., 2013. Endoplasmic reticulum stress and related pathological processes. Journal of pharmacological & biomedical analysis. 1**,** 1000107.

Morissette, M. C., et al., 2015. Disruption of pulmonary lipid homeostasis drives cigarette smoke-induced lung inflammation in mice. Eur Respir J.

Naito, Y., et al., 2014. Heme oxygenase-1 and anti-inflammatory M2 macrophages. Archives of biochemistry and biophysics. 564**,** 83-88.

Nicola, M. L., et al., 2014. Young "healthy" smokers have functional and inflammatory changes in the nasal and the lower airways. Chest. 145**,** 998-1005.

Novak, R., et al., 2012. Galectin-1 and galectin-3 expression profiles in classically and alternatively activated human macrophages. Biochim Biophys Acta. 1820**,** 1383-90.

Nuwaysir, E. F., et al., 1999. Microarrays and toxicology: the advent of toxicogenomics. Mol Carcinog. 24**,** 153-9.

OECD, 2013. Guidance document on developing and assessing adverse outcome pathways. Series on Testing and Assessment No. 184. OECD Environment, Health and Safety Publications. ENV/JM/MONO(2013)6.

Oviedo, A., et al., submitted (this issue). Evaluation of the Tobacco Heating System 2.2. Part 6: 90-day OECD 413 rat inhalation study with systems toxicology endpoints demonstrates reduced exposure effects of a mentholated version compared with mentholated and non-mentholated cigarette smoke.

Pagliuca, G., et al., 2015. Cytologic and functional alterations of nasal mucosa in smokers: temporary or permanent damage? Otolaryngol Head Neck Surg. 152**,** 740-5.

Phillips, B., et al., 2015. Toxicity of aerosols of nicotine and pyruvic acid (separate and combined) in Sprague-Dawley rats in a 28-day OECD 412 inhalation study and assessment of systems toxicology. Inhal Toxicol. 27**,** 405-31.

Piade, J. J., et al., 2014. Toxicological assessment of kretek cigarettes Part 3: kretek and American-blended cigarettes, inhalation toxicity. Regul Toxicol Pharmacol. 70 Suppl 1**,** S26-40.

R Development Core Team, R: A Language and Environment for Statistical Computing. 2007.

Sauer, J. M., et al., 2015. Systems Toxicology: The Future of Risk Assessment. Int J Toxicol. 34**,** 346-8.

Schaller, J.-P., et al., submitted (this issue)-a. Evaluation of the Tobacco Heating System 2.2. Part 2: Chemical composition, genotoxicity, cytotoxicity, and physical properties of the aerosol.

Schaller, J.-P., et al., submitted (this issue)-b. Evaluation of the Tobacco Heating System 2.2. Part 3: Influence of the tobacco blend on the formation of harmful and potentially harmful constituents in the aerosol.

Schlage, W. K., et al., 1998a. Cytokeratin expression patterns in the rat respiratory tract as markers of epithelial differentiation in inhalation toxicology. I. Determination of normal cytokeratin expression patterns in nose, larynx, trachea, and lung. Toxicologic pathology. 26**,** 324-343.

Schlage, W. K., et al., 1998b. Cytokeratin expression patterns in the rat respiratory tract as markers of epithelial differentiation in inhalation toxicology. II. Changes in cytokeratin expression patterns following 8-day exposure to room-aged cigarette sidestream smoke. Toxicologic pathology. 26**,** 344-360.

Schlage, W. K., et al., 2011. A computable cellular stress network model for non-diseased pulmonary and cardiovascular tissue. BMC Syst Biol. 5**,** 168.

Sewer, A., et al., submitted (this issue). Evaluation of the Tobacco Heating System 2.2. Part 5: MicroRNA expression from a 90-day rat inhalation study indicates reduced effects of the aerosol on lung tissue compared with cigarette smoke exposure.

Shaykhiev, R., et al., 2009. Smoking-dependent reprogramming of alveolar macrophage polarization: implication for pathogenesis of chronic obstructive pulmonary disease. The Journal of immunology. 183**,** 2867-2883.

Simet, S. M., et al., 2010. Long-term cigarette smoke exposure in a mouse model of ciliated epithelial cell function. Am J Respir Cell Mol Biol. 43**,** 635-40.

Smith, M., et al., submitted (this issue). Evaluation of the Tobacco Heating System 2.2. Part 1: Description of the System and the Scientific Assessment Program.

Smyth, G. K., 2004. Linear models and empirical bayes methods for assessing differential expression in microarray experiments. Stat Appl Genet Mol Biol. 3**,** Article3.

Stämpfli, M. R., Anderson, G. P., 2009. How cigarette smoke skews immune responses to promote infection, lung disease and cancer. Nature Reviews Immunology. 9**,** 377-384.

Stephens, M. L., et al., 2012. Accelerating the development of 21st-century toxicology: outcome of a Human Toxicology Project Consortium workshop. Toxicological Sciences. 125**,** 327-334.

Sturla, S. J., et al., 2014. Systems toxicology: from basic research to risk assessment. Chemical research in toxicology. 27**,** 314-329.

Szklarczyk, D., et al., 2015. STRING v10: protein-protein interaction networks, integrated over the tree of life. Nucleic Acids Res. 43**,** D447-52.

Talhout, R., et al., 2011. Hazardous compounds in tobacco smoke. International journal of environmental research and public health. 8**,** 613-628.

Telenga, E. D., et al., 2014. Untargeted lipidomic analysis in chronic obstructive pulmonary disease. Uncovering sphingolipids. Am J Respir Crit Care Med. 190**,** 155-64.

Tesfaigzi, J., Carlson, D. M., 1999. Expression, regulation, and function of the SPR family of proteins. Cell biochemistry and biophysics. 30**,** 243-265.

Titz, B., et al., 2016. Effects of cigarette smoke, cessation and switching to two heat-not-burn tobacco products on lung lipid metabolism in C57BL/6 and Apoe-/- mice - an integrative systems toxicology analysis. Toxicol Sci. 149**,** 441-457.

Titz, B., et al., 2014. Proteomics for systems toxicology. Computational and structural biotechnology journal. 11**,** 73-90.

Titz, B., et al., 2015a. Analysis of Proteomic Data for Toxicological Applications. Computational Systems Toxicology. Humana Press, pp. 257-284.

Titz, B., et al., 2015b. Alterations in the sputum proteome and transcriptome in smokers and early-stage COPD subjects. Journal of proteomics. 128**,** 306-320.

Valitutti, S., et al., 1997. Degradation of T cell receptor (TCR)-CD3-zeta complexes after antigenic stimulation. J Exp Med. 185**,** 1859-64.

Vanscheeuwijck, P. M., et al., 2002. Evaluation of the potential effects of ingredients added to cigarettes. Part 4: subchronic inhalation toxicity. Food Chem Toxicol. 40**,** 113-31.

Väremo, L., et al., 2013. Enriching the gene set analysis of genome-wide data by incorporating directionality of gene expression and combining statistical hypotheses and methods. Nucleic acids research. 41**,** 4378-4391.

Vizcaíno, J. A., et al., 2014. ProteomeXchange provides globally coordinated proteomics data submission and dissemination. Nature biotechnology. 32**,** 223-226.

Westra, J. W., et al., 2011. Construction of a computable cell proliferation network focused on non-diseased lung cells. BMC systems biology. 5**,** 105.

Westra, J. W., et al., 2013. A modular cell-type focused inflammatory process network model for non-diseased pulmonary tissue. Bioinformatics and biology insights. 7**,** 167.

White, M. J., Gomer, R. H., 2015. Trypsin, Tryptase, and Thrombin Polarize Macrophages towards a Pro-Fibrotic M2a Phenotype. PLoS One. 10**,** e0138748.

Wong, E. T., et al., submitted (this issue). Evaluation of the Tobacco Heating System 2.2. Part 4: 90-day OECD 413 rat inhalation study with systems toxicology endpoints demonstrates reduced exposure effects compared with cigarette smoke.

Wooten, J. B., et al., 2006. Tobacco smoke constituents affecting oxidative stress. Cigarette Smoke and Oxidative Stress. Springer, pp. 5-46.

Wright, J. L., Churg, A., 2010. Animal models of cigarette smoke-induced chronic obstructive pulmonary disease. Expert Rev Respir Med. 4**,** 723-34.

Xue, J., et al., 2014. Transcriptome-based network analysis reveals a spectrum model of human macrophage activation. Immunity. 40**,** 274-288.

Yang, Y., Uhlig, S., 2011. The role of sphingolipids in respiratory disease. Ther Adv Respir Dis. 5**,** 325-44.

Yu, B., et al., 2008. Acute tobacco smoke-induced airways inflammation in spontaneously hypertensive rats. Inhal Toxicol. 20**,** 623-33.

Zuo, L., et al., 2014. Interrelated role of cigarette smoking, oxidative stress, and immune response in COPD and corresponding treatments. Am J Physiol Lung Cell Mol Physiol. 307**,** L205-18.

Figure captions

Figure 1. Design of the 90-day systems toxicology study to assess effects of CS and THS2.2M exposures on rat respiratory organs. Groups of six male and six female rats were exposed for 90 days to fresh air (Sham) or cigarette smoke of three reference cigarettes: a standard reference cigarette (3R4F), and a low menthol (MRC(LM)) and high menthol (MRC(HM)) reference cigarette (all at 23 µg nicotine/L). In addition, groups of rats were exposed to aerosol from THS2.2M (15, 23, and 50 µg/L nicotine). The 90-day exposure period was followed by a 42-day recovery period with rats exposed to fresh air (indicated groups and female rats only). Rats were exposed for 6 h per day, for 5 days per week. Respiratory nasal epithelium and lung tissue samples were collected for proteomics, transcriptomics, and histopathology. Lipidomics analysis was conducted for the lung tissue samples.

Figure 2. Response of the respiratory nasal epithelium to CS exposure. (A) Star plots showing relative network-level biological impact factors (RBIF) for each exposure group compared with the Sham groups. The total area in each star plot represents the RBIF of each comparison relative to the comparison with the overall largest BIF (MRC(LM), males, 90 days). The areas of the segments show the aggregation of network perturbation amplitude computed for each family of biological network models (see key). For each exposure group comparison, the relative contribution of the individual network perturbation amplitude are indicated. (B) Gene set enrichment analysis for the transcriptomics and proteomics data. Set enrichment was assessed by gene-set analysis with the mean of the absolute log2 fold-change as the gene set statistic (from mSigDB c5 collection). Gene (Q1) and sample permutation (Q2) was used to assess statistical significance. Gene sets with an adjusted p-value < 0.05 for both Q1 and Q2 in any comparison were selected. Gene sets were clustered by similarity of the contributing genes (annotated by representative gene set, see color bar on the left of the heatmap). The mean log2 fold-change (normalized per gene set) is color-coded (see color key). See Supplementary Figure 3 for details. The exposure groups are indicated above the heatmap. Reference cigarette exposure in red, THS2.2M exposure in blue, R1 = 3R4F, R2 = MRC(LM), R3 = MRC(HM), TL = THS2.2M(L), TM = THS2.2M(M), TH = THS2.2M(H). Note that the first 12 and the last six exposure groups for the proteomics data were analyzed as two independent iTRAQ sets. Set 2 is marked, see methods for details.

Figure 3. Molecular marker panels capture the response of the respiratory nasal epithelium to CS exposure. (A) Expression profiles for marker panel of epithelium cell types and basal lamina components. The protein and gene abundance and expression fold-changes compared with the respective Sham groups are color-coded and statistical significance is marked (adjusted p-value, x = < 0.05, * = < 0.01). Missing values are marked in grey. (B) Expression profiles for panel of immune-cell markers. Note that not all relevant markers (e.g., the B-cell marker CD19) were identified in the transcriptomics and proteomics analyses. The exposure groups are indicated above the heatmaps (A and B) and are defined in the caption to Figure 2B.

Figure 4. Response of the lung tissue to CS exposure. (A) Star plots showing relative network-level biological impact factors (RBIFs) for each exposure group compared with the Sham groups. The total area in each star plot represents the RBIF of each comparison relative to the comparison with the MRC(LM), females, 90-days group. See the caption to Figure 2A for other details. (B) Functional association clustering for transcriptomics data of the lung tissue. Functional clusters affected by the exposure conditions were identified and compared across the different clusters. Lower panel shows the identified clusters and their associated functional categories (see key). Each node represents a gene, lines represent functional associations, and identified gene clusters are grouped and circled. The top panel shows the differential expression response for each gene in the association network. The node color represents the –log10 adjusted p-value (see color key). (C) Functional association clustering for proteomics data of the lung tissue. In the lower panel, each node represents a protein, lines represent functional associations, and identified protein clusters are grouped and circled. The top panel shows the differential abundance response for each protein in the association network. See the caption to 4B for other details. Note that several clusters with immune-related molecules were identified.

Figure 5. Immune-related molecular marker panel captures the response of the lung tissue to CS exposure. (A) Expression profiles for panel of immune-cell markers. The protein and gene abundance and expression fold-changes compared with the respective Sham groups are color-coded and statistical significance is marked

(adjusted p-value, x = < 0.05, * = < 0.01). Missing values are marked in grey. (B) Quantitative scores of exposure effects on the macrophage signaling pathway. The bars show the overall network perturbation amplitude (NPA) based on the transcriptomics data, the error bars show the 95% confidence interval. Three statistics are shown: the red star indicates statistical significance with respect to the biological replicates, the green star (o statistic) indicates significance with respect to permutation of the downstream genes of the network nodes, and the blue star (k statistic) indicates significance with respect to permutation of the network topology ($p < 0.05$). (C) Quantitative scores of exposure effects on the neutrophil signaling pathway. See the caption to 5B for other details. (D) Expression profiles for M2 macrophage-related genes/proteins. The exposure groups are indicated above the heatmaps (A and D) and are defined in the caption to Figure 2B.

Figure 6. Cellular stress response in lung tissue after CS exposure. (A) Quantitative scores of exposure effects on the oxidative stress pathway. (B) Quantitative scores of exposure effects on the xenobiotic metabolism pathway. The bars show the overall network perturbation amplitude (NPA) based on the transcriptomics data, the error bars show the 95% confidence interval. Three statistics are shown: the red star indicates statistical significance with respect to the biological replicates, the green star (o statistic) indicates significance with respect to permutation of the downstream genes of the network nodes, and the blue star (k statistic) indicates significance with respect to permutation of the network topology. (C) Expression/abundance profiles for cellular stress-related gene/protein sets. The reactive-oxygen species (ROS) and xenobiotic gene set is the union of the metabolism of xenobiotics by the cytochrome P450 gene set from the KEGG database and the hallmark reactive -oxygen species pathway from mSigDB. The unfolded-protein response (UPR) pathway includes common UPR markers. Profiles for significantly affected proteins/genes are shown (adjusted p-value < 0.05). The fold-changes compared with the respective Sham groups are color-coded and statistical significance is marked (FDR-adjusted p-value, x = < 0.05, * = < 0.01). Missing values are marked in grey. The exposure groups are indicated above the heatmap and are defined in the caption to Figure 2B.

Figure 7. Effects of CS exposure on the lung lipidome. (A) Abundance profiles for lipid species with significant differential abundance. Each row represents a lipid species, each column an exposure condition compared with the respective Sham group. The fold-change compared with Sham exposure is color-coded (see color key). Significantly abundant differences are indicated (* = adjusted p-value < 0.05). The molar contribution of significantly abundant lipid species to their lipid class is indicated by the shade of the significance indicator. (B) Schematic summary of the ceramide-centered sphingolipid metabolic network with the gene expression response profiles of the significantly altered enzymes. See Supplementary Figure 7 for more details.

Supplementary Material

Evaluation of the Tobacco Heating System 2.2. Part 7: Systems toxicological assessment of a mentholated version revealed reduced cellular and molecular exposure effects compared with mentholated and non-mentholated cigarette smoke

Ulrike Kogel[a,*], Bjoern Titz[a,*], Walter K. Schlage[b], Catherine Nury[a], Florian Martin[a], Alberto Oviedo[c], Stefan Lebrun[a], Ashraf Elamin[a], Emmanuel Guedj[a], Keyur Trivedi[a], Nikolai V. Ivanov[a], Patrick Vanscheeuwijck[a], Manuel C. Peitsch[a], Julia Hoeng[a]

[a] Philip Morris International Research and Development, Philip Morris Products S.A., Quai Jeanrenaud 5, 2000 Neuchatel, Switzerland (part of Philip Morris International group of companies)

[b] Biology consultant, Max-Baermann-Str. 21, 51429 Bergisch Gladbach, Germany

[c] Philip Morris International Research Laboratories, 50 Science Park Road, Singapore, Singapore (part of Philip Morris International group of companies)

[*] UK and BT contributed equally to this manuscript.

Corresponding author:

Julia Hoeng, PhD

E-mail: julia.hoeng@pmi.com

Tel: +41 (58) 242 2214

Fax: +41 (58) 242 2811

Supplementary Figure 1. Number of identified genes and proteins with significant differential expression/abundance. (A) Numbers of significant differentially expressed genes (DEGs) identified in respiratory nasal epithelium of the exposure groups compared with the corresponding Sham-exposed rats. Numbers of up- and down-regulated genes with adjusted p-value < 0.05 are shown. **(B)** Numbers of differentially abundant proteins (DEPs) identified in respiratory nasal epithelium of the exposure groups compared with the corresponding Sham-exposed rats. **(C)** Number of significant differentially expressed genes (DEGs) identified in lung tissue for the exposure groups compared with the corresponding Sham-exposed rats. Numbers of up- and down-regulated genes with adjusted p-value < 0.05 are shown. **(D)** Numbers of differentially abundant proteins (DEPs) identified in lung tissue for the exposure groups compared with the corresponding Sham-exposed rats. Note that the first 12 and the last six exposure groups for the proteomics data were analyzed as two independent iTRAQ sets. Set 2 is marked, see methods for details.

Supplementary Figure 2. Exposure response of individual network models. Network perturbation amplitude (NPA) heatmaps of all subnetworks tested. Network models have been described in the literature: cell proliferation (Westra et al., 2011); cell stress (Schlage et al., 2011); apoptosis, autophagy, DNA damage, necroptosis, and senescence (Gebel et al., 2013); and inflammation (Westra et al., 2013). **(A)** Results for respiratory nasal epithelium of male rats. **(B)** Results for respiratory nasal epithelium of female rats. **(C)** Results for lung tissue of male rats. **(D)** Results for lung tissue of female rats. Note: each heatmap indicates the amount of perturbation, but not the direction; therefore, high perturbation can also indicate down-regulated processes. Note that the color bars below the heatmaps indicate the different exposure conditions. CFA, cell fate; CPR, cell proliferation; CST, cell stress; IPN, inflammatory process network; TRA, tissue repair and angiogenesis.

Supplementary Figure 3. Gene-set enrichment for rat respiratory nasal epithelium. Gene set enrichment analysis for transcriptomics and proteomics data. Set enrichment was assessed by gene-set

analysis with the mean of the absolute log2 fold-change as the gene set statistic (mSigDB c5 collection). Gene (Q1) and sample permutation (Q2) were used to assess statistical significance. Gene sets with an adjusted p-value < 0.05 for both Q1 and Q2 in any comparison were selected. Gene sets were clustered by similarity of the contributing genes (annotated by representative gene set) and the mean log2 fold-change (normalized per gene set) was color-coded (see color key). In each cell the significance of the gene-set – exposure association is indicated by a maximum of four stars: positions 1 and 2 = Q1 hypothesis; positions 3 and 4 = Q2 hypothesis; positions 1 and 3 = non-directional; positions 2 and 4 = directional (adjusted p-value < 0.05). Color bar on the left of the heatmap shows the gene set clustering.

Supplementary Figure 4. Functional association clusters for the lung transcriptomics and proteomics data. Each node represents a gene (left panel) or protein (right panel), lines represent functional associations, and identified gene/protein clusters are grouped and circled.

Supplementary Figure 5. Gene-set enrichment for rat lung tissue. Gene set enrichment analysis for transcriptomics and proteomics data. Set enrichment was assessed by gene-set analysis with the mean of the absolute log2 fold-change as the gene set statistic (mSigDB c5 collection). Gene (Q1) and sample permutation (Q2) was used to assess statistical significance. Gene sets with an adjusted p-value < 0.05 for both Q1 and Q2 in any comparison were selected. Gene sets were clustered by similarity of the contributing genes (annotated by representative gene set) and the mean log2 fold-change (normalized per gene set) was color-coded (see color key). In each cell the significance of the gene-set – exposure association is indicated by a maximum of four stars: positions 1 and 2 = Q1 hypothesis; positions 3 and 4 = Q2 hypothesis; positions 1 and 3 = non-directional; positions 2 and 4 = directional (adjusted p-value < 0.05).

Supplementary Figure 6. Macrophage M1/M2 polarization profiles for rat lung tissue. Volcano plots show the effect size (log2 fold-change) and significance (−log10 adjusted p-value) for genes that were

associated with the M1 and M2 macrophage differentiation states (Shaykhiev et al., 2009). **(A)** M2 signature genes. **(B)** M1 signature genes.

Supplementary Figure 7. Effects of CS exposure on sphingolipid metabolic enzymes. (A) Gene and protein expression/abundance profiles for the sphingolipid metabolism pathway from the KEGG database. **(B)** Expression changes mapped onto the sphingolipid metabolism pathway. Fold-changes in exposed groups compared with Sham exposure are color coded. Note that mapping can aggregate expression values for several iso-enzymes and the labels do not necessarily correspond to the most significantly affected iso-enzymes, as for example in the case of Degs1 and Degs2. This mapping serves as an overview and a schematic summary of the ceramide-centered sphingolipid metabolic network for the significantly affected enzymes is shown in Figure 7B.

Supplementary Table 1 [Excel file]: Molecular markers for epithelial and immune cell types. (A) Molecular marker panel for respiratory nasal epithelial cell types. All the markers that were used to characterize the epithelial cell types are listed. **(B)** Molecular marker panel for immune cell types taken from the literature. All the markers that were used to characterize the inflammatory cell types are listed.

Supplementary Table 2 [Excel file]: Lipidomics raw data.

Evaluation of the Tobacco Heating System 2.2. Part 7: Systems toxicological assessment of a mentholated version revealed reduced cellular and molecular exposure effects compared with mentholated and non-mentholated cigarette smoke

Ulrike Kogel[a,*], Bjoern Titz[a,*], Walter K. Schlage[b], Catherine Nury[a], Florian Martin[a], Alberto Oviedo[c], Stefan Lebrun[a], Ashraf Elamin[a], Emmanuel Guedj[a], Keyur Trivedi[a], Nikolai V. Ivanov[a], Patrick Vanscheeuwijck[a], Manuel C. Peitsch[a], Julia Hoeng[a]

[a] Philip Morris International Research and Development, Philip Morris Products S.A., Quai Jeanrenaud 5, 2000 Neuchatel, Switzerland (part of Philip Morris International group of companies)

[b] Biology consultant, Max-Baermann-Str. 21, 51429 Bergisch Gladbach, Germany

[c] Philip Morris International Research Laboratories, 50 Science Park Road, Singapore, Singapore (part of Philip Morris International group of companies)

[*] UK and BT contributed equally to this manuscript.

Corresponding author:

Julia Hoeng, PhD

E-mail: julia.hoeng@pmi.com

Tel: +41 (58) 242 2214

Fax: +41 (58) 242 2811

Abstract[1]

Modified risk tobacco products (MRTPs) are being developed with the aim of reducing smoking-related health risks. The Tobacco Heating System 2.2 (THS2.2) is a candidate MRTP that uses the *heat-not-burn* principle. Here, systems toxicology approaches were engaged to assess the respiratory effects of mentholated THS2.2 (THS2.2M) in a 90-day rat inhalation study (OECD test guideline 413). The standard endpoints were complemented by transcriptomics and quantitative proteomics analyses of respiratory nasal epithelium and lung tissue and by lipidomics analysis of lung tissue. The adaptive response of the respiratory nasal epithelium to conventional cigarette smoke (CS) included squamous cell metaplasia and an inflammatory response, with high correspondence between the molecular and histopathological results. In contrast to CS exposure, the adaptive tissue and molecular changes to THS2.2M aerosol exposure were much weaker and were limited mostly to the highest THS2.2M concentration in female rats. In the lung, CS exposure induced an inflammatory response, triggered cellular stress responses, and affected sphingolipid metabolism. These responses were not observed or were much lower after THS2.2M aerosol exposure. Overall, this system toxicology analysis complements and reconfirms the results from classical toxicological endpoints and further suggests potentially reduced health risks of THS2.2M.

Keywords: modified risk tobacco product; systems toxicology; transcriptomics; proteomics; lipidomics; subchronic inhalation toxicity

[1] *Abbreviations:* THS2.2, Tobacco Heating System 2.2; THS2.2M, mentholated THS2.2; HPHC, harmful and potentially harmful constituent; CS, cigarette smoke; MRTP, modified risk tobacco product; FDR, false-discovery rate; iTRAQ, isobaric tag for relative and absolute quantitation; MRC, mentholated reference cigarette; LM, low menthol; HM, high menthol.

Introduction

The U.S. Family Smoking Prevention and Tobacco Control Act (FSPTCA) defines a Modified Risk Tobacco Product (MRTP) as “any tobacco product that is sold or distributed for use to reduce harm or the risk of tobacco related disease associated with commercially marketed tobacco products” (Family Smoking Prevention and Tobacco Control Act). This publication is part of a series of nine publications describing the nonclinical and part of the clinical assessment of a candidate MRTP, THS2.2 regular and a mentholated version (THS2.2M). THS2.2 and THS2.2M are based on the concept that heating tobacco, rather than burning it, reduces or eliminates the formation of harmful and potentially harmful constituents in the inhaled aerosol. The series of publications provides part of the overall scientific program to assess the potential for THS2.2 to be a reduced risk product. The first publication in this series describes THS2.2 and the assessment program for MRTPs ((Smith et al., submitted (this issue))). This is followed by six publications, including this one, that describe the nonclinical assessment of THS2.2 regular and THS2.2M (Kogel et al., submitted (this issue));(Oviedo et al., submitted (this issue));(Schaller et al., submitted (this issue)-a; Schaller et al., submitted (this issue)-b);(Sewer et al., submitted (this issue); Wong et al., submitted (this issue)). The eighth publication in the series describes a clinical study to assess whether the reduced formation of Harmful and Potentially Harmful Constituents (HPHC) for THS2.2 regular also leads to reduced exposure to HPHCs when the product is used in a clinical setting (Haziza et al., submitted (this issue)). A final publication utilizes data gathered from the reduced exposure clinical study on THS2.2 regular to determine if a systems pharmacology approach can identify exposure response markers in peripheral blood of smokers switching to THS2.2 (Martin et al., submitted (this issue)).

In this part, the systems toxicology arm of a 90-day rat inhalation study for the assessment of THS2.2M compared with cigarette smoke (CS) from reference cigarettes is presented. The overall study was conducted according to OECD test guideline 413: the exposure characteristics, classical endpoints, and

62 global molecular response profiles are summarized in our accompanying manuscript (part 6 (Oviedo et
63 al., submitted (this issue)).

64 A challenge with standard toxicological endpoints is that they are often detectable only after substantial
65 damage has already occurred and therefore can lack sensitivity (Ellinger-Ziegelbauer et al., 2011). In
66 addition, the limited mechanistic insights gained can hamper the refinement and eventual replacement
67 of these traditional animal tests (OECD, 2013). Thus, (i) to increase sensitivity, (ii) to obtain additional
68 insights into the molecular mechanisms of toxicity, and (iii) to gain knowledge that could eventually be
69 applied to reduce the number of animal studies, we complement the standard endpoints in these studies
70 with systems toxicology approaches – using transcriptomics, proteomics, and lipidomics measurements
71 (Sauer et al., 2015; Sturla et al., 2014).

72 Briefly, in this study, groups of male and female rats were exposed for 90 days to three different
73 concentrations of THS2.2M aerosol: 15 µg nicotine/L (low, THS2.2M(L)), 23 µg nicotine/L (medium,
74 THS2.2M(M)), and 50 µg nicotine/L (high, THS2.2M(H)) (Figure 1). THS2.2M aerosol exposure was
75 compared with CS from three different reference cigarettes: the 3R4F standard reference cigarette, and
76 corresponding low (LM) and high (HM) mentholated reference cigarettes (MRCs). Importantly, the
77 nicotine concentration in the CS of these reference cigarettes (23 µg/L) was matched to the nicotine
78 concentration in the aerosol of the medium THS2.2M (THS2.2M(M)). In addition, for female subsets from
79 the exposure groups Sham, 3R4F, MRC(HM), and THS2.2M(H), the recovery of the exposure-related
80 effects after a subsequent fresh-air exposure for 42 days was assessed (Figure 1). For the systems
81 toxicology analyses, respiratory nasal epithelium and lung tissue were collected and the molecular
82 exposure responses of the transcriptome and proteome were measured. In addition, exposure effects on
83 lung lipids were measured using lipidomics. These data were analyzed bioinformatically (Martin et al.,
84 2014; Titz et al., 2014; Titz et al., 2015a) and evaluated in the context of the overall study, for example, in
85 relationship to the histopathology results.

Altogether, our systems toxicology approach demonstrates the added benefit of these mechanistic details (e.g., on the decreased involvement of specific cell types and molecular response programs) and further supports the reduction in biological effects caused by THS2.2M aerosol exposure compared with CS from the reference cigarettes.

Materials and Methods

Experimental design

The study was conducted to characterize potential adverse effects caused by subchronic exposure to an aerosol from the mentholated tobacco heating system THS2.2M, a *heat-not-burn* tobacco product, and to compare them with the effects induced by CS generated from three reference cigarettes (Figure 1) (part 6, (Oviedo et al., submitted (this issue))). In addition to the recommendations in OECD TG413 for study designs, additional rats were included for the purpose of obtaining 'omics' endpoints. These rats were subjected to the same exposure conditions and handling times as the rats in the OECD study. As required, three dose levels of the THS2.2M aerosols were tested. Respiratory nasal epithelium and lung tissue were collected from the exposed rats and after a recovery period of 42 days, and used for the generation of transcriptomic, proteomics, and lipidomics data.

Reference cigarettes and THS2.2M

Standard reference 3R4F cigarettes were purchased from the University of Kentucky (Lexington, KY, USA, http://www.ca.uky.edu/refcig). In addition, two MRCs were produced by Philip Morris International, Neuchatel. The MRCs were designed so that the nicotine, total particulate matter, and CO levels in the smoke matched the levels of the 3R4F reference cigarette. The menthol yield in the smoke from the MRCs was 2.04 mg/cig (MRC(LM)) and 2.58 mg/cig (MRC(HM)) when smoked according to the ISO 3308 standard (International Organization for Standardization: 3308, 1991). For more details see (part 6, (Oviedo et al., submitted (this issue))). The reference cigarette 3R4F was used as the internal reference in this study.

THS2.2 has three distinct components: (i) a *tobacco stick* with unique processed tobacco made from tobacco powder, (ii) a holder into which the *tobacco stick* is inserted and which heats the tobacco material by means of an electronically controlled heating blade, and (iii) a charger that is used to recharge the holder after each use. The holder heats the *tobacco stick* at a temperature not exceeding 350°C (for more

details please refer to (Smith et al., submitted (this issue)). The mentholated version of THS2.2 (THS2.2M), assessed here (blend type *FR1/Menthol*), produces a menthol yield in the aerosol condensate of 2.09 mg/cig when smoked according to ISO 3308 standard (International Organization for Standardization: 3308, 1991). The THS2.2M were provided by Philip Morris Products S.A., Neuchâtel, Switzerland. For more details see (part 6, (Oviedo et al., submitted (this issue))); and for more information on the chemical analysis of smoke constituents see (Schaller et al., submitted (this issue)-a).

Animals

All procedures involving animals were performed in an AAALAC (Association for Assessment and Accreditation of Laboratory Animal Care International) accredited, AVA-licensed (Agri-Food & Veterinary Authority of Singapore) facility with approval from an Institutional Animal Care and Use Committee, in compliance with the National Advisory Committee for Laboratory Animal Research Guidelines on the Care and Use of Animals for Scientific Purposes.

Outbred male and female Sprague-Dawley rats [Crl:CD(SD)], bred under specific pathogen-free conditions, were obtained from Charles River, USA. The rats were approximately 6–7 weeks old on arrival and their health status was attested by the health check certificate provided by the breeder. The rats were kept and exposed in an animal laboratory with restricted access under controlled conditions of good hygiene. The laboratory air was filtered and positive pressure was maintained inside the laboratory. The room temperature was maintained at 22 ± 3°C and the relative humidity at 54 ± 4 %. The light/dark cycle was 12 h/12 h. All rats were individually identified by subcutaneously implanted transponders. The rats were acclimatized for a minimum of 16 days prior to exposure. For more details see (part 6, (Oviedo et al., submitted (this issue))).

Smoke and aerosol generation and animal exposure

The rats were nose-only exposed for a period of 13 weeks (6 h/d, 5 d/week) to filtered air (Sham), reference CS (23 µg/L nicotine) generated from the three reference cigarettes, or to three concentrations of THS2.2M aerosol (15, 23, 50 µg/L nicotine). For more details including on the smoke and aerosol generation, monitoring of the aerosol composition, exposure conditions, and markers of exposure see the ~~previous~~ part 6 of this series (Oviedo et al., submitted (this issue)).

For the molecular end points analyzed here, six male and six female rats were allocated to each of the following groups: the filtered, conditioned air group (Sham), and six smoke exposure groups, RC (3R4F) 23 µg nicotine/L; MRC(LM) 23 µg nicotine/L; MRC(HM) 23 µg nicotine/L; THS2.2M(L) 15 µg nicotine/L; THS2.2M(M) 23 µg nicotine/L; and THS2.2M(H) 50 µg nicotine/L. In addition, six female rats for each of the Sham, 3R4F, MRC(HM), and THS2.2M(H) groups were kept for a 42 days recovery period. For more details see (part 6, (Oviedo et al., submitted (this issue))).

Tissue preparation for 'omics' endpoints

Dissection was performed 16–20 hours after the last exposure. Prior to organ removal, a whole body perfusion with cold saline was performed. For the transcriptomics analysis, respiratory nasal epithelium (RNE) was isolated from the left side of the nose. For the proteomics analysis, RNE was isolated from the right side of the nose. The left lung lobe was cryosectioned into 40 µm slices, and the slices were collected alternating for transcriptomics and proteomics analysis.

Transcriptomics analysis

RNA from the RNE and lung samples was isolated using a miRNeasy extraction kit (Qiagen, Hilden, Germany) with the modification that RLT buffer (Qiagen) with beta-mercaptoethanol was used to lyse the lung slices. RNA was processed for hybridization on GeneChip® Rat Genome 230 2.0 Arrays (Affymetrix, Santa Clara, USA) using a High-Throughput 3' In Vitro Transcription PLUS kit (Affymetrix). Four RNE

158 samples were eliminated because of low RNA concentration or poor RNA quality. Five lungs samples were
159 not processed in the Affymetrix pipeline because the RNA concentration or quality was insufficient.

160 Raw data files were processed in the custom Chip Description File environment Rat2302_Rn_ENTREZG
161 v19.0.0 (rat2302rnentrezgcdf) (Dai et al., 2005) and normalized using frozen robust microarray analysis
162 (fRMA) (McCall et al., 2010). The normalization vector needed for fRMA was created using a set of 1023
163 microarray rat samples from 11 tissues and the R package frmaTools version 1.18.0. Quality controls,
164 including log-intensities, normalized-unscaled standard error (NUSE), relative log expression (RLE),
165 median absolute value RLE (MARLE), and pseudo-images as well as raw image plots, were performed with
166 the affyPLM package (Bioconductor, USA) (Bolstad et al., 2003). Following the quality control procedures,
167 raw p-values were generated for contrasts between Sham and exposed groups with the limma package
168 (Smyth, 2004), and adjusted using the Benjamini–Hochberg false discovery rate (FDR) multiple test
169 correction (Gentleman et al., 2004).

170 ***Proteomics analysis***

171 Proteome alterations were assessed by isobaric-tag based quantification using the iTRAQ® approach (Titz
172 et al., 2015a). For this, rat right RNE samples were homogenized and sonicated in tissue lysis buffer
173 (BioRad, Hercules, CA, USA) in random order and the proteins were precipitated with acetone. Frozen rat
174 lung tissue slices were homogenized using a bead-assisted procedure in Tissue Lyser II (Qiagen, Valencia,
175 CA, USA) in tissue lysis buffer before acetone precipitation. Protein precipitates were resuspended in 0.5
176 M triethylammonium bicarbonate (TEAB, Sigma-Aldrich, St. Louis, MO, USA), 1 M urea (Sigma-Aldrich)
177 and 0.1% SDS (Sigma-Aldrich). Then, 50 µg of the suspension was processed using the iTRAQ 8-plex
178 labeling procedure according to the manufacturer's instructions (AB Sciex, Framingham, MA, USA).
179 Trypsin (Promega, Madison, WI, USA) was added to the samples in a 1:10 trypsin to protein ratio (w/w)

followed by overnight digestion at 37°C. The tryptic digested samples were labeled with the reporter-ion tags for the different exposure groups for two separate iTRAQ analysis sets.

Two multiplexed iTRAQ analysis sets were prepared to allow for all relevant comparisons. iTRAQ set 1 contained all the 90-day time point samples. Each 8-plex labeling replicate set included one sample of each 90-day exposed sample (Sham, RC(3R4F), MRC(LM), MRC(HM), THS2.2M(L), THS2.2M(M), and THS2.2M(H)) and one pooled reference mix containing all replicates from the 90-day time point. For each of the 12 replicates in iTRAQ set 1, either a male or female sample was picked randomly. Within each replicate labeling set, the sample to channel mapping was randomized. iTRAQ set 2 was used to focus on the exposure and 90+42d recovery effect for female rats only. Each 8-plex labeling set included one of each 90+42-day sample (Sham, RC(3R4F), MRC(HM), and THS2.2M(H)) and a female sample of each corresponding 90-day time point. Again, the biological replicates were randomly assigned to the (six) replicate labeling sets and for each set the sample to channel mapping was randomized. Missing samples were replaced randomly by another replicate from the same group. These duplicate, placeholder samples were removed after data analysis and processing.

All the labeled samples that belonged to one iTRAQ replicate set were pooled and dried in a SpeedVac (RVC 2-25 CD Plus, Martin Christ, Osterode am Harz, Germany). Samples were desalted by passing them first through 0.5 mL bed volume detergent removal columns (Pierce, Rockford, IL, USA) and then through 1 cc C18 reversed phase SepPak columns (Waters, Milford, MA, USA) according to the manufacturers' manuals. Samples were dried in a SpeedVac and resuspended in nanoLC buffer A (5% acetonitrile (Sigma-Aldrich), 0.2% formic acid (Sigma-Aldrich)).

Samples were analyzed in random order using an Easy nanoLC 1000 instrument (Thermo Scientific, Waltham, MA, USA) connected online to a Q-Exactive (Thermo Scientific) mass-analyzer. Peptides were separated on a 50 cm long C18 RP RSLC Easyspray column (2 µm particle size; Thermo Scientific) at a flow

rate of 200 nL/min with a 200 min gradient from nanoLC buffer A to 40% acetonitrile with 0.2% formic acid. Each sample was injected twice with two different analysis methods: a fast and a sensitive method, as described by Kelstrup et al. (Kelstrup et al., 2012), on the same column. The outputs of both mass-spectrometry runs were combined as merged mass-lists and searched against the rat reference proteome set (UniProt, version October 2013, canonical isoforms only) using Proteome Discoverer version 1.4.0.288 software (Thermo Scientific). SequestHT (implemented in Proteome Discoverer) was used as the search tool and iTRAQ-reporter ion intensities were determined from Proteome Discoverer. The Percolator node of Proteome Discoverer was used to estimate peptide-level adjusted p-values (q-values). iTRAQ peptide-level quantification data were exported and further processed in the R statistical environment (R Development Core Team, 2007). The quantification data were filtered for a q-value < 0.01 and for "unique" quantification results as defined in Proteome Discoverer. A global variance stabilizing normalization (VSN) was performed with the corresponding Bioconductor package in R (Huber et al., 2002; Hultin-Rosenberg et al., 2013). Each iTRAQ reporter ion set was normalized to its median and protein expression values were calculated as the median of these normalized peptide-level quantification values (Herbrich et al., 2013). To detect differentially abundant proteins, a linear model was fitted for each exposure condition and the corresponding Sham group, and p-values were calculated from moderated t-statistics with the empirical Bayes approach (Gentleman et al., 2004). The Benjamini-Hochberg False Discovery Rate (FDR) method was then used to correct for multiple testing effects. Proteins with an adjusted p-value < 0.05 were considered as differentially abundant.

Lipidomics analysis

Lipid molecules were extracted from lung tissue and quantified by Zora Biosciences (Espoo, Finland) according to internal Standard Operating Procedures, Lab Method Sheets, and data Processing Method Sheets (Ansari et al., 2016). Lipid levels were normalized to their respective internal standards and tissue weight. Concentrations of molecular lipids are presented as pmol/µg wet tissue.

Statistical analysis of the lipidomics data was similar to the analyses of the transcriptomics and proteomics data. Samples with a total summed lipid concentration below the first quartile (1.5 x the interquartile range) were excluded. For the detection of differentially abundant lipids, only lipid species that were present/quantified in at least 50% of the samples of each compared group were included. A linear model was fitted for each exposure condition and the corresponding Sham group, and p-values from a moderated t-statistic were calculated with the empirical Bayes approach (Gentleman et al., 2004). The Benjamini–Hochberg FDR method was used to correct for multiple testing effects. Lipids with an adjusted p-value < 0.05 were considered differentially abundant.

Systems biology network analysis

To quantitatively assess the perturbation of relevant biological response systems, we employed previously defined cellular network models (Boué et al., 2015; Schlage et al., 2011) in conjunction with a network scoring algorithm that predicts the activation of these cellular networks based on transcriptomics data (Martin et al., 2014; Martin et al., 2012). Briefly, this approach relies on two-layer causal network models, in which the lower layer represents the transcriptional changes and the upper layer represents the actual causal network model. Both layers are linked and transcriptional changes in the lower layer are used to deduce the activity of the components in the upper layer, which are then aggregated into the final network score. The method uses gene expression data without a fold change or p-value cut off. The biological mechanisms covered by the networks reflect relevant processes of the respiratory system including inflammation, cellular fate, tissue repair and angiogenesis, cellular stress, and cellular proliferation. Each network was built in a modular way, where each module (sub-network) describes a specific biological aspect of the entire network. The modules can be decomposed to provide another level of detail (Kogel et al., 2014).

Additional data analysis methods

Gene sets were obtained from the Molecular Signatures Database (mSigDB) (Liberzon et al., 2011). Set analysis was supported by the Piano package in the R statistical environment (Väremo et al., 2013). Set enrichment was assessed by gene-set analysis with the (absolute) log2 fold-change as the gene/protein statistic and the mean as the set statistic. Gene/protein permutation and sample permutation were used to assess statistical significance. P-value adjustment was done with the Benjamini-Hochberg procedure. Sparse partial least squares approach was conducted in the canonical mode with the mixOmics package in R (Lê Cao et al., 2009). Functional associations among proteins were obtained from the STRING database (Szklarczyk et al., 2015). Functional clusters were annotated manually guided by ToppGene (Chen et al., 2009). Immune-cell markers were taken from the literature (Supplementary Table 1).

Data availability

The mass spectrometry proteomics data are available from the ProteomeXchange Consortium via the PRIDE partner repository (http://www.ebi.ac.uk/pride/archive/)(Vizcaíno et al., 2014). The database identifiers for the lung and respiratory nasal epithelium datasets are PXD003580 ~~(Username: reviewer48978@ebi.ac.uk; Password: 92Yf6clk; reviewer account information; data will be made public when manuscript is published)~~ and PXD003591 ~~(Username: reviewer48401@ebi.ac.uk; Password: o54W9z5v)~~. The lipidomics data are available in Supplementary Table 2. The transcriptomics data have been submitted to ArrayExpress with the identifier ~~:~~ E-MTAB-4493 ~~(Username: Reviewer_E-MTAB-4493, Password: fbjjacu6)~~.

Results

Histological and molecular exposure response of the respiratory nasal epithelium

Consistent with the common exposure response to CS exposure (Gaworski et al., 1997; Kogel et al., 2014; Vanscheeuwijck et al., 2002), the reference cigarette exposures in this study resulted in several typical histopathological changes in the rat respiratory nasal epithelium (RNE) (see part 6, (Oviedo et al., submitted (this issue))). These changes included squamous cell metaplasia, basal cell hyperplasia, and mixed cell infiltrates in the submucosa. The latter indicated an inflammatory response in the tissue exposed to CS. In contrast, the RNE of rats exposed to THS2.2M aerosol showed fewer and less severe histopathological changes; only the highest THS2.2M aerosol concentration was associated with squamous cell metaplasia and a mixed cell infiltrate in the submucosa. Of note, after the 42-day recovery period several changes induced by CS-exposure including squamous cell metaplasia and the mixed cell infiltrate reverted only partially, whereas in the THS2.2M exposed groups the histopathological changes in the RNE reverted nearly completely.

To analyze the molecular changes that occurred in the RNE, we identified the significantly (FDR-adjusted p-value < 0.05) differentially expressed/abundant genes and proteins after exposure to CS from the reference cigarettes and THS2.2M aerosol compared with Sham exposure (Supplementary Figure 1A and B). Reference smoke exposure after 90 days induced extensive changes in both the transcriptome and the proteome. For example, more than 8000 genes and 1300 proteins were statistically significantly affected by the 90-day exposure to MRC(LM) in female rats. In contrast, the THS2.2M(L) and THS2.2M(M) aerosols induced a very low to absent differential response in the RNE. While THS2.2M(H) induced molecular changes, these remained well below the changes induced by the reference cigarettes (at twice the concentration with respect to the applied nicotine ~~concentration~~).

To reveal which biological processes were most prominently perturbed by the exposure conditions, a threshold-free, network-based systems biology approach was applied. This approach relies on our published collections of hierarchically structured biological network models (Boué et al., 2015; Gebel et al., 2013; Schlage et al., 2011; Westra et al., 2011; Westra et al., 2013). These manually curated models reflect relevant respiratory system processes that contribute to inflammation, cellular fate, tissue repair and angiogenesis, cellular stress, and cellular proliferation. For each of these network models, the degree of network perturbation caused by exposures to different aerosols is computed based on the measured changes in the transcriptome of the target tissue, and the overall biological impact for all networks is summarized based on the contributions of the different biological process categories (Martin et al., 2014). After 90 days of exposure to smoke from the three reference cigarettes, the transcriptomes of both male and female rats displayed network perturbations with similar levels of contributions from all five biological networks (Figure 2B). RNE exposed to aerosol from THS2.2M showed a much lower overall network perturbation; and a clear response was detected only for female rats exposed to THS2.2M(H). Exposure effects for 3R4F and MRC(HM) reverted partially after the 42-day recovery period. The perturbations detected for the subnetworks of these five biological processes are represented in Supplementary Figure 2 A and B.

To complement this analysis, we also identified significantly affected gene and protein sets (FDR-adjusted p-value < 0.05, Figure 2B, Supplementary Figure 3). Overall, the effects observed for gene sets were much less pronounced in RNE exposed to THS2.2M aerosol compared with CS exposure. Clustering of the enrichment results revealed several biological processes affected by CS exposure that could be linked to the observed adaptive changes of the RNE, such as epithelial cell differentiation, extracellular structure organization and tissue remodeling, and cell proliferation and migration processes (Figure 2B). Moreover, immune-response processes were found to be enriched.

Effects of exposure on molecular marker panels for respiratory nasal epithelium

To more specifically evaluate how the changes in tissue architecture are reflected at the molecular level, known markers for different epithelial cell types (e.g., basal cells, goblet cells, and squamous cells) and basal lamina components were assessed (Figure 3A, Supplementary Table 1A). This panel included several keratins, which have been identified as differentiation markers for rat nasal epithelium (Schlage et al., 1998a; Schlage et al., 1998b). For example, Krt14 and Krt15, which have been associated with a hyper- and metaplastic respiratory epithelium (Schlage et al., 1998b), were clearly up-regulated and increased in protein level abundance in the CS exposed groups. The small proline-rich proteins (Sprr1a and Sprr3) also were up-regulated on the gene expression level and increased partly in protein abundance. Sprr1a and Sprr3 are components of the cross-linked envelope of epithelial cells and a human ortholog has been identified as a biomarker for squamous metaplasia (Tesfaigzi and Carlson, 1999). Furthermore, basal lamina components were clearly up-regulated and increased in abundance, which likely reflects the active tissue remodeling processes in the CS-exposed RNE. The up-regulation and increased abundance of proliferating cell nuclear antigen (Pcna) supported an overall more proliferative state of the CS- exposed RNE. Overall, rats exposed to CS from the reference cigarettes showed a clear increase in these and other basal cell and squamous cell markers, which is in line with the histopathological observation of basal cell hyperplasia and squamous metaplasia without and with cornification. Further, the molecular analysis indicated an increase in goblet cell numbers and a goblet cell response (e.g., increase in the mucins Muc5ac and Muc5b). THS2.2M aerosols induced these markers of an adaptive tissue response to a much lower degree, and significant effects were observed only for the highest THS2.2M (THS2.2M(H)) concentration, in female rats.

In addition, a marker panel for immune cell types (Figure 3B, Supplementary Table 1B) was evaluated to investigate if the mixed cell infiltrate that was found in the histological evaluation could also be detected at the molecular level. Markers for both macrophages (e.g., Cd14, Cd68, and Lgals3) and neutrophils (e.g., Mpo, Lcn2, and Camp) were clearly up-regulated and increased in abundance upon CS exposure. Markers

for T-cells (e.g., the Cd3 T-cell receptor components) and B-cells also were up-regulated, but this was less pronounced and was detected only at the RNA level. In contrast, THS2.2M exposure only marginally affected these immune-cell markers; indeed, macrophage and neutrophil markers were up-regulated and increased in abundance only for THS2.2M(H) in female rats. While this response to THS2.2M(H) exposure was not detectable after the 42 day recovery period, a macrophage and neutrophil response was still detectable for 3R4F and MRC(HM) after the recovery period.

In summary, the systems toxicology analysis reconfirmed and complemented the histopathology results by providing insights into the effects on specific cell types and the cellular adaptation programs that were impacted by CS and to a lesser degree by THS2.2M aerosol exposure in the RNE.

Histological and molecular exposure response of the lung tissue

As described in the accompanying manuscript in this series (Oviedo et al., submitted (this issue)), histopathological evaluation of the lung revealed an increase of pigmented and unpigmented macrophages in the alveolar lumen, and goblet cell hyperplasia in the bronchi. Those are typical smoke-related as well as dose-dependent adaptive and inflammatory responses of the lung after exposure to CS in inhalation studies (Coggins et al., 1989; Piade et al., 2014; Vanscheeuwijck et al., 2002). In contrast, the histopathology evaluation of the lungs exposed to THS2.2M aerosol showed a lower response compared with the lungs from rats exposed to CS (part 6,(Oviedo et al., submitted (this issue))). Furthermore, whereas CS exposure resulted in an increase in the free cell counts in bronchoalveolar lavage fluid (BALF) including neutrophils and macrophages, and several inflammatory mediators such as Mcp1/3 and Csf1, THS2.2M aerosol exposure resulted in very limited changes in these immune-related endpoints (part 6, (Oviedo et al., submitted (this issue)).

To complement these comparisons and to gain further insights into the differential molecular responses, microarray-based mRNA expression profiling and quantitative proteomics was conducted for the lung

tissue. CS resulted in a maximum of 2865 differentially expressed genes for female rats exposed to MRC(LM) (adjusted p-value < 0.05, Supplementary Figure 1C), while very few genes were differentially expressed after THS2.2M exposure compared with the Sham group (a maximum of 45 genes were differentially expressed in lung tissue from female rats exposed to THS2.2M(H)). After the 42-day recovery phase, differentially expressed genes in response to CS were still detectable but their numbers were reduced (Supplementary Figure 1C). On the whole, the differential protein abundance in response to the exposures confirmed the trends observed for the transcriptomics data (Supplementary Figure 1D), but at the same significance threshold (adjusted p-value < 0.05) the number of differentially abundant proteins was lower (a maximum of 166 proteins for females exposed to MRC(HM)) than the number of differentially expressed genes.

Again, the threshold-free, network-based systems biology approach was applied for quantification of the response of the network models based on the lung transcriptomics data (Figure 4A) (Martin et al., 2014). After 90 days of exposure to CS from the three reference cigarettes, similar levels of network perturbations were detected in the lung tissue of male and female rats with contributions from all five networks: inflammation, cellular fate, tissue repair and angiogenesis, cellular stress, and cellular proliferation. The responses of the individual scored subnetwork models are shown in Supplementary Figure 2C and D. The THS2.2M aerosol produced a much lower overall network perturbation compared with reference CS exposures. Overall, in male rats, the response to THS2.2M exposure was low and increased slightly with concentration, whereas, in female rats, the response to THS2.2M exposure was higher than in male rats, but well below the response to CS exposure. The effects induced by 3R4F and MRC(HM) in females recovered only partially after the 42-days recovery period.

To further complement this analysis, a functional association clustering approach was applied to both the transcriptomic and the proteomic data (Figure 4B and C, Supplementary Figure 4) (Fang and Gough, 2014; Titz et al., 2015a). Functionally associated genes/proteins were linked and differentially

385 expressed/abundant functional clusters were identified. The identified gene and protein clusters included
386 immune-related, oxidative-stress and xenobiotic response, unfolded-protein response, oxidative
387 phosphorylation, and metabolism clusters. In general, the components of these clusters were up-
388 regulated upon exposure to CS from the reference cigarettes and to aerosols from THS2.2M; however,
389 the exposure response to THS2.2M aerosol was lower. Thus, the data-driven functional interpretation
390 approach confirmed the lower effects observed for THS2.2M aerosol exposure compared with CS
391 exposure. Gene and protein set enrichment analyses further confirmed the overall trends and especially
392 highlighted processes linked to the inflammatory response (Supplementary Figure 5).

393 ***Effects of exposure on molecular markers for the immune response in the lung***

394 To follow-up on the effects of CS on the lung immune system, the expression/abundance of immune-cell
395 markers was evaluated (Figure 5A). CS exposure resulted in a clear increase in macrophage markers such
396 as Cd14 and Cd68 and of neutrophil-associated proteins/genes such as Lcn2 and Mpo. In contrast,
397 lymphoid cell markers, especially T-cell markers such as Cd2 and Cd3, were significantly decreased in
398 response to CS exposure. THS2.2M exposure did not significantly affect the abundance of macrophage or
399 neutrophil markers; however, a dose-dependent reduction in T-cell markers was observed, with Cd3d and
400 Cd8b being significantly reduced in female rats in response to THS2.2M(H) exposure.

401 To further support and quantify these differences, it was measured how the exposure conditions affected
402 both the macrophage and the neutrophil signaling network models (Figure 5B and C). In both models, the
403 response to THS2.2M exposure was very limited. Interestingly, both processes were found to be still
404 activated in the CS exposed groups after the 42-day recovery period, which is in overall agreement with
405 the marker profiles (Figure 5A), histopathological evaluation, and BALF profiling results (part 6, (Oviedo et
406 al., submitted (this issue))).

It has been reported that CS induces an immune state, which involves polarization of macrophages toward the M2 phenotype (Shaykhiev et al., 2009; Stämpfli and Anderson, 2009; Titz et al., 2015b). Whereas M1 macrophages are associated with classical immune-responses, M2 macrophages have been, for example, implicated in tissue repair processes (Mantovani et al., 2013). Here, the prominent up-regulation of Retnla (resistin-like protein a) was noted (Figure 5D). Retnla (also called FIZZ1) is one of the key markers for M2 macrophages (Martinez et al., 2006). Other key M2 markers such as Arg1 and chitinases (Chi3l1/Ym-1, Chia), and important contributors to M2 polarization such as Hmox1 (Heme oxygenase-1) (Naito et al., 2014) and Lgals3 (galectin-3) (Novak et al., 2012; White and Gomer, 2015) were also increased upon CS exposure. Furthermore, CS exposure resulted in a general induction of markers that were defined previously for human M2 macrophages (Supplementary Figure 6A) (Shaykhiev et al., 2009). In contrast, however, the marker genes defined for human M1 macrophages did not show a clear trend; for example the M1 macrophage marker Cd86 was up-regulated and the M1-associated components of the interferon signaling axis (Irf1/7) was down-regulated (Supplementary Figure 6B). In addition, several cytokines that indicate a pro-inflammatory response were increased in BALF (e.g., Mcp1/3) (part 6, (Oviedo et al., submitted (this issue))). Of note, Csf1 (M-CSF), which is associated with M2 polarization, was also significantly increased upon CS exposure (Hamilton et al., 2014).

Overall, this analysis demonstrated a strong and specific effect of the CS from all three reference cigarettes on the lung immune system. In contrast, THS2.2M aerosol exposure resulted in a much more limited effect on the lung immune system.

Analysis of the cellular stress response in the lung tissue

Xenobiotic metabolism and oxidative stress responses are commonly induced by CS (Wooten et al., 2006). The response of the oxidative stress and the xenobiotic metabolism response subnetworks that are part of the cellular stress (CST) network compendium were compared (Supplementary Figure 2C and D). An

oxidative stress response was observed in rats exposed to CS for all three reference cigarettes (Figure 6A). Interestingly, this response was only partially reduced after the 42-day recovery period. In contrast, the three tested THS2.2M aerosol concentrations induced only a limited (although, still significant) effect on the oxidative stress network in both sexes. The xenobiotic metabolism response network demonstrated a similar response difference between rats exposed to CS and THS2.2M aerosol, but this response appeared to recover more completely after the 42-day exposure to filtered air (Figure 6B).

To reconfirm these observations and to obtain additional molecular detail, the differential expression response of gene sets related to these cellular stress responses was evaluated; namely, the reactive-oxygen species (ROS) and xenobiotic response, and the functionally related unfolded-protein response (UPR) (Figure 6C). CS activated an extensive oxidative stress response program, which involved the glutathione system (e.g., glutamate-cysteine ligase (Gclc), glutaredoxin (Glrx), glutathione-S-transferases (GSTs)), the thioredoxin system (thioredoxin (Txn2) and thioredoxin reductase 1 (Txnrd1)), superoxide dismutase 2 (Sod2) and quinone NAD(P)H dehydrogenase 1 (Nqo1), and metabolic adaptations toward NAPDH generation (glucose-6-phosphate dehydrogenase (G6pd)). Other genes/proteins that were up-regulated/increased by CS and involved in the xenobiotic response included aldehyde dehydrogenase 3 (Aldh3a1/Aldh3b1) and the aldo-keto reductase 1c3 (Akr1c3). Oxidative damage to proteins has been reported to also induce endoplasmic reticulum stress and the unfolded-protein response (UPR) (Hengstermann and Müller, 2008; Jorgensen et al., 2008; Kelsen et al., 2008). Here, CS induced the expression of several UPR marker genes and, in female rats, significantly increased the abundance of the UPR proteins calreticulin (Calr), Grp-78 (Hspa5), and Pdia6 (Mei et al., 2013). This suggests an adverse, possibly ROS-mediated, effect of CS on lung protein metabolism, which was much reduced in the THS2.2M aerosol exposure groups.

Taken together, these results suggest that CS exposure triggered a clear stress response in the lung tissue of the rats, which included broad oxidative stress, xenobiotic, and unfolded-protein responses and was confirmed at the transcriptome and the proteome levels. In contrast, THS2.2M aerosols, even at the highest concentration, triggered a much lower response in these cellular stress pathways.

Analysis of the lung lipidome

CS exposure has been associated with extensive alterations in the lung lipid metabolism (Bodas et al., 2015; Morissette et al., 2015; Telenga et al., 2014; Titz et al., 2016). Here, a lipidomics analysis revealed changes in lung lipids for the tested exposure conditions (Figure 7A). The most consistent effects on the lipidome observed in this study were on several sphingolipid classes: sphingomyelins (SM), ceramides (Cer), glucosyl-/galactosyl-ceramides (Glc/GalCer), lactosyl-ceramide (LacCer), and globotriaosyl-ceramides (Gb3), which was in line with previous studies (Bodas et al., 2015; Telenga et al., 2014; Titz et al., 2016; Yang and Uhlig, 2011). Of note, d18:1/18:0 and d18:1/20:0 Glc/GalCers decreased in response to CS exposure in this and a previous ApoE$^{-/-}$ mouse study (Titz et al., 2016), which likely indicates chain-length specific properties of these sphingolipids (Grösch et al., 2012).

Whether these changes in sphingolipid levels were reflected in the enzymes involved in sphingolipid metabolism was examined. While only a few of these enzymes were quantified at the protein level, several genes encoding sphingolipid metabolism enzymes showed significant differential mRNA expression (Supplementary Figure 7A). To determine whether the differential expression followed any particular pattern, the changes were mapped onto the sphingolipid metabolism map (Supplementary Figure 7B) and the main effects related to the measured sphingolipid classes are summarized in Figure 7B. The mRNA transcript of the *de novo* ceramide synthesis enzyme Degs2 and the transcripts of the degradation enzymes for the glycosylated-ceramide lipids (e.g., Gba, Galc, and Glb1) were significantly up-regulated by reference CS exposure. In contrast, the transcript of Acer2, an enzyme that converts ceramide to

475 sphingosine, was significantly down-regulated. These expression changes generally pointed to ceramide
476 as the central component of the sphingolipid pathway — with the increase in the sphingolipid degradation
477 enzymes supporting the role of dynamic sphingolipid equilibrium in the response to CS exposure.

478 In summary, reference CS significantly affected the sphingo-lipidome and transcriptome, whereas the
479 effects of THS2.2M aerosol were much less and not statistically significant. While the expression changes
480 of the genes encoding sphingolipid metabolic enzymes showed a distinct pattern, the relationship with
481 the observed changes in lipid levels is complex. Nevertheless, these changes likely contribute to the
482 dynamic sphingolipid equilibrium as part of the overall regulation of tissue responses.

Discussion

In this paper the results from the systems toxicology arm ("OECD PLUS") of a standard 90-day rat inhalation study are reported that was conducted according to the OECD TG413 (part 6, (Oviedo et al., submitted (this issue))). Molecular profiling results complemented the classical endpoints and showed a consistent reduction in the biological effects in the rat RNE and lung tissue for THS2.2M aerosol exposed compared with CS exposed rats.

Overall, this study exemplified how classical toxicology endpoints (e.g., histopathology) can be complemented effectively by extensive molecular measurements and computational analyses within a systems toxicology framework (Sturla et al., 2014). The systems toxicology approach facilitates a deeper (mechanistic) understanding of the complex biological responses to toxicant exposure, and supports a more comprehensive and possibly more sensitive assessment. Toxicants can affect all levels of the biological organization, including the transcriptome, proteome, and lipidome. Because of the maturity of the technology, transcriptomics analyses were engaged first to globally capture molecular responses to toxicants (Lovett, 2000; Nuwaysir et al., 1999). Although the potential benefits of including proteomics measurement for toxicity assessment were proposed much earlier (Burchiel et al., 2001), technical limitations made the effective use of proteomics for systems toxicology investigations challenging. However, with the development of new instrumentation, proteomics technology is now evolving rapidly and more and more studies are using proteomic data to support deeper insights into the mechanisms of toxicity (Titz et al., 2016; Titz et al., 2014). Similarly, lipidomics — also supported by the rapid progress in mass-spectrometry based assays — can be expected to contribute more and more to the elucidation of toxicological responses (Fernando et al., 2011). In this study, we applied all three technologies to compare the biological response of male and female rats to THS2.2M aerosol and CS. With this, we were able to identify the biological effects of CS exposure across these three levels of molecular organization. As expected, the detected responses were highly interconnected — including to the classical

histopathological endpoints. All in all, we found that the measurements on these three biological levels complemented each other (see below) and mutually increased the confidence in our conclusions, especially on the reduced biological effects of THS2.2M aerosol compared with CS exposure, which was found consistently on all three biological levels.

For RNE, we showed that in agreement with the observed massive adaptive changes in the architecture of this tissue, a large number of genes and proteins were significantly differentially regulated after CS exposure. By analyzing the enrichment of biological processes and signaling pathways, we found that there was high consistency between the molecular and histopathological findings. For example, we identified several processes affected by CS exposure that could be linked to the observed adaptive changes of the RNE, such as hyperplasia, stratification, and squamous differentiation of the RNE, extracellular matrix alteration and tissue remodeling, as well as cell proliferation and migration processes in general (Figure 2). Assuming that the up-regulation of specific cell markers largely reflects an increase of the respective cell types, we found an increase in basal cells and squamous-differentiated epithelial cells of squamous epithelium, specifically in the rats exposed to CS. In contrast, most of the tested markers that were differentially expressed in the RNE of rats exposed to CS, were not significantly affected in the RNE of rats exposed to THS2.2M aerosol. Some exceptions were found in female rats exposed to the high concentration of THS2.2M. For example markers such Sprr1 were significantly affected, which is also in concordance with the histological results (part 6, (Oviedo et al., submitted (this issue)).

Markers for ciliated cells such as Foxj1 and dynein subunits tended to be down-regulated, which correlates with the observed disappearance of ciliated cells in the areas of goblet cell hyperplasia and squamous metaplasia (see Figure 2). Ciliated cells are the hallmarks of respiratory epithelium and are found not only in the nasal cavity but throughout the respiratory tract; therefore, this finding is in line with previous literature, which showed that exposure to CS is associated with a decrease in cilia and ciliated cells (Simet et al., 2010). The airway epithelium of smokers has shorter cilia than that of non-smokers (Leopold et al.,

2009). Air-liquid interface *in vitro* cultures were shown to recapitulate the effect of CS on shortening cilia length and, in this system, CS extract was reported to have a broad inhibiting effect on the expression of a variety of genes related to ciliogenesis (Brekman et al., 2014). Further, the overexpression of the cilia-related transcription factor FOXJ1 was found to prevent the CS extract-mediated inhibition of cilia growth (Brekman et al., 2014).

Among the markers specific for secretory cells, Muc5b and, to a lesser degree, Muc5ac were found to be up-regulated in the RNE samples following CS exposure, although goblet cell hyperplasia (a higher number of mucus-producing cells) was observed in the histological sections of the region where the samples were taken from. This effect might be explained by the fact that a local loss of goblet cells was also found in other regions along the nasal septum and dorsal meatus (part 6, (Oviedo et al., submitted (this issue))). This observation represents a clear limit of molecular-level analyses. The spatial heterogeneity in tissues cannot be resolved, but separating different areas by laser capture microdissection may help overcome this shortcoming.

On the other hand, molecular methods were successful in characterizing the observed mixed cell infiltrates in more detail. Marker analysis indicated that these cells were likely macrophages and neutrophils, and less pronounced T- or B-cells. Young healthy smokers were reported to have increased numbers of macrophages, and exfoliated ciliated and goblet cells, as well as higher myeloperoxidase concentrations in their nasal lavage fluid compared with nonsmokers, and their nasal mucociliary clearance was higher (Nicola et al., 2014). However, other studies either found no differences in the nasal mucosa of smokers compared with non-smokers (Vachier et al., 2004), or reported reduced mucociliary clearance and ciliary motility, as well as a decreased ratio of ciliated to goblet cells in nasal mucosa biopsies from smokers compared with nonsmokers and former smokers (no difference was detected between nonsmokers and former smokers) (Pagliuca et al., 2015).

As obligate nose-breathers, rodents inhale CS exclusively through their nasal airways. In ~~constrast~~contrast, humans usually inhale CS through the mouth. Nasal tissue exposure in humans occurs mostly during exhalation of inhaled mainstream CS and additionally by some sidestream smoke in the surrounding atmosphere. Hence, the less pronounced and less consistent CS effects on human nasal epithelium must be seen against a background of individual variability in smoke uptake and smoking habit.

The airways of rats and mice generally undergo adaptive responses to CS exposure, and long-term exposure of lung tissue to CS can result in more permanent tissue changes in the deeper lung that are associated with chronic obstructive pulmonary disease (COPD) development (Chung and Adcock, 2008; Fischer et al., 2015; Titz et al., 2015b). In general, 90-day rat CS inhalation studies do not result in clear signs of a COPD-like disease such as emphysema; nevertheless, rats develop distinct pulmonary inflammation. It is generally recognized that rat models address asthma and chronic bronchitis, while emphysema development can be observed more easily in susceptible mouse strains (Wright and Churg, 2010; Yu et al., 2008). Accordingly, in this rat study, reference CS exposure resulted in an extensive inflammatory response, oxidative stress response, and perturbation of tissue repair networks, all of which are known to be associated with and contribute to the development of lung disease, including chronic bronchitis and small airway remodeling (Figure 4) (Chung and Adcock, 2008; Fischer et al., 2015; Zuo et al., 2014).

The inflammatory response of the lung was detected by transcriptome and the proteome analyses using three approaches: biological network-based analysis, gene-set analysis, and functional association clustering. Consistently, all three approaches showed the up-regulation of inflammatory processes upon exposure to CS but not to THS2.2M aerosol, and supported the overall conclusion that the effects of THS2.2M exposure were strongly reduced (even for the highest concentration ~~of 50 µg/L nicotine~~) compared with CS exposure. Specifically, we found evidence of the involvement of macrophages and neutrophils in this CS response (Figure 5). These molecular profiling results were well aligned with the

other endpoints of this study (part 6, (Oviedo et al., submitted (this issue))). Free immune cells and inflammatory mediators also were specifically increased in the BALF of CS-exposed rats, and the histopathology showed an increase in macrophages scattered within alveoli and aggregated in alveolar spaces upon CS exposure.

An interesting observation was that markers for M2 macrophages (e.g., Retnla, Arg1, and Chi3l1) were increased in lung tissue upon CS exposure (Figure 5D, Supplementary Figure 6A). The M1/M2 polarization concept of macrophages was initially defined as analogous to the Th1/Th2 T-cell concept, and the two states have been associated with different modes of activation (e.g., IFNγ vs. IL-4/IL-13) and different immune responses (e.g., viral vs. parasite clearance) (Mantovani et al., 2013). Consistent with our finding for CS exposure, several studies have reported the polarization of macrophages toward the M2 phenotype (Shaykhiev et al., 2009; Stämpfli and Anderson, 2009; Titz et al., 2015b). All in all, the engagement of the M2 macrophage population, which is known to be involved in lung repair processes (Johnston et al., 2012), suggests they may help the lung tissue to cope with the effects of CS exposure. However, it is important to note that macrophage differentiation and response is clearly more complex and does not fully fit into binary schemes (Martinez and Gordon, 2014) — as exemplified here by the less consistent response of the M1 polarization markers (Supplementary Figure 6A). Our observations can further motivate more systematic investigations into how the full spectrum of macrophage activation states contributes to the response of the lung to toxicological challenges (e.g., (Morissette et al., 2015; Xue et al., 2014)).

T-cell markers were lower in the lung tissues of CS-exposed rats than in the lung tissues of sham-exposed animals. Furthermore, gene/protein enrichment analysis indicated down-regulation of T cell activation (Supplementary Figure 5). For example, *in vitro* activated T cells cultured in the presence of CS extract were found to display a dose-dependent decrease in cell proliferation, which was associated with the induction of cellular apoptosis (Hernandez et al., 2013). The T cell receptor (TCR) is a multimeric protein complex composed of a clonotypic αβ heterodimer, a CD3 γδε chains, and a ζ homodimer (Valitutti et al.,

1997). Here, we found that the CD3 γδε and ζ chains in the lung tissue decreased upon CS exposure. Interestingly, the process of TCR-antigen (peptide-MHC) interaction is self-limited. The triggered TCRs are rapidly removed from the cell surface and are degraded in the lysosomes (Valitutti et al., 1997). Therefore, lower T-cell numbers or TCR down-regulation are possible alternative explanations that can best be resolved with additional experiments in future studies.

The constituents in CS pose an extensive xenobiotic and oxidative challenge for the lung tissue (Talhout et al., 2011). To counteract this challenge, lung tissue activates several oxidative and xenobiotic stress response systems (Cantin, 2010). Inflammatory and oxidative stress are tightly interconnected and likely facilitate each other (Morissette et al., 2015; Zuo et al., 2014). Here, we observed a clear xenobiotic and oxidative stress response in the lung upon CS exposure, and this response was much more limited upon exposure to THS2.2M aerosol (Figure 6). Cyp1a1 was the only xenobiotic enzyme that was significantly up-regulated upon THS2.2M exposure, which could likely be explained — in the absence of CS-typical inducers such as polycyclic aromatic hydrocarbons — by the up-regulation effect that nicotine-only exposure had on the expression of this gene (Phillips et al., 2015). Further supporting the strong xenobiotic and oxidative stress burden upon CS exposure, the lung tissue also showed a clear unfolded-protein response (UPR). The UPR reflects stress on the endoplasmic reticulum caused by proteins that have unfold as a result of, for example, oxidative damage (Hengstermann and Müller, 2008; Jorgensen et al., 2008; Kelsen et al., 2008). Taken together, the molecular analyses clearly revealed a strong stress burden on the lung tissue by CS exposure, and this burden was much reduced for all concentrations of THS2.2M aerosol exposure.

CS exposure also has been associated with extensive alterations in lung lipid metabolism (Lee et al., 2015; Lundstrom et al., 2011; Morissette et al., 2015; Telenga et al., 2014; Titz et al., 2016). The most consistent effect of CS exposure observed in this study was a significant increase in several sphingolipids (SM, Cer, Glc/GalCer, LacCer, and Gb3) (Figure 7A). Previously, we observed similar increases in sphingolipids in the

626 lung of mice upon CS exposure (Titz et al., 2016). Of note, this finding might also be related to
627 accumulating literature evidence that indicates the involvement of sphingolipid alterations in several lung
628 diseases including COPD (Lee et al., 2015; Yang and Uhlig, 2011). In a recent example, Telenga et al.
629 profiled the sputum lipidome of COPD subjects and found increased levels of several sphingolipids,
630 including ceramide and glycosphingolipids, compared with sputum lipidome of smokers without COPD
631 (Telenga et al., 2014). Of these glycosphingolipids, CS-induced accumulation of LacCer in the lung of COPD
632 subjects has been specifically implicated in processes that lead to emphysema (Bodas et al., 2015). While
633 the observed changes in the abundances of sphingolipid metabolic enzymes are more difficult to
634 interpret, overall they support changes in the dynamic equilibrium of sphingolipids — centered on
635 ceramide — that are induced by CS exposure (Figure 7B). As such, these effects likely reflect the complex
636 sphingosine network response, including feedback mechanisms, that as a whole determines their
637 phenotypic effects (Köberlin et al., 2015). We can conclude that CS had a clear effect on the sphingolipid
638 metabolism and induced a state that is similar to previously reported disease-related changes. In contrast,
639 THS2.2M aerosol exposure had much lower effects on sphingolipid metabolism.

640 **CONCLUSIONS**

641 In summary, this systems toxicology analysis supported an integrated product risk assessment of
642 THS2.2M. Consistently, the THS2.2M aerosols (even at the highest ~~nicotine~~ concentration) showed much
643 lower effects compared with smoke from reference cigarettes on the molecular profiles and molecular
644 response networks of respiratory nasal epithelium and lung tissue. They included biological processes
645 crucially linked to the development of lung disease, such as inflammation- and oxidative stress-related
646 processes. Thus, our systems toxicology endpoints complemented and augmented the more classical
647 endpoints of this OECD TG413 90-day rat inhalation study. Furthermore, this study revealed activated
648 toxicity pathways and associated candidate biomarkers that could further facilitate the development of
649 21st century toxicology assessment approaches (Krewski et al., 2010; Langley et al., 2015; Stephens et al.,

2012). Limitations of the employed omics technologies included the lack of spatial and cellular resolution of the detected changes, the lack of global activity measurements for the detected proteins, and the lack of information how the observed molecular changes are specifically linked to disease outcomes. In the future, complementary technologies could be adapted to fill these gaps and, importantly, the dense matrix of the systems biology-derived molecular data ~~may~~ could be used to ~~enhance the linking of~~more directly link the outcomes from the general purpose 90-day OECD TG413 subchronic inhalation studies~~y~~ to the more disease-specific results from animal models of, for example, COPD, cardiovascular disease, and lung cancer.

Acknowledgements

The authors would like to thank the study team, especially acknowledging the technical assistance and support of Camille Schilt, Lola Hamied, Karine Baumer, Polina Mironova, Remi Dulize, Sophie Scheuner, Sophie Dijon, Sam Ansari as well as Jenny Ho, Wei Teck Tan, Subash Krishnan and the bioresearch and aerosol team at PMIRL Singapore. The authors thank Maurice Smith and Emilija Veljkovic for their critical review.

Conflict of interest statement

The work reported in this publication involved a candidate Modified Risk Tobacco Product developed by Philip Morris International (PMI) and was solely funded by PMI. All authors are (or were) employees of PMI R&D or worked for PMI R&D under contractual agreements.

References

Field Code Changed

Ansari, S., et al., 2016. Comprehensive systems biology analysis of a 7-month cigarette smoke inhalation study in C57BL/6 mice. Sci Data. 3**,** 150077.

Bodas, M., et al., 2015. Lactosylceramide-accumulation in lipid-rafts mediate aberrant-autophagy, inflammation and apoptosis in cigarette smoke induced emphysema. Apoptosis. 20**,** 725-739.

Boué, S., et al., 2015. Causal biological network database: a comprehensive platform of causal biological network models focused on the pulmonary and vascular systems. Database. 2015**,** bav030.

Brekman, A., et al., 2014. FOXJ1 prevents cilia growth inhibition by cigarette smoke in human airway epithelium in vitro. Am J Respir Cell Mol Biol. 51**,** 688-700.

Burchiel, S. W., et al., 2001. Analysis of genetic and epigenetic mechanisms of toxicity: potential roles of toxicogenomics and proteomics in toxicology. Toxicological Sciences. 59**,** 193-195.

Cantin, A. M., 2010. Cellular response to cigarette smoke and oxidants: adapting to survive. Proc Am Thorac Soc. 7**,** 368-75.

Chen, J., et al., 2009. ToppGene Suite for gene list enrichment analysis and candidate gene prioritization. Nucleic Acids Res. 37**,** W305-11.

Chung, K., Adcock, I., 2008. Multifaceted mechanisms in COPD: inflammation, immunity, and tissue repair and destruction. The European respiratory journal. 31**,** 1334.

Coggins, C. R., et al., 1989. Ninety-day inhalation study in rats, comparing smoke from cigarettes that heat tobacco with those that burn tobacco. Fundam Appl Toxicol. 13**,** 460-83.

Ellinger-Ziegelbauer, H., et al., 2011. The enhanced value of combining conventional and "omics" analyses in early assessment of drug-induced hepatobiliary injury. Toxicol Appl Pharmacol. 252**,** 97-111.

Family Smoking Prevention and Tobacco Control Act. Public Law No. 111-131 (June 22, 2009).

Fang, H., Gough, J., 2014. The 'dnet' approach promotes emerging research on cancer patient survival. Genome Med. 6**,** 64.

Fernando, H., et al., 2011. Lipidomic changes in rat liver after long-term exposure to ethanol. Toxicol Appl Pharmacol. 255**,** 127-37.

Fischer, B. M., et al., 2015. COPD: balancing oxidants and antioxidants. Int J Chron Obstruct Pulmon Dis. 10**,** 261-276.

Formatted: French (Switzerland)

Gaworski, C. L., et al., 1997. 13-week inhalation toxicity study of menthol cigarette smoke. Food Chem Toxicol. 35**,** 683-92.

Gebel, S., et al., 2013. Construction of a computable network model for DNA damage, autophagy, cell death, and senescence. Bioinformatics and biology insights. 7**,** 97.

Gentleman, R. C., et al., 2004. Bioconductor: open software development for computational biology and bioinformatics. Genome biology. 5**,** R80.

Grösch, S., et al., 2012. Chain length-specific properties of ceramides. Progress in lipid research. 51**,** 50-62.

Hamilton, T. A., et al., 2014. Myeloid colony-stimulating factors as regulators of macrophage polarization. Front Immunol. 5**,** 554.

Haziza, C., et al., submitted (this issue). Evaluation of the Tobacco Heating System 2.2. Part 8: 5-Day randomized reduced exposure clinical trial in Poland.

Hengstermann, A., Müller, T., 2008. Endoplasmic reticulum stress induced by aqueous extracts of cigarette smoke in 3T3 cells activates the unfolded-protein-response-dependent PERK pathway of cell survival. Free Radical Biology and Medicine. 44**,** 1097-1107.

Herbrich, S. M., et al., 2013. Statistical Inference from Multiple iTRAQ Experiments without Using Common Reference Standards. Journal of proteome research. 12**,** 594-604.

Hernandez, C. P., et al., 2013. Effects of cigarette smoke extract on primary activated T cells. Cell Immunol. 282, 38-43.
Huber, W., et al., 2002. Variance stabilization applied to microarray data calibration and to the quantification of differential expression. Bioinformatics. 18, S96-S104.
Hultin-Rosenberg, L., et al., 2013. Defining, comparing, and improving iTRAQ quantification in mass spectrometry proteomics data. Mol Cell Proteomics. 12, 2021-31.
International Organization for Standardization: 3308, ISO 3308. Routine analytical cigarette-smoking machine. Definitions and standard conditions. Amended 2000. International Organization for Standardization Geneva, Switzerland, 1991.
Johnston, L. K., et al., 2012. Pulmonary macrophage subpopulations in the induction and resolution of acute lung injury. American journal of respiratory cell and molecular biology. 47, 417-426.
Jorgensen, E., et al., 2008. Cigarette smoke induces endoplasmic reticulum stress and the unfolded protein response in normal and malignant human lung cells. BMC cancer. 8, 229.
Kelsen, S. G., et al., 2008. Cigarette smoke induces an unfolded protein response in the human lung: a proteomic approach. American journal of respiratory cell and molecular biology. 38, 541-550.
Kelstrup, C. D., et al., 2012. Optimized fast and sensitive acquisition methods for shotgun proteomics on a quadrupole orbitrap mass spectrometer. Journal of proteome research. 11, 3487-3497.
Köberlin, M. S., et al., 2015. A conserved circular network of coregulated lipids modulates innate immune responses. Cell. 162, 170-183.
Kogel, U., et al., 2014. A 28-day rat inhalation study with an integrated molecular toxicology endpoint demonstrates reduced exposure effects for a prototypic modified risk tobacco product compared with conventional cigarettes. Food and Chemical Toxicology. 68, 204-217.
Kogel, U., et al., submitted (this issue). Evaluation of the Tobacco Heating System 2.2. Part 7: Systems toxicological assessment of a mentholated version revealed reduced cellular and molecular exposure effects compared with mentholated and non-mentholated cigarette smoke.
Krewski, D., et al., 2010. Toxicity testing in the 21st century: a vision and a strategy. Journal of Toxicology and Environmental Health, Part B. 13, 51-138.
Langley, G., et al., 2015. Lessons from Toxicology: Developing a 21st-Century Paradigm for Medical Research. Environ Health Perspect. 123, A268-72.
Lê Cao, K.-A., et al., 2009. integrOmics: an R package to unravel relationships between two omics datasets. Bioinformatics. 25, 2855-2856.
Lee, J., et al., 2015. Sphingolipids as cell fate regulators in lung development and disease. Apoptosis. 20, 740-57.
Leopold, P. L., et al., 2009. Smoking is associated with shortened airway cilia. PLoS One. 4, e8157.
Liberzon, A., et al., 2011. Molecular signatures database (MSigDB) 3.0. Bioinformatics. 27, 1739-1740.
Lovett, R. A., 2000. Toxicogenomics. Toxicologists brace for genomics revolution. Science. 289, 536-7.
Lundstrom, S. L., et al., 2011. Lipid mediator profiling in pulmonary disease. Curr Pharm Biotechnol. 12, 1026-52.
Mantovani, A., et al., 2013. Macrophage plasticity and polarization in tissue repair and remodelling. The Journal of pathology. 229, 176-185.
Martin, F., et al., 2014. Quantification of biological network perturbations for mechanistic insight and diagnostics using two-layer causal models. BMC Bioinformatics. 15, 238.
Martin, F., et al., submitted (this issue). Evaluation of the Tobacco Heating System 2.2. Part 9: Application of systems pharmacology to identify exposure response markers in peripheral blood of smokers switching to THS2.2.
Martin, F., et al., 2012. Assessment of network perturbation amplitudes by applying high-throughput data to causal biological networks. BMC systems biology. 6, 54.

Martinez, F. O., Gordon, S., 2014. The M1 and M2 paradigm of macrophage activation: time for reassessment. F1000prime reports. 6.
Martinez, F. O., et al., 2006. Transcriptional profiling of the human monocyte-to-macrophage differentiation and polarization: new molecules and patterns of gene expression. The Journal of Immunology. 177**,** 7303-7311.
Mei, Y., et al., 2013. Endoplasmic reticulum stress and related pathological processes. Journal of pharmacological & biomedical analysis. 1**,** 1000107.
Morissette, M. C., et al., 2015. Disruption of pulmonary lipid homeostasis drives cigarette smoke-induced lung inflammation in mice. Eur Respir J.
Naito, Y., et al., 2014. Heme oxygenase-1 and anti-inflammatory M2 macrophages. Archives of biochemistry and biophysics. 564**,** 83-88.
Nicola, M. L., et al., 2014. Young "healthy" smokers have functional and inflammatory changes in the nasal and the lower airways. Chest. 145**,** 998-1005.
Novak, R., et al., 2012. Galectin-1 and galectin-3 expression profiles in classically and alternatively activated human macrophages. Biochim Biophys Acta. 1820**,** 1383-90.
Nuwaysir, E. F., et al., 1999. Microarrays and toxicology: the advent of toxicogenomics. Mol Carcinog. 24**,** 153-9.
OECD, 2013. Guidance document on developing and assessing adverse outcome pathways. Series on Testing and Assessment No. 184. OECD Environment, Health and Safety Publications. ENV/JM/MONO(2013)6.
Oviedo, A., et al., submitted (this issue). Evaluation of the Tobacco Heating System 2.2. Part 6: 90-day OECD 413 rat inhalation study with systems toxicology endpoints demonstrates reduced exposure effects of a mentholated version compared with mentholated and non-mentholated cigarette smoke.
Pagliuca, G., et al., 2015. Cytologic and functional alterations of nasal mucosa in smokers: temporary or permanent damage? Otolaryngol Head Neck Surg. 152**,** 740-5.
Phillips, B., et al., 2015. Toxicity of aerosols of nicotine and pyruvic acid (separate and combined) in Sprague-Dawley rats in a 28-day OECD 412 inhalation study and assessment of systems toxicology. Inhal Toxicol. 27**,** 405-31.
Piade, J. J., et al., 2014. Toxicological assessment of kretek cigarettes Part 3: kretek and American-blended cigarettes, inhalation toxicity. Regul Toxicol Pharmacol. 70 Suppl 1**,** S26-40.
R Development Core Team, R: A Language and Environment for Statistical Computing. 2007.
Sauer, J. M., et al., 2015. Systems Toxicology: The Future of Risk Assessment. Int J Toxicol. 34**,** 346-8.
Schaller, J.-P., et al., submitted (this issue)-a. Evaluation of the Tobacco Heating System 2.2. Part 2: Chemical composition, genotoxicity, cytotoxicity, and physical properties of the aerosol.
Schaller, J.-P., et al., submitted (this issue)-b. Evaluation of the Tobacco Heating System 2.2. Part 3: Influence of the tobacco blend on the formation of harmful and potentially harmful constituents in the aerosol.
Schlage, W. K., et al., 1998a. Cytokeratin expression patterns in the rat respiratory tract as markers of epithelial differentiation in inhalation toxicology. I. Determination of normal cytokeratin expression patterns in nose, larynx, trachea, and lung. Toxicologic pathology. 26**,** 324-343.
Schlage, W. K., et al., 1998b. Cytokeratin expression patterns in the rat respiratory tract as markers of epithelial differentiation in inhalation toxicology. II. Changes in cytokeratin expression patterns following 8-day exposure to room-aged cigarette sidestream smoke. Toxicologic pathology. 26**,** 344-360.
Schlage, W. K., et al., 2011. A computable cellular stress network model for non-diseased pulmonary and cardiovascular tissue. BMC Syst Biol. 5**,** 168.

Formatted: French (Switzerland)

Sewer, A., et al., submitted (this issue). Evaluation of the Tobacco Heating System 2.2. Part 5: MicroRNA expression from a 90-day rat inhalation study indicates reduced effects of the aerosol on lung tissue compared with cigarette smoke exposure.
Shaykhiev, R., et al., 2009. Smoking-dependent reprogramming of alveolar macrophage polarization: implication for pathogenesis of chronic obstructive pulmonary disease. The Journal of immunology. 183**,** 2867-2883.
Simet, S. M., et al., 2010. Long-term cigarette smoke exposure in a mouse model of ciliated epithelial cell function. Am J Respir Cell Mol Biol. 43**,** 635-40.
Smith, M., et al., submitted (this issue). Evaluation of the Tobacco Heating System 2.2. Part 1: Description of the System and the Scientific Assessment Program.
Smyth, G. K., 2004. Linear models and empirical bayes methods for assessing differential expression in microarray experiments. Stat Appl Genet Mol Biol. 3**,** Article3.
Stämpfli, M. R., Anderson, G. P., 2009. How cigarette smoke skews immune responses to promote infection, lung disease and cancer. Nature Reviews Immunology. 9**,** 377-384.
Stephens, M. L., et al., 2012. Accelerating the development of 21st-century toxicology: outcome of a Human Toxicology Project Consortium workshop. Toxicological Sciences. 125**,** 327-334.
Sturla, S. J., et al., 2014. Systems toxicology: from basic research to risk assessment. Chemical research in toxicology. 27**,** 314-329.
Szklarczyk, D., et al., 2015. STRING v10: protein-protein interaction networks, integrated over the tree of life. Nucleic Acids Res. 43**,** D447-52.
Talhout, R., et al., 2011. Hazardous compounds in tobacco smoke. International journal of environmental research and public health. 8**,** 613-628.
Telenga, E. D., et al., 2014. Untargeted lipidomic analysis in chronic obstructive pulmonary disease. Uncovering sphingolipids. Am J Respir Crit Care Med. 190**,** 155-64.
Tesfaigzi, J., Carlson, D. M., 1999. Expression, regulation, and function of the SPR family of proteins. Cell biochemistry and biophysics. 30**,** 243-265.
Titz, B., et al., 2016. Effects of cigarette smoke, cessation and switching to two heat-not-burn tobacco products on lung lipid metabolism in C57BL/6 and Apoe-/- mice - an integrative systems toxicology analysis. Toxicol Sci. 149**,** 441-457.
Titz, B., et al., 2014. Proteomics for systems toxicology. Computational and structural biotechnology journal. 11**,** 73-90.
Titz, B., et al., 2015a. Analysis of Proteomic Data for Toxicological Applications. Computational Systems Toxicology. Humana Press, pp. 257-284.
Titz, B., et al., 2015b. Alterations in the sputum proteome and transcriptome in smokers and early-stage COPD subjects. Journal of proteomics. 128**,** 306-320.
Valitutti, S., et al., 1997. Degradation of T cell receptor (TCR)-CD3-zeta complexes after antigenic stimulation. J Exp Med. 185**,** 1859-64.
Vanscheeuwijck, P. M., et al., 2002. Evaluation of the potential effects of ingredients added to cigarettes. Part 4: subchronic inhalation toxicity. Food Chem Toxicol. 40**,** 113-31.
Väremo, L., et al., 2013. Enriching the gene set analysis of genome-wide data by incorporating directionality of gene expression and combining statistical hypotheses and methods. Nucleic acids research. 41**,** 4378-4391.
Vizcaíno, J. A., et al., 2014. ProteomeXchange provides globally coordinated proteomics data submission and dissemination. Nature biotechnology. 32**,** 223-226.
Westra, J. W., et al., 2011. Construction of a computable cell proliferation network focused on non-diseased lung cells. BMC systems biology. 5**,** 105.
Westra, J. W., et al., 2013. A modular cell-type focused inflammatory process network model for non-diseased pulmonary tissue. Bioinformatics and biology insights. 7**,** 167.

White, M. J., Gomer, R. H., 2015. Trypsin, Tryptase, and Thrombin Polarize Macrophages towards a Pro-Fibrotic M2a Phenotype. PLoS One. 10**,** e0138748.
Wong, E. T., et al., submitted (this issue). Evaluation of the Tobacco Heating System 2.2. Part 4: 90-day OECD 413 rat inhalation study with systems toxicology endpoints demonstrates reduced exposure effects compared with cigarette smoke.
Wooten, J. B., et al., 2006. Tobacco smoke constituents affecting oxidative stress. Cigarette Smoke and Oxidative Stress. Springer, pp. 5-46.
Wright, J. L., Churg, A., 2010. Animal models of cigarette smoke-induced chronic obstructive pulmonary disease. Expert Rev Respir Med. 4**,** 723-34.
Xue, J., et al., 2014. Transcriptome-based network analysis reveals a spectrum model of human macrophage activation. Immunity. 40**,** 274-288.
Yang, Y., Uhlig, S., 2011. The role of sphingolipids in respiratory disease. Ther Adv Respir Dis. 5**,** 325-44.
Yu, B., et al., 2008. Acute tobacco smoke-induced airways inflammation in spontaneously hypertensive rats. Inhal Toxicol. 20**,** 623-33.
Zuo, L., et al., 2014. Interrelated role of cigarette smoking, oxidative stress, and immune response in COPD and corresponding treatments. Am J Physiol Lung Cell Mol Physiol. 307**,** L205-18.

Formatted: French (Switzerland)

Figure captions

Figure 1. Design of the 90-day systems toxicology study to assess effects of CS and THS2.2M exposures on rat respiratory organs. Groups of six male and six female rats were exposed for 90 days to fresh air (Sham) or cigarette smoke of three reference cigarettes: a standard reference cigarette (3R4F), and a low menthol (MRC(LM)) and high menthol (MRC(HM)) reference cigarette (all at 23 µg nicotine/L). In addition, groups of rats were exposed to aerosol from THS2.2M (15, 23, and 50 µg/L nicotine). The 90-day exposure period was followed by a 42-day recovery period with rats exposed to fresh air (indicated groups and female rats only). Rats were exposed for 6 h per day, for 5 days per week. Respiratory nasal epithelium and lung tissue samples were collected for proteomics, transcriptomics, and histopathology. Lipidomics analysis was conducted for the lung tissue samples.

Figure 2. Response of the respiratory nasal epithelium to CS exposure. (A) Star plots showing relative network-level biological impact factors (RBIF) for each exposure group compared with the Sham groups. The total area in each star plot represents the RBIF of each comparison relative to the comparison with the overall largest BIF (MRC(LM), males, 90 days). The areas of the segments show the aggregation of network perturbation amplitude computed for each family of biological network models (see key). For each exposure group comparison, the relative contribution of the individual network perturbation amplitude are indicated. (B) Gene set enrichment analysis for the transcriptomics and proteomics data. Set enrichment was assessed by gene-set analysis with the mean of the absolute log2 fold-change as the gene set statistic (from mSigDB c5 collection). Gene (Q1) and sample permutation (Q2) was used to assess statistical significance. Gene sets with an adjusted p-value < 0.05 for both Q1 and Q2 in any comparison were selected. Gene sets were clustered by similarity of the contributing genes (annotated by representative gene set, see color bar on the left of the heatmap). The mean log2 fold-change (normalized per gene set) is color-coded (see color key). See Supplementary Figure 3 for details. The exposure groups are indicated above the heatmap. Reference cigarette exposure in red, THS2.2M exposure in blue, R1 = 3R4F, R2 = MRC(LM), R3 = MRC(HM), TL = THS2.2M(L), TM = THS2.2M(M), TH = THS2.2M(H). Note that the first 12 and the last six exposure groups for the proteomics data were analyzed as two independent iTRAQ sets. Set 2 is marked, see methods for details.

Figure 3. Molecular marker panels capture the response of the respiratory nasal epithelium to CS exposure. (A) Expression profiles for marker panel of epithelium cell types and basal lamina components. The protein and gene abundance and expression fold-changes compared with the respective Sham groups are color-coded and statistical significance is marked (adjusted p-value, x = < 0.05, * = < 0.01). Missing values are marked in grey. (B) Expression profiles for panel of immune-cell markers. Note that not all relevant markers (e.g., the B-cell marker CD19) were identified in the transcriptomics and proteomics analyses. The exposure groups are indicated above the heatmaps (A and B) and are defined in the caption to Figure 2B.

Figure 4. Response of the lung tissue to CS exposure. (A) Star plots showing relative network-level biological impact factors (RBIFs) for each exposure group compared with the Sham groups. The total area in each star plot represents the RBIF of each comparison relative to the comparison with the MRC(LM), females, 90-days group. See the caption to Figure 2A for other details. (B) Functional association clustering for transcriptomics data of the lung tissue. Functional clusters affected by the exposure conditions were identified and compared across the different clusters. Lower panel shows the identified clusters and their associated functional categories (see key). Each node represents a gene, lines represent functional associations, and identified gene clusters are grouped and circled. The top panel shows the differential expression response for each gene in the association network. The node color represents the –log10 adjusted p-value (see color key). (C) Functional association clustering for proteomics data of the lung tissue. In the lower panel, each node represents a protein, lines represent functional associations, and identified protein clusters are grouped and circled. The top panel shows the differential abundance response for each protein in the association network. See the caption to 4B for other details. Note that several clusters with immune-related molecules were identified.

Figure 5. Immune-related molecular marker panel captures the response of the lung tissue to CS exposure. (A) Expression profiles for panel of immune-cell markers. The protein and gene abundance and expression fold-changes compared with the respective Sham groups are color-coded and statistical significance is marked (adjusted p-value, x = < 0.05, * = < 0.01). Missing values are marked in grey. (B) Quantitative scores of exposure effects on the

macrophage signaling pathway. The bars show the overall network perturbation amplitude (NPA) based on the transcriptomics data, the error bars show the 95% confidence interval. Three statistics are shown: the red star indicates statistical significance with respect to the biological replicates, the green star (o statistic) indicates significance with respect to permutation of the downstream genes of the network nodes, and the blue star (k statistic) indicates significance with respect to permutation of the network topology ($p < 0.05$). (C) Quantitative scores of exposure effects on the neutrophil signaling pathway. See the caption to 5B for other details. (D) Expression profiles for M2 macrophage-related genes/proteins. The exposure groups are indicated above the heatmaps (A and D) and are defined in the caption to Figure 2B.

Figure 6. Cellular stress response in lung tissue after CS exposure. (A) Quantitative scores of exposure effects on the oxidative stress pathway. (B) Quantitative scores of exposure effects on the xenobiotic metabolism pathway. The bars show the overall network perturbation amplitude (NPA) based on the transcriptomics data, the error bars show the 95% confidence interval. Three statistics are shown: the red star indicates statistical significance with respect to the biological replicates, the green star (o statistic) indicates significance with respect to permutation of the downstream genes of the network nodes, and the blue star (k statistic) indicates significance with respect to permutation of the network topology. (C) Expression/abundance profiles for cellular stress-related gene/protein sets. The reactive-oxygen species (ROS) and xenobiotic gene set is the union of the metabolism of xenobiotics by the cytochrome P450 gene set from the KEGG database and the hallmark reactive -oxygen species pathway from mSigDB. The unfolded-protein response (UPR) pathway includes common UPR markers. Profiles for significantly affected proteins/genes are shown (adjusted p-value < 0.05). The fold-changes compared with the respective Sham groups are color-coded and statistical significance is marked (FDR-adjusted p-value, x = < 0.05, * = < 0.01). Missing values are marked in grey. The exposure groups are indicated above the heatmap and are defined in the caption to Figure 2B.

Figure 7. Effects of CS exposure on the lung lipidome. (A) Abundance profiles for lipid species with significant differential abundance. Each row represents a lipid species, each column an exposure condition compared with the respective Sham group. The fold-change compared with Sham exposure is color-coded (see color key). Significantly abundant differences are indicated (* = adjusted p-value < 0.05). The molar contribution of significantly abundant lipid species to their lipid class is indicated by the shade of the significance indicator. (B) Schematic summary of the ceramide-centered sphingolipid metabolic network with the gene expression response profiles of the significantly altered enzymes. See Supplementary Figure 7 for more details.

Supplementary Material

Evaluation of the Tobacco Heating System 2.2. Part 7: Systems toxicological assessment of a mentholated version revealed reduced cellular and molecular exposure effects compared with mentholated and non-mentholated cigarette smoke

Ulrike Kogel[a,*], Bjoern Titz[a,*], Walter K. Schlage[b], Catherine Nury[a], Florian Martin[a], Alberto Oviedo[c], Stefan Lebrun[a], Ashraf Elamin[a], Emmanuel Guedj[a], Keyur Trivedi[a], Nikolai V. Ivanov[a], Patrick Vanscheeuwijck[a], Manuel C. Peitsch[a], Julia Hoeng[a]

[a] Philip Morris International Research and Development, Philip Morris Products S.A., Quai Jeanrenaud 5, 2000 Neuchatel, Switzerland (part of Philip Morris International group of companies)

[b] Biology consultant, Max-Baermann-Str. 21, 51429 Bergisch Gladbach, Germany

[c] Philip Morris International Research Laboratories, 50 Science Park Road, Singapore, Singapore (part of Philip Morris International group of companies)

[*] UK and BT contributed equally to this manuscript.

Corresponding author:

Julia Hoeng, PhD

E-mail: julia.hoeng@pmi.com

Tel: +41 (58) 242 2214

Fax: +41 (58) 242 2811

Supplementary Figure 1. Number of identified genes and proteins with significant differential expression/abundance. (A) Numbers of significant differentially expressed genes (DEGs) identified in respiratory nasal epithelium of the exposure groups compared with the corresponding Sham-exposed rats. Numbers of up- and down-regulated genes with adjusted p-value < 0.05 are shown. **(B)** Numbers of differentially abundant proteins (DEPs) identified in respiratory nasal epithelium of the exposure groups compared with the corresponding Sham-exposed rats. **(C)** Number of significant differentially expressed genes (DEGs) identified in lung tissue for the exposure groups compared with the corresponding Sham-exposed rats. Numbers of up- and down-regulated genes with adjusted p-value < 0.05 are shown. **(D)** Numbers of differentially abundant proteins (DEPs) identified in lung tissue for the exposure groups compared with the corresponding Sham-exposed rats. Note that the first 12 and the last six exposure groups for the proteomics data were analyzed as two independent iTRAQ sets. Set 2 is marked, see methods for details.

Supplementary Figure 2. Exposure response of individual network models. Network perturbation amplitude (NPA) heatmaps of all subnetworks tested. Network models have been described in the literature: cell proliferation (Westra et al., 2011); cell stress (Schlage et al., 2011); apoptosis, autophagy, DNA damage, necroptosis, and senescence (Gebel et al., 2013); and inflammation (Westra et al., 2013). **(A)** Results for respiratory nasal epithelium of male rats. **(B)** Results for respiratory nasal epithelium of female rats. **(C)** Results for lung tissue of male rats. **(D)** Results for lung tissue of female rats. Note: each heatmap indicates the amount of perturbation, but not the direction; therefore, high perturbation can also indicate down-regulated processes. Note that the color bars below the heatmaps indicate the different exposure conditions. CFA, cell fate; CPR, cell proliferation; CST, cell stress; IPN, inflammatory process network; TRA, tissue repair and angiogenesis.

Supplementary Figure 3. Gene-set enrichment for rat respiratory nasal epithelium. Gene set enrichment analysis for transcriptomics and proteomics data. Set enrichment was assessed by gene-set analysis with

the mean of the absolute log2 fold-change as the gene set statistic (mSigDB c5 collection). Gene (Q1) and sample permutation (Q2) were used to assess statistical significance. Gene sets with an adjusted p-value < 0.05 for both Q1 and Q2 in any comparison were selected. Gene sets were clustered by similarity of the contributing genes (annotated by representative gene set) and the mean log2 fold-change (normalized per gene set) was color-coded (see color key). In each cell the significance of the gene-set – exposure association is indicated by a maximum of four stars: positions 1 and 2 = Q1 hypothesis; positions 3 and 4 = Q2 hypothesis; positions 1 and 3 = non-directional; positions 2 and 4 = directional (adjusted p-value < 0.05). Color bar on the left of the heatmap shows the gene set clustering.

Supplementary Figure 4. Functional association clusters for the lung transcriptomics and proteomics data. Each node represents a gene (left panel) or protein (right panel), lines represent functional associations, and identified gene/protein clusters are grouped and circled.

Supplementary Figure 5. Gene-set enrichment for rat lung tissue. Gene set enrichment analysis for transcriptomics and proteomics data. Set enrichment was assessed by gene-set analysis with the mean of the absolute log2 fold-change as the gene set statistic (mSigDB c5 collection). Gene (Q1) and sample permutation (Q2) was used to assess statistical significance. Gene sets with an adjusted p-value < 0.05 for both Q1 and Q2 in any comparison were selected. Gene sets were clustered by similarity of the contributing genes (annotated by representative gene set) and the mean log2 fold-change (normalized per gene set) was color-coded (see color key). In each cell the significance of the gene-set – exposure association is indicated by a maximum of four stars: positions 1 and 2 = Q1 hypothesis; positions 3 and 4 = Q2 hypothesis; positions 1 and 3 = non-directional; positions 2 and 4 = directional (adjusted p-value < 0.05).

Supplementary Figure 6. Macrophage M1/M2 polarization profiles for rat lung tissue. Volcano plots show the effect size (log2 fold-change) and significance (−log10 adjusted p-value) for genes that were

associated with the M1 and M2 macrophage differentiation states (Shaykhiev et al., 2009). **(A)** M2 signature genes. **(B)** M1 signature genes.

Supplementary Figure 7. Effects of CS exposure on sphingolipid metabolic enzymes. (A) Gene and protein expression/abundance profiles for the sphingolipid metabolism pathway from the KEGG database. **(B)** Expression changes mapped onto the sphingolipid metabolism pathway. Fold-changes in exposed groups compared with Sham exposure are color coded. Note that mapping can aggregate expression values for several iso-enzymes and the labels do not necessarily correspond to the most significantly affected iso-enzymes, as for example in the case of Degs1 and Degs2. This mapping serves as an overview and a schematic summary of the ceramide-centered sphingolipid metabolic network for the significantly affected enzymes is shown in Figure 7B.

Supplementary Table 1 [Excel file]: Molecular markers for epithelial and immune cell types. (A) Molecular marker panel for respiratory nasal epithelial cell types. All the markers that were used to characterize the epithelial cell types are listed. **(B)** Molecular marker panel for immune cell types taken from the literature. All the markers that were used to characterize the inflammatory cell types are listed.

Supplementary Table 2 [Excel file]: Lipidomics raw data.